

October 1968

FINAL REPORT

STUDY OF AN AURORAL ZONE ROCKET EXPERIMENT

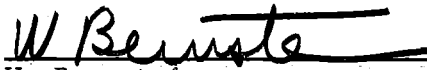
Prepared for


NASA Headquarters  
Washington, D. C.

Contract No. NASW-1474


Space Sciences Laboratory  
Systems Laboratories  
TRW SYSTEMS GROUP  
One Space Park  
Redondo Beach, California 90278

Prepared by:


  
W. Bernstein

  
G. T. Inouye

  
N. L. Sanders

  
R. L. Wax

Approved by:

  
A. Rosen, Director  
Space Sciences Laboratory

## TABLE OF CONTENTS

	<u>Page</u>
SUMMARY . . . . .	1
I. INTRODUCTION . . . . .	2
II. DESCRIPTION OF THE PAYLOAD . . . . .	3
A. Summary of the Experiments . . . . .	3
B. Detailed Description of the Experimental Payload . . . . .	3
C. DC Electric Field Experiments. . . . .	6
D. Fluxgate Magnetometer . . . . .	8
E. Hg Photometer . . . . .	8
F. Search Coil Magnetometer . . . . .	9
G. High and Low Voltage Power . . . . .	9
H. Telemetry Assignments . . . . .	10
I. Arrangement of the Payload in the Rocket . . . . .	10
J. Problems in Performance . . . . .	11
III. LAUNCH CONDITIONS AND FLIGHT HISTORY . . . . .	12
A. Criteria for Launch . . . . .	12
B. Actual Launch Conditions . . . . .	14
C. Flight History . . . . .	15
IV. RESULTS . . . . .	16
A. Ground Based Measurements . . . . .	16
B. Flight Experiments . . . . .	17
VII. DISCUSSION OF RESULTS . . . . .	20
A. Hydrogen Energy Spectra and Flux . . . . .	20
B. Electron Spectra . . . . .	22
C. Cessation of Precipitation . . . . .	23
D. Evidence for Rapid Fluctuations in Precipitation Rate. . . . .	24
E. Energy Balance . . . . .	25
F. H <sup>0</sup> Total Hydrogen Flux Detector . . . . .	26
G. Doppler Shifted Hydrogen Balmer Line Emission . . . . .	28
H. AC Electric Field Measurement . . . . .	29
I. DC Electric Field Measurements . . . . .	32
CONCLUSIONS . . . . .	34
ACKNOWLEDGEMENTS . . . . .	35
LIST OF PUBLICATIONS SUPPORTED BY THIS PROGRAM . . . . .	36
APPENDIX . . . . .	37
REFERENCES . . . . .	39
FIGURE CAPTIONS . . . . .	41

SUMMARY

This report contains a description of the experimental payload of a Nike-Tomahawk sounding rocket, and an exposition of the scientific results derived from its launch into a breakup aurora from Ft. Churchill, Manitoba, Canada on April 25, 1968. The important scientific results included:

1. The adequacy and utility of an energetic neutral hydrogen spectrometer has been demonstrated in a flight experiment.
2. The measured precipitated total hydrogen fluxes were  $\sim 5 \times 10^8 \text{ cm}^{-2} \text{ sec}^{-1} \text{ str}^{-1}$  with an e-fold energy of  $\sim 1 \text{ keV}$ .
3. The measured doppler shifted  $H_\beta$  intensity and altitude profile were consistent with those theoretically predicted for the observed hydrogen fluxes and energy spectra.
4. Peaked electron energy spectra were observed. During the flight, the peak energy abruptly shifted from the interval  $1.1 - 2.5 \text{ keV}$  to the interval  $2.5 - 6 \text{ keV}$ . The maximum electron fluxes were  $\sim 10^8 \text{ cm}^{-2} \text{ sec}^{-1} \text{ str}^{-1} \text{ keV}^{-1}$ .
5. The total energy precipitation was  $\sim 10 \text{ ergs/cm}^2 \text{ sec}$  during the flight. The energy precipitated by the energetic hydrogen alone ranged from 25-50% of the total rate.
6. A unique event in which both hydrogen and electron precipitation ceased abruptly was observed.
7. DC electric fields of  $25 - 50 \text{ mv/m}$  in the North-South direction were observed.
8. The AC electric field experiment results were very similar to those previously reported for a temperate latitude flight and showed severe modulation at the spin frequency and its harmonics. The behavior of the fields showed no correlation with particle precipitation rates.

## I. INTRODUCTION

This program was initiated in 1967 with two related objectives in mind. Firstly, it was desired to conduct a simple and inexpensive flight demonstration of two neutral hydrogen experiments, which had been conceived at TRW for eventual use as detectors for energetic neutral hydrogen atoms in the interplanetary medium, in an environment where measurable fluxes of energetic hydrogen atoms were expected. Secondly, it was desired that these measurements, providing more than just an instrument test, would contribute significant scientific information. Because an auroral experiment admirably satisfied both these objectives, the two neutral hydrogen detectors were incorporated into a comprehensive Nike-Tomahawk rocket payload. The rocket, NASA 18.33CE, was launched into a post breakup aurora from Ft. Churchill, Manitoba, Canada on 25 April 1968.

Our philosophy in the payload selection was directed toward obtaining a rather complete measurement of the flux and energy spectrum of the precipitated energetic particles, protons, hydrogen atoms, and electrons. The direct particle measurements were supplemented by both ground based and vehicle borne photometers to permit study of the particle-light relationships and to give a greater degree of confidence in the particle measurements. Also, we included experiments to measure both electric and magnetic fields and thus study possible relationships between their characteristics and the behavior of the precipitating particles.

The final payload provided a sufficient number of experiments with sufficient redundancy to permit a reasonable assessment of instrument performance and also to yield significant scientific information.

This report includes a concise description of the complete payload, auroral conditions for the flight, the limitations of the equipment, the results, and our assessment of the significance of these results with respect to auroral physics. A brief description of some laboratory studies of Bendix Continuous Channel Multiplier (CCM) characteristics are found in the Appendix.

## II. DESCRIPTION OF THE PAYLOAD

### A. Summary of the Experiments

The instruments flown on Nike-Tomahawk rocket NASA 18.33 CE included:

1. An energy spectrometer for energetic neutral hydrogen atoms in the range 0.6 - 22 keV.
2. A detector for measuring the fluxes of only energetic neutral hydrogen atoms or total energetic hydrogen including neutral atoms, protons, and negative ions.
3. An energy spectrometer for protons and electrons in the range 0.5 - 21 keV.
4. Two AC electric field detectors, oriented to yield both the electric field perpendicular to the spin axis of the rocket ( $E_{\perp}$ ) and parallel to the spin axis ( $E_{\parallel}$ ) over the frequency range 10 Hz - 30 kHz.
5. A DC electric field detector oriented to measure  $E_{\perp}$ .
6. Two fluxgate magnetometers oriented to measure  $B_{\perp}$  and  $B_{\parallel}$  to the vehicle spin axis in order to give the aspect of the rocket with respect to the earth's magnetic field.
7. Two sensitive search coil magnetometers oriented to measure  $B_{\parallel}$  and  $B_{\perp}$  to the vehicle spin axis in order to investigate ionospheric current systems and fast magnetic fluctuations.
8. A filter photometer system to determine the doppler shifted  $H_{\beta}$  light intensity as a function of altitude.

### B. Detailed Description of the Experimental Payload

Several detailed descriptions of the experiments and their data processing systems have been published during the course of this work. Because copies of these publications are appended to this report, we will supplement this published information only where required.

## 1. H<sup>0</sup> Energy Spectrometer

A complete description of this instrument is given in the appended paper<sup>(1)</sup> which was presented at the 1968 COSPAR meeting in Toyko. Basically, this instrument, shown schematically in Fig. 1, consisted of a charged particle deflection system, a stripping foil for the ionization of incident energetic neutral atoms, a hemispherical electrostatic analyzer and two 8 mm diameter Bendix continuous channel multipliers (channeltrons) used as detectors. Incident protons <30 keV and electrons <80 keV were rejected by the combined electrostatic and magnetic deflection systems. A known fraction of the incident neutrals were ionized in transit of the 2  $\mu\text{g}/\text{cm}^2$  carbon foil\* at the entrance to the analyzer and subsequently analyzed. The resolution of the analyzer was ~22% and varied only slightly with the energy of the incident particle. The analyzer factor was 5 kV/keV; thus 4 kV allowed measurement of 20 keV particles leaving the foil. The geometrical factor was  $4.3 \times 10^{-2} \text{ cm}^2 \text{ ster}$ . The efficiency of the instrument, defined as the ratio of the number of protons reaching the detectors to the total number of atoms incident on the foil, was energy dependent and ranged from  $10^{-3}$  at 2 keV to  $2 \times 10^{-1}$  at 20 keV.

A -4 kV, 100 Hz, non-linear sawtooth voltage was applied to one plate of the analyzer to provide a sampling of the energy spectrum every 10 msec. The detected events were time sorted into five energy channels 0.6 - 1.5, 1.5 - 3.4, 3.4 - 7, 7 - 11.5, and 11.5 - 22 keV respectively. Each event detected in a channel turned on a constant current source for a fixed time which charged a capacitor to provide an analog signal to the telemetry system. When the capacitor voltage reached five volts, it was reset to zero. More complete details of the circuitry, programming, and calibration are found in the appended paper.

## 2. The Neutral and Total Hydrogen Flux Detector

This detector also is described in greater detail in an appended publication<sup>(2)</sup>. Basically it consisted of an electrostatic deflection system

---

\*Purchased from the Yisum Research Development Corp., Jerusalem, Israel

for removal of incident protons and a magnetic deflection system for removal of electrons, a  $2 \mu\text{gm}/\text{cm}^2$  carbon scattering foil, and an 8 mm diameter channeltron detector mounted  $22^\circ$  off axis. The scattering technique was employed in order to reduce the UV sensitivity of the channeltron. In this configuration, the detector efficiency was approximately independent of incident energy over the range 2 - 20 keV and was  $\sim 7 \times 10^{-3}$ . The geometrical factor was  $\sim 2.2 \times 10^{-2} \text{ cm}^2 \text{ ster}$ . With the electrostatic voltage on, only neutral particles were detected; with the voltage off, the total hydrogen flux ( $\text{H}^0 + \text{H}^+ + \text{H}^-$ ) was detected. This voltage was turned on for one second and off for one second, continuously. Thus the ratio,  $\text{H}^0/\text{H}^0 + \text{H}^+ + \text{H}^-$ , was obtained every two seconds.

The detected events were stored and transmitted in a manner similar to that described for the  $\text{H}^0$  spectrometer. The only modification was that the capacitor voltage was reset to zero at the completion of each operating mode in addition to the 5 volt reset.

### 3. Proton-Electron Energy Spectrometer

This instrument was a conventional  $90^\circ$  cylindrical electrostatic analyzer and collimator with an analyzer factor of 5 kV/keV. The calculated resolution was 11% for isotropic radiation. This was confirmed by laboratory measurements using the quasi-isotropic source technique described in the appended publication<sup>(3)</sup>. The geometrical factor was  $1.3 \times 10^{-3} \text{ cm}^2 \text{ ster}$ , and since a foil was not employed, the detector efficiency was assumed to be 100% for all particles passing through the analyzer. The outside plate was serrated to reduce scattering effects and UV sensitivity.

The analyzer plate voltage was provided by a pair of 100 Hz, -4 kV sawtooth generators identical to that described for the  $\text{H}^0$  energy spectrometer. The outside analyzer plate was driven by one sweep for a one second period to give electron data. Then the inside plate was driven by the other sweep for one second to provide proton data. Thus every two seconds, complete proton and electron spectra were obtained.

Each sweep cycle was time sorted into five energy channels as described for the  $\text{H}^0$  spectrometer. Although the analyzer factors were the



same for both instruments, the energy channels differed because of the energy loss incurred during particle transit through the foil. For the proton-electron spectrometer, the channels were 0.5 - 1.1, 1.1 - 2.5, 2.5 - 6, 6 - 10.5, and 10.5 - 21 keV. The detected events were stored as described for the  $H^0$  spectrometer with the only modification being the addition of the capacitor reset at the end of each measurement period.

### C. Electric Field Experiments

The electric field experiments were intended to measure AC electric fields oriented parallel and perpendicular to the earth's magnetic field over the frequency range 30 Hz - 30 kHz and to measure DC electric fields perpendicular to the magnetic field. With the exception of the antenna configuration, the instrument was similar to that described by Scarf, Crook, and Fredricks<sup>(4)</sup>; their description is included in the appendix.

A simplified block diagram of the instrument is shown in Fig. 2. Basically it consisted of three separate antenna systems with two duplicate electronic channels for the AC measurements and one channel for the DC measurement. The two AC channels each consisted of a broad band (30 Hz - 1 kHz) output connected directly to the telemetry and six narrow band filter outputs at 1.3, 2.3, 3.9, 7.35, 14.5, and 30 kHz connected to the telemetry commutator.

Because any environmental DC electric field perpendicular to the spin axis, including  $v \times B/c$  induced E field, would be modulated at the spin frequency, a band pass filter at the spin frequency (1 Hz) was employed in the DC channel to eliminate all other frequencies. This technique tended to eliminate any steady potential difference between the two antenna elements (contact potentials, etc.) which would obscure true field measurements. However, variations in these steady potential differences, particularly those associated with the vehicle spin, such as could be caused by shadowing of light or particles which would change contact potentials, were not eliminated by this technique.

Four 4 cm radius spherical collecting surfaces provided the required three sets of antenna elements. The use of such large diameter collecting

spheres introduced a problem of stowage of these elements within the shell prior to deployment. Therefore each collector was made of 12 strips of 2 mil stainless steel which could be twisted to fit when stowed but which expanded to be nearly spherical when deployed. The same pair of collectors were employed for the AC and DC  $E_{\perp}$  measurements. Here separate antennas were achieved by connecting together alternate strips of each collector and then isolating each set from the other. Thus two separate systems were achieved with the sacrifice of only half the collecting area. It should be noted that no attempt was made to clean or coat these collecting surfaces to obtain a more uniform surface work function.

The collectors were placed on small boomlets at the end of a 1 meter boom, which extended 88.6 cm from the rocket shell, in such a manner that one pair was aligned parallel to the spin axis ( $E_{\parallel}$ ) and the other pair formed an array perpendicular to both the axial and radial orientations of the rocket ( $E_{\perp}$ ). In the designation of  $E_{\perp}$  and  $E_{\parallel}$  it was assumed that the rocket spin axis would be reasonably parallel to the magnetic field. The distance between each pair of collectors was  $\sim 40$  cm. The collectors were connected to the electronics package by low capacity coaxial cables about 150 cm long. The antenna array was situated  $\sim 172$  cm from the tip of the rocket payload; the angle at the top of the rocket shell between the rocket axis and the antenna arrays was  $54^{\circ}$ .

Scarf, et al<sup>(4)</sup> have considered the response of such an instrument and antenna array for ambient plasmas of very low density such as those found in the outer magnetosphere or interplanetary medium. In these cases, they conclude that the input impedance of the device would be entirely capacitive and evaluate the response on that basis. At the plasma densities ( $10^5 - 10^6/\text{cm}^3$ ) encountered during this flight, however the sheath resistance should be on the order of  $10^6 - 10^7 \Omega$  and the response should be primarily resistive over the entire frequency range. Since the input resistance was  $5 \times 10^8 \Omega$  and was large compared to this sheath resistance, it is concluded that the response of the antenna array could be interpreted in terms of the theory applicable to conventional, resistively coupled Langmuir probes<sup>(5)</sup>.

#### D. Fluxgate Magnetometer

Two perpendicular fluxgate sensors were mounted inside the rocket shell to provide a measure of the instantaneous vehicle orientation with respect to the earth's magnetic field. The units were of conventional design; a block diagram is shown in Fig. 3.

#### E. H <sub>$\beta$</sub> Photometer

The H <sub>$\beta$</sub>  photometer was intended to measure the altitude profile of the doppler shifted H <sub>$\beta$</sub>  light emitted by the precipitated energetic hydrogen flux. Basically, it was a two channel instrument, one located at  $\lambda = 4858\text{\AA}$  corresponding to the expected maximum of the doppler shifted line and the other set at  $\lambda 4874\text{\AA}$  to provide a measure of the background light intensity in the H <sub>$\beta$</sub>  region. The wavelength sections were provided by two narrow band filters having  $2\text{\AA}$  FWHM\*. RCA 4439 photomultiplier tubes were used for both channels. The light passing through each filter was focussed by a 5.08 cm focal length lens with a lens stop set to gather light from a cone with a  $4^\circ$  half angle opening off the spin axis of the rocket. Thus the wavelengths transmitted through the filters were close to those stipulated above. The stop also served to define the solid angle of the detectors.

A block diagram of the complete photometer is shown in Fig. 4. Because of the large uncertainty existing in the expected magnitude of output currents, logarithmic amplification was employed prior to the telemetry.

In order to begin these measurements at as low an altitude as possible, the photomultiplier tubes and associated high voltage supplies were completely potted in RTV-11. Thus background measurements were initiated immediately after low voltage turn on and light measurements began with nose cose deployment.

---

\*Purchased from Thin Film Products, Inc., Cambridge, Mass.

#### F. Search Coil Magnetometer

A block diagram of the search coil magnetometer is shown in Fig. 5. The sensors were two identical iron cored coils six inches in length with 200,000 turns of AWG 46 copper wire. The sensitivity was about  $7 \mu\text{V}/\gamma$  at 1 Hz and had a broad self resonance at about 1 kHz due to its self-inductance and distributed capacitance. Following a low-noise preamplifier in each channel, wideband telemetry was provided to look for magnetic fluctuations in the 20 to 2000 Hz range. Symmetrical logarithmic amplifiers were used to provide a wide dynamic range.

Ionospheric current systems are expected to produce a magnetic field change of the order of a hundred gamma within a few tens of seconds. To detect this change in the large sinusoidal variation of the  $B_{\perp}$  sensor, the signal was peak rectified by a careful adjustment of the discharge current of the filter capacitor. Thus, the magnitude of the ripple was a measure of the change in amplitude of the sinusoid since its last peak. To increase the number of measurements during the ionospheric transit, the sinusoid was inverted and again peak rectified to provide two field increment measurements per rotation. The  $B_{\parallel}$  measurement of field change was not contaminated by these large spin effects. A high sensitivity to magnitude changes was achieved by a sampling technique similar to the one used for the  $B_{\perp}$  measurement.

To obtain the vector direction of the ionospheric current system, a sensitive measurement of any change in the phase of the  $B_{\perp}$  sinusoid is required. It is possible for a change in the field direction to manifest itself only by a change of phase. This would be the case if a rocket were shot up vertically into a horizontal North-South current sheet. The phase was measured by comparing the zero crossings of the  $B_{\perp}$  sinusoid against a time scale defined by a crystal controlled oscillator. As with the  $B_{\perp}$  magnitude, measurements were limited to two per rocket rotation.

#### G. High and Low Voltage Power

A single supply was used to provide low voltage power for all the experiments. Voltage regulation was provided to compensate for uncertainties

in the final loaded battery voltage. Although separate high voltage supplies were included to power the channeltrons of each separate experiment, it was later decided to operate these supplies in parallel with adequate decoupling to provide greater redundancy. Lastly, a separate high voltage power supply was employed for the intermittent electrostatic deflection voltage employed in the total hydrogen flux experiment.

#### H. Telemetry Assignments

The complete payload required the use of two telemetry transmitters. In general, the outputs from each experiment were divided between the two transmitters to eliminate the possibility of a total loss of data from any given experiment because of a transmitter failure.

##### I. Arrangement of the Payload in the Rocket

The physical arrangement of the payload is shown in Fig. 6. From top to bottom the arrangement was as follows:

1. All of the particle detectors and the photometer had their apertures pointed upward in the direction of the rocket spin axis. All channeltrons and discriminators were housed in this top section. The channeltrons were contained within the rocket shell so that they were not exposed to the ambient ionosphere during the flight.
2. The high voltage sweep power supplies for the energy spectrometers.
3. The high voltage DC power supplies for the channeltrons.
4. The electronics for the electric field experiment, and the fluxgate sensor units.
5. The boom section containing one boom with four spherical antennas for the electric field meter and one boom having two perpendicular search coil sensors on it. In this section were mounted two 5 rps, 28 pole commutators and various test points for the payload electronics. The electronics package for the search coil magnetometer also was mounted in this section.

6. The counting and timing circuits for the various experiments.
7. The low voltage power supply and the fluxgate electronics.
8. The interconnect plugs for the telemetry unit supplied by the Sounding Rocket Branch of GSFC.

The complete payload stage was 9' 4 3/4" high and weighed ~200 pounds. This included the experiments, ejectable nose cone, the telemetry section, and a de-spin section.

#### J. Problems in Performance

Several major difficulties occurred during the course of the flight which either resulted in the loss of data or increased difficulties in the data reduction effort. These include

1. At 159 seconds after launch, one of the two telemetry transmitters failed with the following results: (a) only the E<sub>1</sub> broadband channel and the E<sub>1</sub> DC channel of the electric field experiment remained operative, (b) both the proton-electron and H<sup>O</sup> energy spectrometers lost three data channels and five point differential energy spectra could no longer be obtained, (c) one aspect magnetometer channel was noisy but still readable. Consequently our more detailed studies are limited to the early portion of the flight.

2. The search coil magnetometer appeared to be operative prior to deployment but subsequently went into a high noise mode for the remainder of the flight. There is some possibility that the cables to the search coils were severed during boom deployment because none of the boom switches indicated deployment. However, the aspect data indicate that both booms did deploy as intended.

3. Ninety-five seconds after launch or 18 seconds after high voltage turn on, the one second clock output signal became erratic. Because this timing system selected the operating modes for several instruments, they no longer sampled the environment as prescribed. The sampling was continued in an erratic but known manner. We have not identified any malfunctions in the timing sequences controlling the energy selection of the spectrometers.

4. At the same time as the interference in the timing signal sequences occurred, bursts of counts appeared at times in the proton-electron spectrometer data. These counts could not have been caused by high voltage corona or breakdown for several reasons: (a) they did not appear until 18 seconds after turn-on of the high voltage, (b) they did not affect the  $H^0$  analyzer or the  $H^0$  total detector, (c) the repetition rate was somewhat regular, and (d) each burst contained only a limited large number of counts, usually about 100. Although it would be possible for corona or breakdown to account for some of these observations, we feel strongly that they cannot explain the total pattern. We have ignored these bursts in the derivation of counting rates since their occurrence was sufficiently infrequent and obvious that meaningful data could be extracted from the quiescent periods. These effects had not previously been observed in ground based tests and no obvious explanation is readily at hand.

5. The use of a single instrument for protons and electrons with a dynamic range in counting rate of  $\sim 10^4$  resulted in a very low observed proton counting rate. Thus the proton data are limited by poor statistical accuracy and a far greater sensitivity to contamination by the described spurious counts. Because of these problems, it is difficult to assign a calculated error to the proton data. A reasonable estimate might be as large as  $\pm$  a factor of three. Because the electron counting rates were very much higher, the electron data are far more accurate.

### III. LAUNCH CONDITIONS AND FLIGHT HISTORY

#### A. Criteria for Launch

The presence of energetic hydrogen auroral precipitation was a mandatory requirement for this flight. At most auroral latitudes there are three time periods in a usual day when energetic hydrogen precipitation is present: (1) in the evening around 1700 or 1800 local time, (2) during the auroral breakup event at about midnight or later, and (3) in the morning around 0300 to 0600 local time. It was decided before reaching the launch site that we would attempt to launch into a breakup aurora. This was decided

because (1) the fluxes of both hydrogen and electrons are large in such events; (2) the presence of strong auroral electrojets are far more likely during breakup and so it would be more likely to obtain meaningful observations by search coil magnetometer and the electric field meter; (3) because both electrons and hydrogen are precipitating in contrast to the evening and morning times when electron fluxes are low, one can hope to learn more about the precipitation mechanism by noting the similarities and differences of the two components; (4) our past experience better qualified us to anticipate the time development of the breakup in order to determine when to launch the rocket; and (5) there exists a larger number of past observations of the breakup type aurora to which our data could be compared.

The minimum flux of hydrogen that we could observe was on the order of  $10^5$  particles  $\text{cm}^{-2} \text{sec}^{-1} \text{str}^{-1} \text{keV}^{-1}$  but, of course, we desired a flux at least 100 times as large. After considering the theories of Chamberlin<sup>(6)</sup> and Eather<sup>(7)</sup> we decided that an intensity of >30 Rayleighs of doppler shifted  $\text{H}_\beta$  emission observed from the ground would indicate a suitable flux of precipitated energetic hydrogen. This light flux was set as the prime launch condition. However, on arriving at Ft. Churchill, we found that Dr. F. Creutzberg had initiated a general survey of the  $\text{H}_\beta$  intensity at Ft. Churchill using a tilting filter spectrophotometer somewhat similar to that employed by Eather and Jacka<sup>(8)</sup>. During the prior three months of this survey the maximum observed  $\text{H}_\beta$  intensity had been on the order of 20 R. Although this intensity was surprisingly low relative to other observations and theoretical predictions, we altered our prime launch condition to an  $\text{H}_\beta$  intensity of 5 R observed on this instrument.

A secondary launch condition was the presence of a Class I to Class II visible aurora indicating significant electron precipitation. The presence of at least a 100γ magnetic bay so that the search coil magnetometer would yield usable data was a third condition. It was felt that there would be a strong possibility that all three conditions could be met by a typical breakup aurora.



### B. Actual Launch Conditions

The rocket was flown from Ft. Churchill, Manitoba, Canada on 25 April 1968. The geographic coordinates of the site are 49° N, 94° W; and geomagnetic coordinates are 69° N, 38° W.

The launch window was only about  $\pm 1\frac{1}{2}$  hours from local midnight because sunrise at high altitude would make the vehicle photometer and particle measurements suspect. At 0001:40 local time, 0601:40 UT, the rocket was launched into a moderate breakup event. The magnetic field was in the recovery phase of a 140γ negative bay which was accompanied by a bright breakup about 18 minutes before the breakup into which the rocket was launched. The magnetic field was still depressed by an approximately constant 100γ during the flight. There was very little 30 MHz riometer absorption before or during the flight. It is estimated that the aurorally enhanced absorption was less than 1/2 db.

The tracking radar gave the data shown in Table I for the rocket position in the vertical plane of flight. The direction of launch was 15.0 degrees south of east. The last column of the table shows heights computed by assuming that the data at 2:14 (LOS-1) and 2:58 (LOS-2) gave the proper positions on a free fall trajectory. These assumptions give a maximum trajectory height of 235 km at 06:05:31. The equation for computing the height vs time curves is

$$H = 235 - \frac{1}{2} g [t(\text{sec}) - 5:31]^2 \text{ kilometers}$$

where  $g = .0098 \text{ km/sec}^2$ . The computed height at 06:02:43 (AOS-2) is very close to the measured height. The other computed values are too low, indicating that the atmospheric effects were not negligible below a height of 45 km. The time at which the rocket descended to 45 km is calculated to be at 06:08:48.

Using the same two points, LOS-1 and LOS-2, for horizontal position gives a horizontal velocity of 0.338 km/sec. This velocity, when used to determine the trajectory, required the atmospheric influence to begin at an

altitude of about 100 km. Using the data at LOS-2, the time at AOS-3, and a distance slightly less than for AOS-3, gave a horizontal velocity of 0.301 km/sec. The equation for the trajectory is

$$H = 235 - \frac{g}{2} \left( \frac{R - 66}{v_x} \right)^2 \text{ kilometers,}$$

where  $v_x = 0.301$  km/sec,  $g = .0098$  km/sec<sup>2</sup>,  $R$  in kilometers. The angle of the rocket,  $\theta$ , from the vertical was close to 10.5 degrees between 45 km and 120 km altitudes.

Ground-based instruments making measurements during the flight were (1) tilting filter spectrometer for  $H_\beta$  emission, (2) a fixed filter photometer for  $H_\beta$ , (3) a fixed filter photometer for the oxygen 5577Å emission, (4) a fixed filter photometer for the nitrogen 3914Å emission, (5) three all-sky cameras, (6) a 30 MHz riometer, and (7) a magnetometer.

### C. Flight History

Twenty seconds after firing, the low voltage power supply was turned on. The photometer, the electric field meter and the two magnetometers began operation. The photometer read at a background level because it was enclosed by the rocket nose cone. The aspect magnetometer gave proper readings. Both the search coil magnetometer and the electric field meter gave noise outputs as should be expected. Forty seconds after launch the nose cone was ejected and the photometer responded to the increased light intensity. The rocket was de-spun to about 1 rps and the booms were deployed 47 seconds after launch. The electric field meter indicated fields as it was deployed and for the remainder of the flight. The search coil magnetometer indicated the beginning of the deployment, but suddenly went into a high noise mode and remained in this condition for the rest of the flight. Seventy-seven seconds after launch, the high voltage was turned on for all of the particle experiments and they all began counting.

## VI. RESULTS

### A. Ground Based Measurements

The ground based optical measurements performed during the flight included:

1. Measurement of the doppler shifted  $H_{\beta}$  intensity was performed by two instruments. The tilting filter spectrophotometer\* required one minute for each scan of the spectrum and had a  $2.5^{\circ}$  field of view. It was held fixed at the point where the rocket would enter the  $\sim 100$  km altitude region on the up-leg portion of the flight.

A  $2^{\circ}$  field of view fixed filter photometer, centered at  $4861\text{\AA}$  with the half intensity width of  $24.7\text{\AA}$  was also employed. During the course of the flight this photometer was directed at three different positions, (a) the point at which the rocket passed the 100 km level on the upleg of the flight, (b) a point at the 100 km level below the apogee point, and (c) the point at which the rocket passed the 100 km level on the downleg. Intensity readings were obtained every 5 sec. Because of the spectral width of the filter, the measured intensities represented the sum of both  $H_{\beta}$  intensity and background.

2. Measurement of atmospheric emissions at  $5577\text{\AA}$  and  $3914\text{\AA}$  were performed with fixed filter photometers. These both had a  $2^{\circ}$  field of view and gave intensity data every 5 seconds. They were initially directed at the 100 km region on the upleg flight, then shifted to the 100 km region below apogee, and then to the 100 km region on the downward leg.

3. All-sky camera photographs, with 2 second exposures every 10 seconds were taken throughout the flight.

The temporal behavior of the ground based photometric measurements beginning one minute after launch are shown in Figs. 7A and B. The tilting filter  $H_{\beta}$  spectrophotometer indicated an  $H_{\beta}$  intensity between 5-8 R throughout the flight whereas the fixed filter photometer indicated an  $H_{\beta}$  intensity of 24 R early in the flight decreasing to values less than 10 R late in the flight.

---

\*The measurements were provided by Dr. F. Creutzberg of the National Research Council of Canada.

The  $\lambda 5577$  photometer indicated a peak intensity of 16.5 kR at 0604:10 decreasing to less than 1 kR late in the flight. The  $\lambda 3914$  intensity showed a time dependence similar to that of  $\lambda 5577$  with a peak intensity of  $\sim 3$  kR.

The all-sky camera pictures showed a breakup aurora in progress at launch. The form was brightest to the north of the rocket trajectory at the beginning of the flight. The form began to move southward and to fade as the rocket neared apogee. In the later half of the flight, the form had become very faint and had moved to the south of the rocket.

## B. Flight Experiments

The data, to be shown in this section for all the particle counting experiments, has been corrected for instrument efficiency, resolution, variable energy channel width, and geometrical factor but no other correction factors have been applied.

### 1. H<sup>0</sup> Energy Spectrometer

Ten second averages of the differential flux of neutral hydrogen in each of the five energy channels are shown in Fig. 8. Channels 1, 3, and 5 were lost at 0604:10 UT as a result of the telemetry failure. In general, during the period of full telemetry coverage, the flux showed an increase of about a factor of two during the first minute of data and then a rapid decrease of about equal magnitude. The peak rate of  $3.5 \times 10^8 \text{ cm}^{-2} \text{ sec}^{-1} \text{ str}^{-1} \text{ keV}^{-1}$  was reached in the lowest channel at 0604:05 UT. After the telemetry failure, there was an apparently larger increase in precipitated flux which peaked at 0604:45 UT; subsequently the neutral flux fell off to a low rate at 0605:30. There is no evidence for a peaked H<sup>0</sup> spectrum, nor did the relative counting rates in the channels show any significant variation indicative of a change in spectral shape.

### 2. Total Hydrogen Flux Detector

The flight record from this instrument is shown in Fig. 9 for the alternate operating modes,  $(\text{H}^0 + \text{H}^+ + \text{H}^-)$  and H<sup>0</sup>. Also shown are ten second averages of the ratio,  $\text{H}^0 / (\text{H}^0 + \text{H}^+ + \text{H}^-)$ . The main features of this data include (a) a counting rate, in both modes, which decreased steadily during the

time 0603:00 UT to 0604:10 UT after which it remained at a nearly constant rate for the remainder of the flight and (b) an initial  $H^0/H^0 + H^+ + H^-$  ratio of  $\sim 0.4$  which increased during the period of decreasing counting rate and stabilized near 0.9 once the nearly constant counting rates were observed.

### 3. Proton Energy Spectrometer

As described earlier, the observed proton counting rates were very low because of the small geometry factor necessary to insure that electrons did not saturate the instrument when it operated in the electron mode. Fig. 10 shows the observed ten second average differential proton flux in the five energy channels during the early portion of the flight. The general time behavior of the proton rate was similar to that observed by the neutral hydrogen energy spectrometer.

### 4. Electron Energy Spectrometer

Ten second averages of the electron energy spectrometer are shown in Fig. 11. The striking feature of these data is the changes in the shape of the spectrum. The spectrum was of a peaked nature during the entire time that data were available from all five channels. In the early part of the flight, Channel 2 showed a strong peak; at 0603:40 UT, the flux in Channel 2 (1.1 - 2.5 keV) decreased and Channel 3 (2.5 - 6 keV) showed the highest rates. By 0605:30, there was a strong indication that the spectrum had softened again. After 0606:30 the counting rates fell to a low value.

### 5. Vehicle Borne $H_\beta$ Intensity Measurements

Fig. 12 shows the time dependence of the  $H_\beta$  light intensity corrected to the zenith measured by the vehicle borne photometers. Background has been subtracted from these fluxes. The  $H_\beta$  intensity dropped from a measured value of  $\sim 103$  R to  $\sim 30$  R as the rocket rose through the light emitting region.

## 5. DC Electric Field Measurements ( $E_{\perp}$ )

The time record of the DC electric field measurement ( $E_{\perp}$ ) is shown in Fig. 13. The plotted voltage is the measured peak-to-peak voltage difference during each spin cycle between the two antennas which were separated by 40 cm. The  $v \times B/c$  induced voltage has not been subtracted from this record. The gap in the record corresponds to a period when the frequency of the output signals appeared to have doubled. Because of the wide dynamic range of the logarithmic output signal, the reading errors correspond to large errors in the field intensity. We attribute much of the fluctuation in field intensity to this reading error.

## 6. AC Electric Field Measurements

The outputs of the 2.3 kHz, 3.9 kHz, 7.35 kHz, and 30 kHz  $E_{\perp}$  channels and the 30 kHz  $E_{\parallel}$  in units of volts are shown in Fig. 14A, B, and C over the time period 3:00 - 3:56 UT. The other channels for both orientations were rather similar. In general, the  $E_{\parallel}$  showed a greater spin modulation than  $E_{\perp}$ ; the degree of modulation decreased with increasing channel frequency in both cases. Also the amplitude of the signals decreased with increasing altitude. Unfortunately the loss of the transmitter prevented measurements during the interesting time period during which particle precipitation ceased abruptly.

Fig. 15 shows selected portions of the  $E_{\perp}$  broadband (30 Hz - 1 kHz) channel; the  $E_{\parallel}$  output was rather similar. Intense bursts of low frequency ( $\sim 30$  Hz) oscillations were seen at all times. After entering the ionosphere at 0603:30 UT, these bursts repeated at the spin frequency. At 0604:00 UT they repeated at twice the spin frequency and at 0604:30 UT they showed signs of recurrence at four times the spin frequency; subsequently the repetition rate decreased to the spin frequency. Bursts of  $\sim 100$  Hz oscillations also occurred, but these only repeated at the spin frequency even during the time periods when the 30 Hz bursts repeated at multiples of the spin frequency. With the exception of these changes in the low frequency burst repetition rate, the patterns were extremely repetitive during the entire flight and showed little evidence of a randomness.

In the early portion of the flight where the data from the higher frequency channels was available, the occurrence of the low frequency bursts was correlated with the observed minima in the high frequency signals.

#### 6. Aspect Magnetometer

Fig. 16 shows the components  $B_{\perp}$  and  $B_{\parallel}$  as measured by the two flux-gate magnetometers and the computed total field  $B_T$ . Precession of the rocket with a period of  $\sim 4.9$  min and a cone angle of  $\sim 18^\circ$  is clearly shown. The rocket spin rate was 3.83 Hz at power turn on, decreased to 3.27 Hz at 0602:19 UT and to 0.69 Hz after de-spin and deployment.

### VII. DISCUSSION OF RESULTS

#### A. Hydrogen Energy Spectra and Flux

The magnitude and energy spectrum of the total energetic hydrogen flux ( $H^0 + H^+ + H^-$ ) can be derived from either the proton or the neutral atom spectra. We assume that energetic neutral atoms do not exist at the top of the atmosphere and thus that the derived total hydrogen flux measured at low altitudes corresponds to the total precipitated proton flux at the top of the atmosphere. Because complete spectra were obtained only early in the flight for altitudes  $< 180$  km because of the telemetry failure, we have assumed that the equilibrium fractions  $F_{1\infty}$  and  $F_{0\infty}$  tabulated by Allison<sup>(9)</sup> for protons passing through nitrogen gas are applicable to these measurements. Unfortunately this tabulation does not extend to energies  $< 4$  keV. Therefore, we have extrapolated the higher energy data for  $F_{1\infty}$  and  $F_{0\infty}$  as shown in Fig. 17.

Fig. 18 shows one representation of a 10 second average energy spectrum of total energetic hydrogen incident at the top of the atmosphere as derived from the neutral energy spectrometer. As can be seen, the spectrum fits well to a power law ( $E^{-n}$ ) dependence with  $n = 3.2$ . In conformity with other presentations, Fig. 19 shows the spectrum plotted for an exponential dependence showing an e-fold energy of  $\sim 1$  keV and a maximum differential flux of  $\sim 5 \times 10^8 \text{ cm}^{-2} \text{ sec}^{-1} \text{ str}^{-1} \text{ keV}^{-1}$ . Also shown in Fig. 19 is the total hydro-

gen spectrum derived from the proton measurements. Because of the errors in the proton measurements, poor statistical accuracy, spurious counts, and erratic sampling time, we do not believe that these two derived spectra are in significant disagreement. On the other hand, it is clear that the errors in the proton experiment are far too large to justify any further physical conclusions. However, the following problems could have been studied by comparing protons and neutrals if the proton counting rates had been more reliable: (1) the existence of charge-exchange equilibrium conditions including the possibility of a transition to non-equilibrium conditions at altitudes  $>200$  Km, (2) the adequacy of the extrapolation of Allison's tabulation of equilibrium fractions and charge-exchange and stripping cross-sections to low energies, (3) possible differences in the charge-exchange and stripping cross-sections between atomic oxygen and molecular nitrogen, and (4) the possible existence of a significant (10 mV/m) electric field parallel to the earth's magnetic field.

For the present, we will employ the energetic neutral hydrogen data for the determination of the total energetic hydrogen flux and energy spectrum because of the smaller errors in the experimental data and the much smaller correction factor required to derive the total hydrogen flux from the measured neutral fraction.

Fig. 20A and B shows plots of the time dependence of the 10 second average maximum flux and e-fold energy of the energetic hydrogen at the top of the atmosphere for the time period prior to the telemetry failure. Changes in flux and e-fold energy of greater than  $\pm 20\%$  are significant. As can be seen, the spectral shape showed very little variation during this period and the fluxes were high,  $\sim 5 \times 10^8 \text{ cm}^{-2} \text{ sec}^{-1} \text{ str}^{-1} \text{ keV}^{-1}$ . After loss of the transmitter, the observed rates in Channels 2 and 4 indicated little change in the shape of the spectrum until precipitation ceased at 0605:30 UT. This type of hydrogen precipitation was similar to that reported by Chase<sup>(10)</sup>, except that our fluxes were somewhat larger.

The observed spectra and fluxes were remarkably close to those one might expect to observe for a thermalized solar wind. Whalen, et al<sup>(11)</sup>, who



have reported hydrogen energy spectra measured during a proton aurora occurring earlier in the evening, found a 12 keV e-folding energy above 30 keV and a flux smaller than ours, i.e., a spectrum bearing little resemblance to a thermalized solar wind. While there is not yet a sufficient number of experimental observations, we feel it is worthwhile to speculate that (1) the hydrogen precipitation in proton auroras occurring before and after the breakup period is excited by a different mechanism from that which is operative during the breakup phase, (2) during the breakup phase thermalization of solar wind protons occurs, but, at best, only a minor fraction of these are energized, and (3) during the breakup phase, the auroral field lines are open to the thermalization region to the extent that direct precipitation of some of these thermalized particles is possible.

#### B. Electron Spectra

During the time period for which complete spectral information is available an electron energy spectrum peaked at low energy and a flux of  $\sim 10^8 \text{ cm}^{-2} \text{ sec}^{-1} \text{ str}^{-1} \text{ keV}$  were observed. Such a peaked spectrum is consistent with other observations by Evans<sup>(12)</sup> and by others<sup>(10, 13)</sup>. Fig. 21 shows two successive ten second average electron spectra; the peak position showed a shift from Channel 2 (1.1 - 2.5 keV) to Channel 3 (2.5 - 6 keV) between these two measurements. Before this shift, the peak was always in Channel 2 and subsequently it remained in Channel 3. After the telemetry failure, the observed rates in Channels 1 and 3 indicated that the peak remained in Channel 3 until 0605:30 UT when precipitation ceased.

During the time of less than ten seconds in which the peak energy of the electrons shifted, the rocket traveled only about 2 km in a direction perpendicular to the magnetic field lines. If one attempts to attribute this change in peak energy to an electric field perpendicular to the magnetic field<sup>(13)</sup>, one obtains a field of at least 1 volt/m; this value is much larger than reported values for  $E_{\perp}$ <sup>(14, 15)</sup> or the fields actually measured. Fields of this magnitude would also result in a very fast  $E \times B/B^2$  drift of auroral forms if applied at these altitudes. Such drifts were not indicated by the all-sky camera photographic data. It therefore seems unlikely to us that this shift in the peak energy of the electron spectrum can be explained in terms of a perpendicular electric field at rocket altitude.

### C. Cessation of Precipitation

Fig.22A shows the rapid decline of the 1.6 - 3.5 keV hydrogen flux during the period 0605 - 0607 UT. The all-sky photographs showed that this decline could have been associated with either a general cessation of auroral activity or a slow movement of the auroral form. Davidson<sup>(16)</sup> has calculated the expected spatial distribution of energetic hydrogen at altitudes below 250 km for two proton beams with different pitch angle distributions at the top of the atmosphere. The initial beam is significantly spread (over tens of kilometers) because the neutrals, produced as a result of charge exchange, are no longer constrained by the magnetic field. For this reason, very rapid spatial variations in precipitated hydrogen are not expected to be observed. However, as can be seen in Fig.22A, a decrease of about a factor of 4 in the proton flux occurred in a time period of less than 10 seconds. During this time, the total distance traversed by the rocket was approximately 10 km and the north-south distance was only about 2 km.

If this variation was spatial, then the pitch angle distribution of the precipitated protons must have been very sharply peaked near zero degrees. An alternative spatial explanation would require that the zone of proton precipitation was moving in the north-south direction at a speed of at least 1 km/sec. On the other hand, a rapid cut-off of precipitation extending over a minimum north-south distance of  $\sim 0.5$  km (proton cyclotron diameter at the top of the atmosphere) would be consistent with the observed results even if one assumes a nearly isotropic pitch angle distribution for the precipitated protons. Here again, any north-south movement of the precipitation zone would increase the rate of fall-off.

Two significant conclusions can therefore be derived from this observation. If the cause for the fast drop was only spatial, then the incident proton pitch angle distribution must have been sharply peaked near zero degrees. If the explanation is temporal, then the region from which the precipitated protons originated must have behaved coherently to shut off the precipitation. We again minimize the possibility of any north-south drift velocity of 1 km/sec because the all-sky camera pictures do not show it.

Fig. 22 B and C show the relationships between the 0.5 - 1 keV and 6 - 10 keV electrons during the period 0605:00 - 0606:20 UT. The counting rate in the 6-10 keV electron peak dropped abruptly at the same time the hydrogen fluxes decreased. This drop corresponded to a decrease of about an order of magnitude in the energy content in the precipitated electrons. About 5 sec earlier, the lowest energy electrons (0.5 - 1.2 keV) showed an increase in flux. Subsequent to the disappearance of the 6 - 10 keV electrons, the flux of low energy electrons began to oscillate with an  $\sim 10$  sec period and then abruptly decreased after about 45 seconds. For the remainder of the flight, the neutral hydrogen spectrometer and the electron-proton spectrometer did not show any significant increase in counting rates over these low levels.

We believe the described sequence of events indicates a close relationship between electron and proton precipitation. It is unlikely that entirely independent precipitation processes for each class of particles could result in the observed pattern.

#### D. Evidence for Rapid Fluctuations in Precipitation Rate

Fig. 23 shows a typical sample of the unreduced data recorded in two energy channels of the energetic neutral hydrogen spectrometer. The abscissa is time and the ordinate is the instantaneous voltage across the storage capacitor. In this case, each recorded event corresponded to a voltage increment of 50 mv or  $10^{-2}$  of full scale. The data indicate that the majority of recorded counts occurred in bursts of 2-7 counts in a time  $\leq 4$  m/sec. This differed considerably from the aforementioned bursts of counts that appeared in the electron-proton spectrometer. In that case the count burst appeared only occasionally and each burst consisted of a larger number of counts. Telemetry filtering limits the rise time of voltage pulses to  $\sim 4$  m/sec, so that this rise time only represents a lower limit to the arrival rate of the events. A statistical analysis on segments of the data indicated only a 0.05 significance on an  $\chi^2$  test; we conclude that the recorded precipitation rate was not random in nature.

The bursts never appeared simultaneously in all channels; this is the strongest argument against their production by either electronic noise or voltage breakdown. Obviously, multiple pulsing by the discriminator on almost every

event could account for the observed pattern. However, great care was taken in the circuit design and in the laboratory test phase to eliminate such multiple pulsing of the discriminator. The resolving time of the channeltron-discriminator arrangement was  $\sim 2 \mu\text{sec}$ ; thus only multiple pulsing of the channeltron itself, as a result of ion feedback effects, could result in multiple counts. This was not observed in the laboratory tests and we see little reason for its occurrence during the flight.

The time required for a complete energy scan was 10 msec; the channel "on" times ranged from  $\sim 0.6$  msec to  $\sim 3$  msec. The facts that simultaneous bursts were not observed in the channels and that a burst duration was less than 10 msec lead to several possible conclusions: (1) The hydrogen precipitation occurs in a series of bursts, of variable energy, each relatively monoenergetic and with a duration  $< 10$  msec. The long time averaging ( $> 1$  sec) employed for statistical reasons would obscure any monoenergetic features. (2) The precipitation occurred in bursts with a broad energy spectrum but with a duration less than the "on" time of any given channel (0.6 - 3 msec). Such a pattern would predict the source to be located only a few Km from the observation location, an unreasonable result. (3) The precipitation occurred in bursts with a broad energy spectrum from a source located sufficiently remote from the rocket that the transit time spread significantly exceeded the time between bursts.

#### E. Energy Balance

The time dependence of the energy flux precipitated by both total energetic hydrogen and by electrons is shown in Fig. 24 for the time period during which full spectral data was recorded. These were calculated by numerical integration of the differential flux curves for each class of particles. The precipitation was assumed to be isotropic. In general, the methods used were somewhat inaccurate and we estimate the error to be  $\pm 50\%$ .

One can also derive a rough estimate of the total energy precipitation from the observed intensity of the  $\text{N}_2^+$  ( $\lambda 3914\text{\AA}$ ) emission using the technique outlined by Chamberlain<sup>(6)</sup>. For the above described time period, this

estimate yields  $\sim 10$  ergs/cm<sup>2</sup> sec. This is in very good agreement with the precipitated energy flux derived from the particle measurements when one considers the assumptions that must be made in the calculation. Some of these assumptions were (1) the energy required per ion pair was 30 ev, (2) the fraction of 3914Å photons per ionization was 2%, and (3) differences in the ionization and excitation efficiencies between H<sup>0</sup>, H<sup>+</sup>, and electrons in the 1 keV energy range were neglected. Lastly the ground based photometer was not pointed at the exact spot where the particle measurements were obtained, which introduces further errors.

Other rocket and satellite flights have indicated that precipitated protons usually carry  $\leq 0.1$  of the total precipitated energy during a breakup aurora<sup>(6, 7, 17)</sup>. The larger fraction observed in this flight may be due to the fact that this flight was near the edge of the auroral form. As shown previously, if protons and electrons enter the atmosphere at the same point, then the protons will deposit their energy over a much larger area because of the spreading associated with charge exchange. Thus, if the precipitated energy in both beams were equal, one would observe maximum density of energy deposition produced by the electron beam near the center of the form but the ratio H/e would increase to greater than unity as one moved outward.

#### F. H<sup>0</sup> Total Hydrogen Flux Detector

There are several reasons why the results of the total hydrogen flux experiment must be questioned. These include

- a. There appears to be no temporal correlation in the fluxes observed with this instrument and those observed with the H<sup>0</sup> energy spectrometer and the proton spectrometer.
- b. The total hydrogen flux, as measured by this instrument, is about a factor of 100 lower than that indicated by both the H<sup>0</sup> energy spectrometer and the proton spectrometer.
- c. The ratio,  $H^0/H^0 + H^+ + H^-$ , shown in Fig. 10 increases smoothly from 0.4 at  $\sim 120$  km to 0.9 at 200 km. However, ratios less than  $\sim 0.9$ <sup>(9)</sup> should only be observed at altitudes sufficiently high

that equilibrium conditions no longer prevail. It is questionable whether such non-equilibrium conditions were achieved even at apogee and therefore it is expected that the ratio,  $H^0/H^+ + H^- + H^0$ , should probably have been altitude independent but definitely not directly dependent on altitude.

We have speculated about reasons for these observed inconsistencies without arriving at any specific conclusion. However, the following statements about the experiment appear to be valid:

1. The observed low counting rates would be consistent with loss of the foil during launch. However, even with the foil completely absent, some scattering should occur for particles incident on the supporting grid. The  $H^0/H^+ + H^- + H^0$  ratio should be independent of the presence of the foil since the measured ratio should only be dependent on the application and removal of the charged particle deflection voltage.
2. The counting rate patterns in both operating modes appear extremely steady and regular throughout the entire flight. They show none of the irregularities and burst patterns which are typical of spurious counts caused by high voltage breakdown.
3. Precautions were taken to enclose the channeltron to prevent counting of the ambient ionosphere. In addition, the 30 volt negative potential applied to the channeltron entrance surface should have precluded the counting of ambient electrons, but should also have been insufficient to accelerate ambient ions to the point where they could be detected efficiently. Also, it is not apparent how the application of the deflection plate voltage could modify any ambient ionosphere which might have reached the channeltron in a manner to yield the observed ratios.
4. As described in the appended reprint<sup>(2)</sup>, the instrument has some UV response and counts could be generated by auroral UV (at lower altitudes) or possibly sunlight (at the higher altitudes). However, such counts would be independent of the deflection plate voltage and are therefore considered unimportant as a source of counts.

5. The observed change in the  $H^0/H^+ + H^- + H^0$  ratio could be accounted for by a gradual softening in the precipitated proton energy spectrum since the ratio decreases with increasing energy. No evidence for such a change in the proton energy spectrum can be derived from either the  $H^0$  or proton spectrometer data, but in both cases the maximum measured energy was limited to 20 keV.
6. The time dependence of the observed ratio could be indicative of an outgassing process. However, it is difficult to conceive of any situation where the pressure in the deflection system could be high enough ( $10^{-3}$  mm Hg) so that the incident particles could either undergo significant scattering or stripping without the presence of comparable or greater pressures in the region near the channeltron. Since our data indicates channeltron breakdown occurs at  $\sim 10^{-4}$  mm Hg, the lack of evidence for HV breakdown indicates that outgassing should not have played a significant role in the type of behavior seen by this instrument.

#### G. Doppler Shifted Hydrogen Balmer Line Emission

The photometer unit was calibrated against a blackbody source at 1000°K; the following results are given in absolute terms based on this configuration. Above 220 km, the rocket probably began to see sunlight since both phototubes showed output currents greater than 1  $\mu$ amp for a several minute period. The  $H_\beta$  intensity during the downleg portion of the flight shows little structure and was consistent with the absence of particle precipitation.

Fig. 12 has shown the measured intensity, corrected to the zenith by a simple cosine factor, of doppler shifted  $H_\beta$  emission as a function of time. The derived volume emission rate, photons/cm<sup>3</sup> sec, is shown in Fig. 25. A strong peak is observed in the region between 120-135 km, but clearly the emission was spread over a larger altitude range, and, in fact, the emission never reached background. The peaks seen at 165 km and 145 km were well correlated with observed increases in the precipitated hydrogen flux; this demonstrates the difficulties in performing an accurate altitude profile measure-

ment during a breakup aurora. It is assumed that the peak at 102 km also was correlated with particle flux increases. The relatively high altitude of the main peak was consistent with the observed soft hydrogen energy spectrum and would be totally inconsistent with electron produced background emission. The observed flattening of the hydrogen spectrum at higher energies could account for the slow fall off in the emission rate observed at altitudes below 120 km.

Throughout the period of observation, it is reasonable to assume that the precipitated hydrogen flux was  $\sim 6 \times 10^9/\text{cm}^2 \text{ sec}$ . Therefore at the peak of the volume emission, the emission rate was  $\sim 4 \times 10^{-9}$  photons/proton cm. This value is extremely close to the value of  $3.8 \times 10^{-9}$  H photons/proton cm obtained from Fig. 9B of Eather and Burrows<sup>(18)</sup> for the  $n = 3$  curve with reductions in flux by a factor of 2 (for reasons given in Eather's review<sup>(7)</sup>) and by a factor of 6 to take into account the  $H\alpha/H\beta$  ratio. The present emission rate curve falls off faster with increasing altitude above the peak than theoretically predicted for isotropic particle fluxes. This may indicate a particle pitch angle distribution more highly peaked in the forward direction. Another possible reason for the rapid fall off with altitude and somewhat lower peak position than theoretically predicted<sup>(18)</sup> is that the atmosphere above Ft. Churchill was probably somewhat colder than the atmosphere they assumed in their treatment.

At present, there does not appear to be any obvious physical explanation for the discrepancy in the  $H\beta$  intensity derived from the vehicle borne photometer together with the particle measurements and that derived from ground based tilting filter photometer. It is possible that the absolute flux calibration of the instruments were incorrect. At this time we are still considering this discrepancy.

#### H. AC Electric Field Measurement

With the exception of the broadband (30 Hz - 1 kHz)  $E_z$  channel, all data from the AC electric field experiment was terminated after 0604:30 UT because of the telemetry failure. This broadband data appeared to be dominated by the large amplitude (10 mV/m) bursts of 30 Hz and 150 Hz signals



which repeated primarily at the spin frequency or at times in multiples thereof. These low frequency bursts appeared at the same times on the  $E_{||}$  channel during its period of operation. The great regularity in the onset pattern, duration, and cessation of successive bursts would appear to preclude any natural source for the occurrence of these bursts.

Fig. 26 is a sample frequency spectrogram of the broadband  $E_{\perp}$  data; the degree of blackening is inversely related to the intensity of the output signal. As can be seen the intensity decreased with increasing frequency; no definite low frequency cutoff was observed.

During the period when particle precipitation ceased, little change, if any, was observed in the broadband  $E_{\perp}$  pattern throughout its frequency range. Densitometer plots, at selected frequencies, of the spectrogram seem to indicate a pattern symmetrical in altitude about apogee with a minimum at apogee. No significant differences were observed between the upleg during which precipitation was present and during the downleg when precipitation was absent. It is very difficult, therefore, to associate the AC electric field amplitudes with the particle precipitation rate.

Both the  $E_{\perp}$  and  $E_{||}$  high frequency channel data showed an intensity modulation of about a factor of 10 at the spin frequency. For the 40 cm antenna separation the amplitudes ranged from a minimum of 10  $\mu$ volts to as high as 5 mV. Just as with the broadband data, the intensity decreased with increasing frequency and altitude. Any high frequency cutoff must have been at a frequency greater than 30 kHz, the highest frequency channel employed. For those channels which did not show strong spin modulation, the magnitude of the intensity appeared to be equal to the minimum magnitude in the modulated channels. During auroral flights, Mozer<sup>(19)</sup> has observed amplitudes similar to these minimum values but he observed a far smaller degree of spin modulation.

The large spin modulation and the general amplitude patterns are consistent with the data described by Shawhan and Gurnett<sup>(20)</sup> for a launch from Wallops Island. The precession modulation clearly seen in their flight was not obvious in our data. However, because our magnetometer data indicated a precession period on the order of 4.9 minutes for this flight, it is possible

that the observed slow decrease in intensity with increasing altitude might have been associated with this long precession period. Shawhan and Gurnett saw a correlation of the observed spin modulation with the alignment of the  $E_{\perp}$  and  $E_{\parallel}$  antennas to the geomagnetic field. In our experiment this was not the case. The orientation of the  $E_{\parallel}$  antenna was almost constant with respect to the field because the magnetometer data showed no indication of a large coning angle during a single spin period. Secondly, the degree of spin modulation was frequency dependent and was almost completely absent in some channels. We therefore conclude for our experiment that orientation with respect to the geomagnetic field alone cannot be significantly related to the degree of modulation.

The phase relationships between channels are shown in Fig. 27. As can be seen, the phase of the signals tended to drift and at times some channels appeared to be as much as  $180^{\circ}$  out of phase with each other. It is difficult to ascribe a specific phase relationship between the different channels.

Although the Shawhan and Gurnett measurements began only above 200 Km and were performed at temperate latitudes whereas the present measurements ranged only from 100 - 180 Km and were performed at auroral latitudes during a breakup aurora, very great similarities exist between the observations. This great similarity, together with the lack of any evidence for a changed broadband pattern at the time precipitation ceased, can lead only to the conclusion that the present measurements show no dependence on auroral activity.

As pointed out by Shawhan and Gurnett, their observations may be the result of the interaction of the vehicle with the environment. The great regularity in our E-field patterns supports such an interpretation. For example, any asymmetrical wake configuration could possibly result in the spin modulation; subsidiary wake configurations would be required to account for the multiple spin frequency observations. Also shadowing from particles, auroral light and even scattered sunlight by the rocket body might be of importance. On the other hand, Mozer<sup>(19)</sup> does not observe modulations of the

amplitude as great as seen in our data even in cases where the shadowing possibilities appear to be similar. Lastly, though we believe it unlikely, there is some possibility that significant portions of the rocket shell had insulating surfaces and that significant differences in the potential of these surfaces occurred during a spin cycle. These potential differences could significantly influence the local plasma parameters to give the observed results. It should be pointed out that the time structure of the particle deflection plate and analyzer sweep voltages bear no resemblance to the observed modulations. We therefore discount any possibility of rocket borne electric fields causing any of these observed E-field patterns.

#### I. DC Electric Field Measurements

The DC electric field ( $E_{\perp}$ ) data shown in Fig. 13 is the peak-to-peak voltage measured between the two antenna elements separated by 40 cm. In order to express the field strength in the more conventional dimensions of mv/m, it is necessary to increase the measured values by a factor of 1.25. Thus the minimum measured field strength was about 33 mv/m prior to apogee.

We have not, as yet, carried out a detailed point-by-point calculation of the induced  $v \times B/c$  electric field and consequently this field has not been subtracted from the measured value. However, we estimate the maximum measured total field ranged between 2 and 3 times the  $v \times B/c$  electric field. We therefore conclude that the ambient  $E_{\perp}$  ranged between 25 - 50 mv/m which is consistent with other observations (14,15).

There was some evidence for an increase in the measured field strength between 0606:00 - 0606:10 UT which includes the time interval during which local precipitation ceased. The subsequent decrease at 0607:30 UT was not accompanied by any measured increase in the measured particle flux. Therefore, we find it difficult to assign a specific relationship between the local rate of particle precipitation and the electric field strength. It should be noted that all-sky camera photographs indicated the presence of the aurora in the sky throughout the flight and there may therefore be little relationship between the electric field strength and the local precipitation rate.

As mentioned earlier, the gap in the record corresponds to the period when the output signals were not regular and well behaved. In general, this period coincided with that when the bursts of low frequency AC electric field signals at multiples of the spin rate were observed. If these low frequency bursts contained frequency components within the range of the spin frequency band pass filter, these could well distort the DC output signals.

In Fig. 28 the phase relationship between the DC  $E_{\perp}$  output and the  $B_{\perp}$  aspect magnetometer output is given for the entire flight. With the exception of a few points, the phase differences lay between 0 and  $-90^{\circ}$ ; at higher altitudes, the phase difference was predominantly near  $-90^{\circ}$ . There was no evidence for a  $180^{\circ}$  reversal in the E field direction throughout the flight. From the antenna orientation with respect to the rocket, we conclude that a measured phase shift of  $\pm 90^{\circ}$  indicated that the antenna was aligned parallel or anti-parallel to the  $B_{\perp}$  component of the geomagnetic field when maximum amplitudes were observed. Therefore we conclude that the electric field was predominantly North-South for the higher altitudes. From the available data, we cannot specifically identify the polarity of this North-South electric field.

At altitudes below 100 km, the magnitude of the DC  $E_{\perp}$  electric field increased rapidly with decreasing altitude. There are several possible explanations for this result which include

1. Below 100 km, the ionospheric electron density decreases very rapidly with decreasing altitude. Therefore our assumption of resistive coupling between the antenna and the plasma may no longer be valid with a consequent change in calibration. Secondly, the dimensions of the antenna sheaths will increase and assumptions based upon the presence of collisionless plasma sheaths will no longer be valid because of the increased atmospheric density. Therefore, the increased field strengths observed at lower altitudes may be entirely spurious.
2. If we assume  $E_{\parallel} = 0$ , the measured results imply that  $\nabla \times E \neq 0$ . The ground based magnetometer data does not give a sufficient  $dB/dt$

to account for these observations. However we have no data on the magnitude and configuration of localized ionospheric current systems which would satisfy Maxwell's equation.

3. A significant  $E_{||}$  electric field at altitudes below 100 km.

Because of its limitation to low altitudes, the effects of this large electric field are not considered to be of importance in particle accelerations or particle auroral phenomena. If the fields were real, they may have made significant modifications of the auroral electrojet current pattern.

### CONCLUSIONS

Although the report is entitled, "Final Report", data reduction and analysis are an almost endless process. We believe that further study of the data would permit more positive answers to some of the questions which have been raised in this report. However, in order to satisfy contractual obligations we have prepared this report of the current status of the data reduction and analysis phase of this program.

Many of the physical conclusions we have reached require further experimental and flight study. It is particularly important to determine whether the described breakup aurora was unique or common, and to study different auroral patterns with the described instrumentation to determine whether generalization of our conclusions is justifiable.

ACKNOWLEDGEMENTS

We wish to acknowledge the contributions of many individuals to the completion of this program. We include, at TRW: R. A. Alexander for the basic electronic design of the particle counting experiments, G. M. Crook and A. Belobradic for the design, fabrication and test of the electric field experiment, D. Blackwell and J. Black for their fabrication effort, E. Offer and W. Simpson who provided invaluable support through the entire program, Mrs. B. Benefield for her help in preparation of the final report, W. Slota, R. Brown, and H. Sanders for design and fabrication of the boom assembly, and G. W. McSherry for his assistance in contractual matters.

Most important support was provided by the NASA Sounding Branch personnel specifically, R. Shamaley, W. Conner, C. Cambell, J. Rast, J. Wood, L. Parker, H. Pedolsky, and J. Cameron and by the Canadian Rocket Range particularly F. Creutzberg.

Discussions with D. Evans, F. Mozer, D. Judge, F. Scarf, W. B. Thompson, I. Axford, and H. T. Mann were most useful during the course of the program.

LIST OF PUBLICATIONS SUPPORTED BY THIS PROGRAM

1. R. L. Wax and W. Bernstein, "Energy Independent Detector for Total Hydrogen Fluxes in the Range 1-10 keV for Space and Laboratory Applications", Review of Scientific Instruments, 11, 1612 (1967).
2. W. Bernstein, N. L. Sanders, R. L. Wax, "Technique for the Generation of Quasi-Isotropic 1-10 keV Proton Fluxes", Review of Scientific Instruments", 10, 1537 (1967).
3. R. M. Alexander, W. Bernstein, N. L. Sanders, and R. L. Wax, "An Instrument for the Measurement of Charged Particles in the Aurora", IEEE Transactions on Nuclear Science, NS-15, 1, 258 (1968).
4. W. Bernstein, R. L. Wax, G. T. Inouye, and N. L. Sanders, "An Energy Spectrometer for Energetic (1-20 keV) Neutral Hydrogen Atoms", COSPAR, Tokyo, 1968.
5. W. Bernstein, G. T. Inouye, N. L. Sanders, and R. L. Wax, "Measurement of Low Energy (1-20 keV) Protons and Neutral Hydrogen Atoms in A Breakup Aurora", to be presented at American Geophysical Union meeting in San Francisco, Dec. 1968.
6. R. L. Wax, W. Bernstein, N. L. Sanders, G. T. Inouye, "Comparison of Measured Total Hydrogen and Electron Fluxes and Spectra (1-20 keV) in a Breakup Aurora", to be presented at American Geophysical Union meeting in San Francisco, Dec. 1968.

## APPENDIX

Channeltron Studies

As part of the general supporting effort, we have carried out some laboratory measurements of channeltron properties in order to assess their adequacy as particle detectors and the requirements imposed on the associated electronics. These data have included (a) measurement of the dependence of output pulse height and pulse height distribution on applied voltage, (b) the dependence of output pulse height on counting rate, (c) magnetic field effects, and (d) operating pressure limitations. Because of the short life required in a rocket mission, we have not attempted any detailed life studies in this program. A simple and reliable technique for high voltage potting has been developed which does not appear to cause any observable deterioration in channeltron properties.

In all measurements, the channeltron was operated in a conventional RC coupled manner. Either a positive high voltage was applied to the anode or a negative high voltage to the cathode.

In Appendix Fig. 1 a series of integral bias curves are shown for various applied high voltages. In this case,  $\text{Sr}^{90}$   $\beta$  rays were used as the exciting source. Above 3200 volts, a relatively narrow pulse height distribution was observed; the output pulse amplitude continued to increase with increasing high voltage. Operation at 3600 volts was finally selected to obtain the maximum pulse height without major risk of breakdown or corona.

In Appendix Fig. 2 a series of integral bias curves are shown for different counting rates with 3600 volts as the applied high voltage. In this case, 2 keV electrons were used as the exciting source. From these data, a pulse height decrement of about a factor of 7 was observed as the counting rate was increased from  $3 \times 10^4/\text{sec}$  to  $2.6 \times 10^5/\text{sec}$ . At the selected discriminator operating bias of  $\sim 60$  mV one can operate reliably at counting rates as high as  $10^5/\text{sec}$  without significant changes in discriminator stability and noise. In general, we considered this counting rate range to be adequate and made no provision to prevent misinterpretation of the data at higher counting rates.



The need for a magnetic deflection system in close proximity to the channeltrons led to some measurements of the influence of such a field on channeltron properties. Qualitatively, a reduction in output pulse height was observed only above 100 gauss for fields perpendicular to the electron paths in the channeltron. There was some evidence for an increased pulse height between 60-100 gauss. Since the field at the channeltron in the flight configuration was less than 10 gauss, the channeltron should not have been affected by the fields.

In general, we have determined that channeltrons operate satisfactorily at ambient pressures below  $3 \times 10^{-4}$  mm Hg. There does not appear to be any significant dependence of the characteristics on pressure below this value. Breakdown occurs at higher pressures; in general recovery from the breakdown condition was fast and complete.

We have found that channeltrons respond quite well to the presence of an ion gauge in the vacuum system. It is not clear whether the response is to UV radiation or electrons leaking out of the gauge. However, it has been necessary to extinguish all ion gauges in order to obtain a meaningful background counting rate. In some instances, however, an ion gauge proves to be a useful exciting source and removes the necessity for installation of such a source in the vacuum system.

Because of space limitations we have used the 8 mm diameter aperture curled model channeltron almost exclusively. It has been necessary that these be potted in order to provide mechanical strength and to simplify mounting. These were potted in RTV-11 poured under vacuum. In only one case did the potting compound leak through the anode cap into the channeltron.

The vacuum system in which these tests were conducted was conventional in every respect. Two diffusion pumps were employed, one mercury and one oil; liquid nitrogen traps were associated with each pump. Provision for overnight pumping was not made; the system was cut off from the pumps each night and kept under vacuum without pumping. The system was also opened to air frequently for modifications in the apparatus. The best base pressure attained was  $\sim 10^{-6}$  mm Hg. No apparent degradation in channeltron characteristics was observed as a result of intermittent operation under these conditions.

## REFERENCES

1. W. Bernstein, R. L. Wax, G. T. Inouye, and N. L. Sanders, "An Energy Spectrometer for Energetic (1-20 keV) Neutral Hydrogen Atoms", presented at the COSPAR Meeting, Tokyo, Japan, 1968.
2. R. L. Wax and W. Bernstein, "Energy-Independent Detector for Total Hydrogen Fluxes in the Range 1-10 keV for Space and Laboratory Applications", Rev. Sci. Instr., 11, 1612-1615 (1967).
3. W. Bernstein, N. L. Sanders, and R. L. Wax, "Technique for the Generation of Quasi-Isotropic 1-10 keV Proton Fluxes", Rev. Sci. Instr., 10, 1537 (1967).
4. F. L. Scarf, G. M. Crook, and R. W. Fredricks, "Preliminary Report on Detection of Electrostatic Ion Waves in the Magnetosphere", J. Geophys. Res., 13, 3045 (1965).
5. F. S. Mozer, "Instrumentation for Measuring Electric Fields in Space", presented at the COSPAR Meeting, Tokyo, Japan, 1968.
6. J. W. Chamberlain, Physics of the Aurora and Airglow, Academic Press, New York, 1961.
7. R. H. Eather, "Auroral Proton Precipitation and Hydrogen Emission", Rev. of Geophysics, 5, 207-285 (1967).
8. R. H. Eather and F. Jacka, "Auroral Hydrogen Emission, Aust. J. Phys., 19, 241-274 (1966).
9. S. K. Allison, "Experimental Results on Charge Changing Collisions of Hydrogen and Helium Atoms and Ions at Kinetic Energies above 0.2 keV", Rev. Mod. Phys., 30, 1137-1168 (1958).
10. L. M. Chase, "Spectral Measurements of Auroral-Zone Particles", J. Geophys. Res., 73, 3469-3476 (1968).
11. B. A. Whalen, I. B. McDiarmid, and E. E. Budzinski, "Rocket Measurements in Proton Aurora", Can. J. Phys., 45, 3247-3255 (1967).
12. D. S. Evans, "A 10 cps Periodicity in the Precipitation of Auroral-Zone Electrons", J. Geophys. Res., 72, 4281-4291 (1967).
13. R. D. Albert, "Energy and Flux Variations of Nearly Monoenergetic Auroral Electrons", J. Geophys. Res., 72, 5811-5815 (1967).
14. F. S. Mozer and P. Bruston, "Electric Field Measurements in the Auroral Ionosphere", J. Geophys. Res., 72, 1109-1114 (1967).

## REFERENCES (Cont'd)

15. H. Foppl, et al, "Preliminary Results of Electric Field Measurements in the Auroral Zone", J. Geophys. Res., 73, 21-26 (1968).
16. G. T. Davidson, "Expected Spatial Distribution of Low Energy Protons Precipitated in the Auroral Zone", J. Geophys. Res., 70, 1061-1068, (1965).
17. C. E. McIlwain, "Direct Measurement of Particles Producing Visible Auroras", J. Geophys. Res., 65, 2727-2747 (1960).
18. R. H. Eather and K. M. Burrows, "Excitation and Ionization by Auroral Protons", Aust. J. Phys., 19, 302-322, (1966).
19. F. S. Mozer, private communication.
20. S. D. Shawhan and D. A. Gurnett, "VLF Electric and Magnetic Fields Observed with the Javelin 8.45 Sounding Rocket", J. Geophys. Res., 73, 5649-5664 (1968).

## FIGURE CAPTIONS

1. Schematic of the energetic neutral hydrogen energy spectrometer.
2. Block diagram of the electric field experiment showing the configuration for the measurement of  $E_{\perp}$  (AC),  $E_{\parallel}$  (AC), and  $E_{\parallel}$  (DC) electric fields.
3. Block diagram of the  $B_{\perp}$  and  $B_{\parallel}$  aspect magnetometer.
4. Block diagram of the vehicle borne  $H_{\beta}$  photometer experiment.
5. Block diagram of the search coil magnetometer experiment.
6. Schematic representation of the experimental payload in the rocket. The booms are shown in both the stowed and deployed positions.
- 7A. Temporal behavior of the 5577Å and 3914Å light intensity measured by the ground based photometers.
- 7B. Temporal behavior of the doppler shifted  $H_{\beta}$  light intensity measured by the ground based tilting filter and fixed filter photometers.
8. Temporal behavior of the energetic neutral hydrogen flux, averaged over 10 second intervals, measured in the 5 energy channels of the  $H^0$  spectrometer (not corrected to zero atmospheric depth).
9. Temporal behavior of the  $H^0$  flux and total hydrogen ( $H^0 + H^+ + H^-$ ) flux measured by the  $H^0$  total flux detector. Also shown is the ratio  $H^0/H^0 + H^+ + H^-$  averaged over 10 second intervals.
10. Temporal behavior of the proton flux, averaged over 10 second intervals, measured in the 5 energy channels of the proton spectrometer (not corrected to zero atmospheric depth).
11. Temporal behavior of the electron fluxes, averaged over 10 second intervals, measured in the 5 energy channels of the electron spectrometer.
12. Temporal behavior of the doppler shifted  $H_{\beta}$  light intensity measured by the vehicle borne photometer where the background has been subtracted.
13. Temporal behavior of the magnitude of the DC  $E_{\perp}$  electric potential developed across the antennas.

## FIGURE CAPTIONS (Cont'd)

- 14A. Temporal behavior of the AC  $E_{\perp}$  2.3 kHz and 7.35 kHz high frequency channels.
- 14B. Temporal behavior of the AC  $E_{\perp}$  3.9 kHz and 30 kHz high frequency channels.
- 14C. Temporal behavior of the AC  $E_{\parallel}$  30 kHz high frequency channel.
- 15. Output signals of the broad band (30 Hz - 1 kHz)  $E_{\perp}$  channel sampled at the following times: (a) 06:03:30, (b) 06:04:00 and (c) 06:04:30. In Fig. (A) the time between the large bursts is  $\sim 0.7$  seconds.
- 16. Aspect magnetometer data showing the measured magnitudes of  $B_{\perp}$  and  $B_{\parallel}$ , the computed total field,  $B_T$ , and the instantaneous value of the angle between the rocket spin axis and the geomagnetic field,  $\theta$ .
- 17. Extrapolation of the equilibrium fractions,  $F_{0\infty}$  and  $F_{+\infty}$  tabulated by Allison to low energies. The lowest energy for which his values are tabulated is 4 keV.
- 18. Power law presentation of the energy spectrum of the total hydrogen flux incident at the top of the atmosphere as derived from the  $H^0$  spectrometer data.
- 19. Comparison of the energy spectrum of the total hydrogen flux incident at the top of the atmosphere as derived from the  $H^0$  spectrometer with that derived from the proton spectrometer.
- 20A. Temporal behavior of the total hydrogen flux incident at the top of the atmosphere.
- 20B. Temporal behavior of the e-folding energy of the total hydrogen flux incident at the top of the atmosphere.
- 21. Successive electron energy spectra showing abrupt shift in the peak energy.
- 22. Observed patterns in the  $H^0$  and electron counting rates at the time of the abrupt cessation of precipitation.

## FIGURE CAPTIONS (Cont'd)

23. Samples of raw counting data from two  $H^0$  spectrometer channels. A single event is represented by an increment of  $10^{-2}$  times the full scale amplitude.
24. Temporal behavior of the rate of energy precipitation by electrons and energetic hydrogen.
25. Altitude profile of the volume emission rate of doppler shifted  $H_\beta$  photons.
26. Frequency spectrogram of the broadband (30 Hz - 1 kHz) AC  $E_\perp$  electric field data. The intense band at 1 Kc is instrumental.
27. Phase relationship of the spin modulated signals observed in several high frequency channels of the AC  $E_\perp$  and  $E_\parallel$  experiment.
28. Phase relationship between the  $E_\perp$  aspect magnetometer outputs and phase of the DC  $E_\perp$  electric field experiment.

## APPENDIX FIGURES

1. Integral bias curves showing the dependence of the channeltron output pulse height on applied high voltage.
2. Integral bias curves showing the dependence of the channeltron output pulse height on counting rate. The applied high voltage was 3600 volts.

TABLE I: Variation of Rocket Altitude with Flight Time

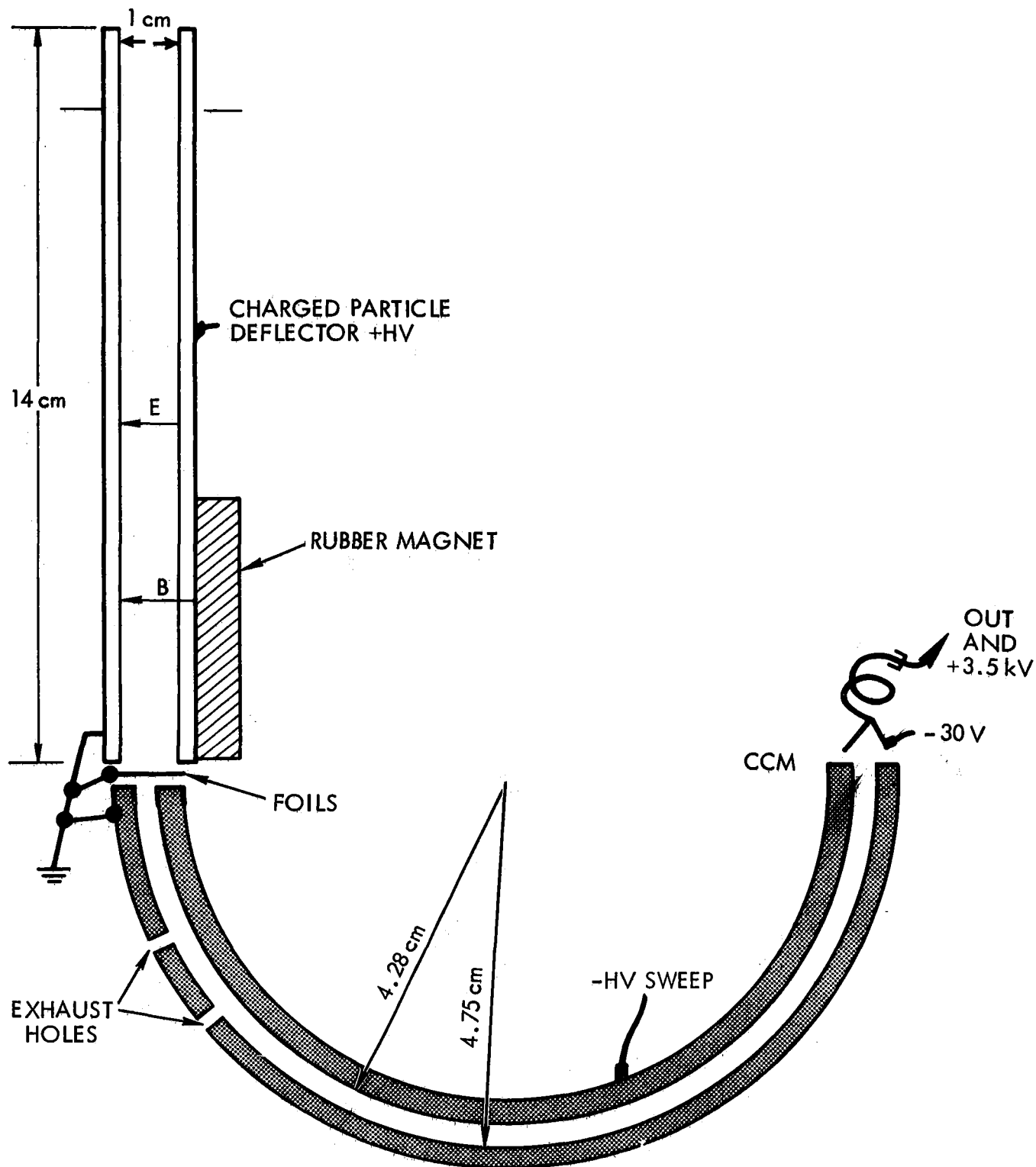


FIGURE 1

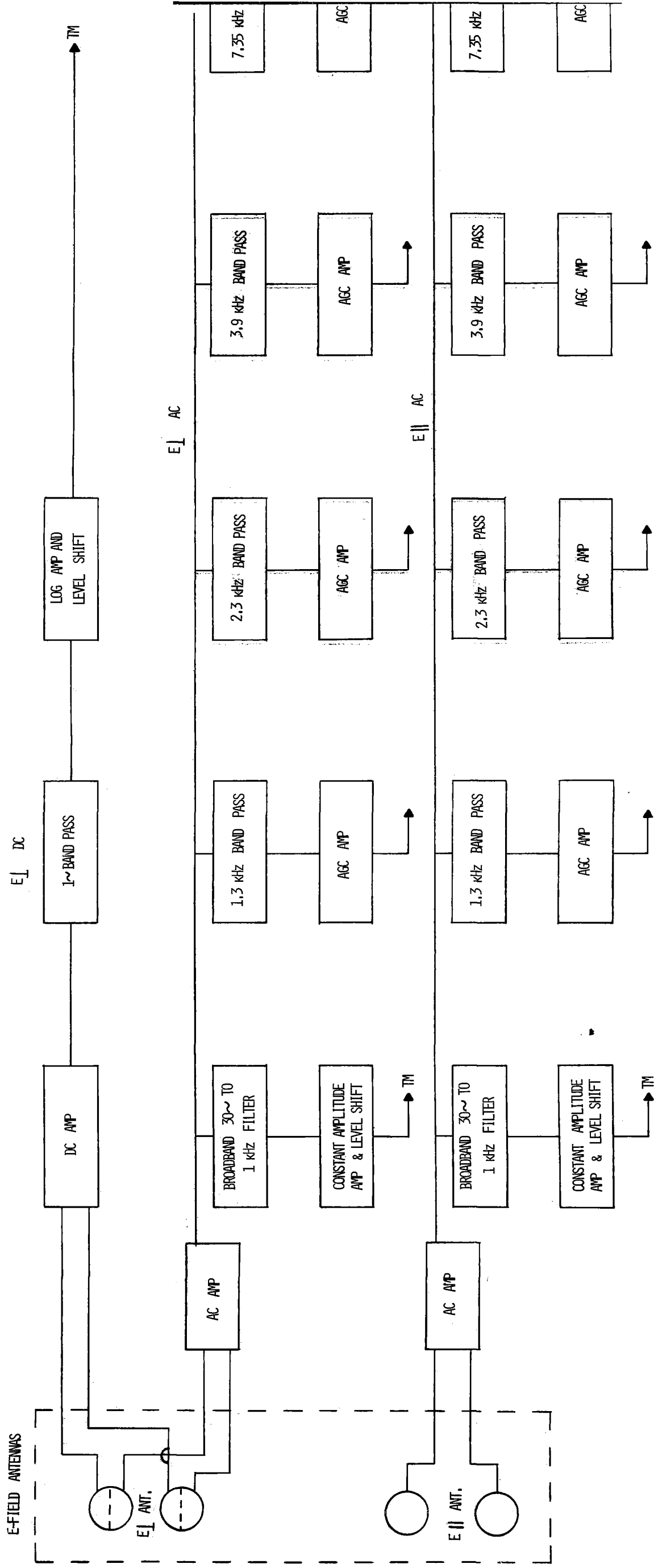
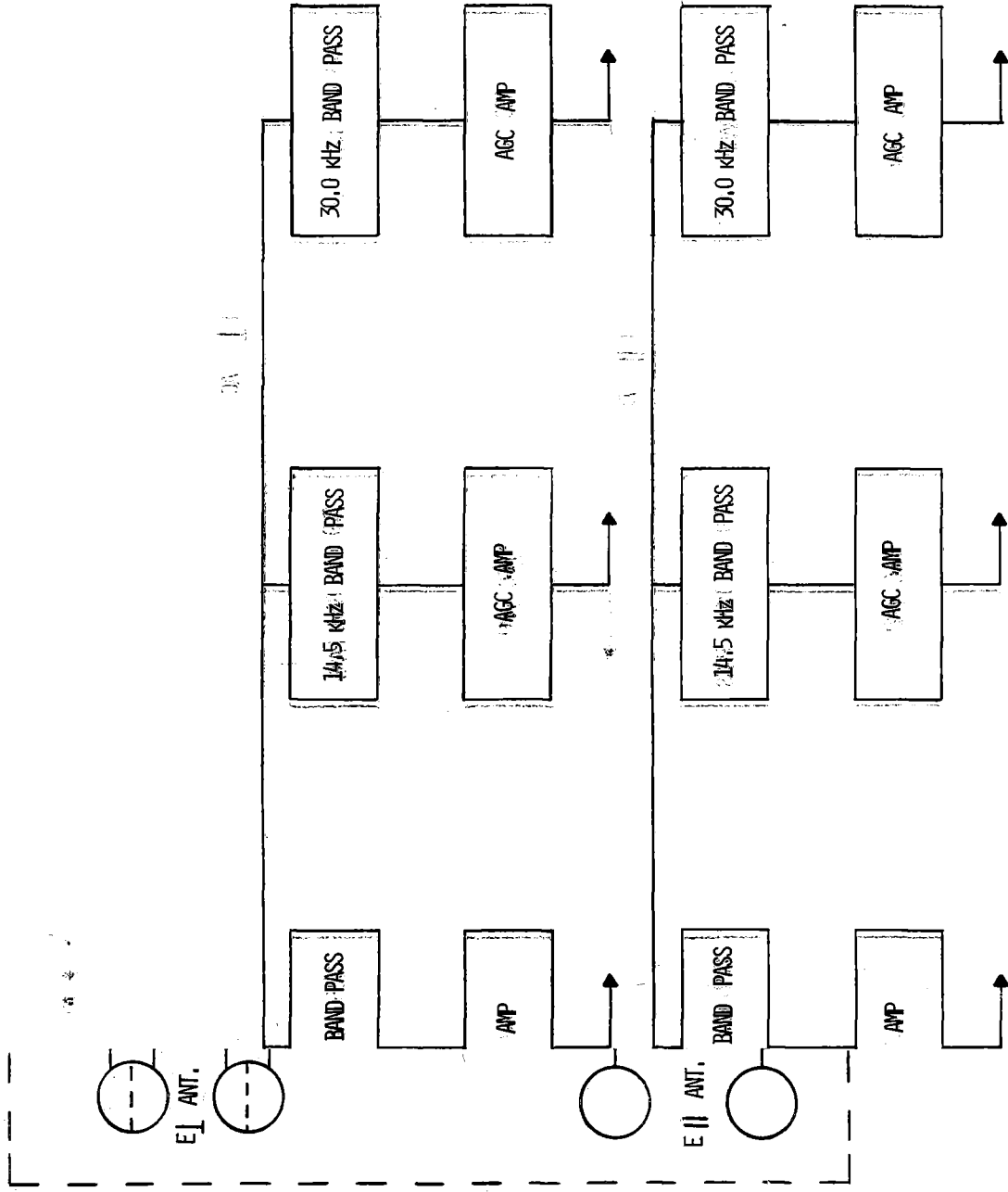


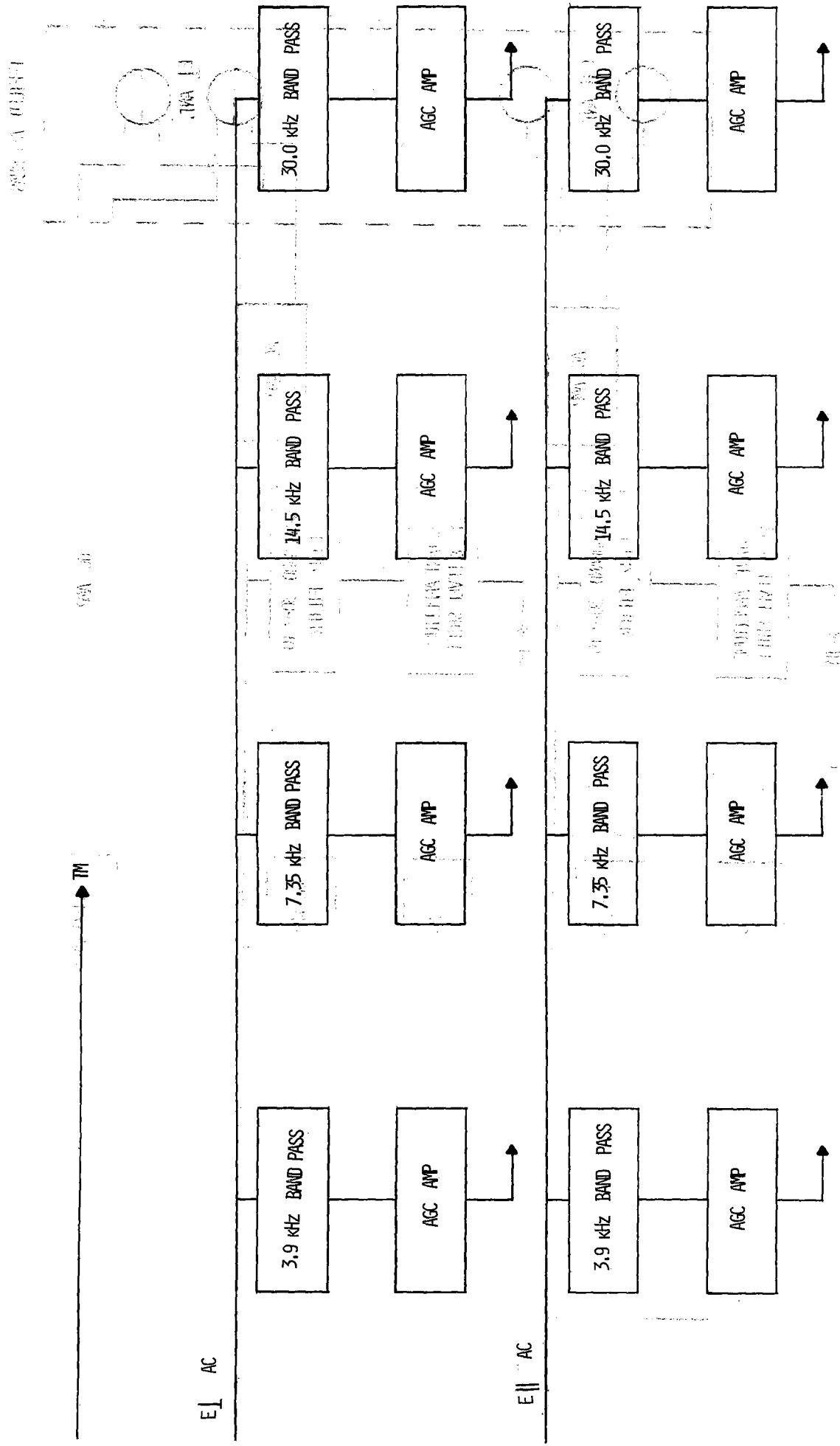
FIGURE 2



E-FIELD /



2



1 of 1

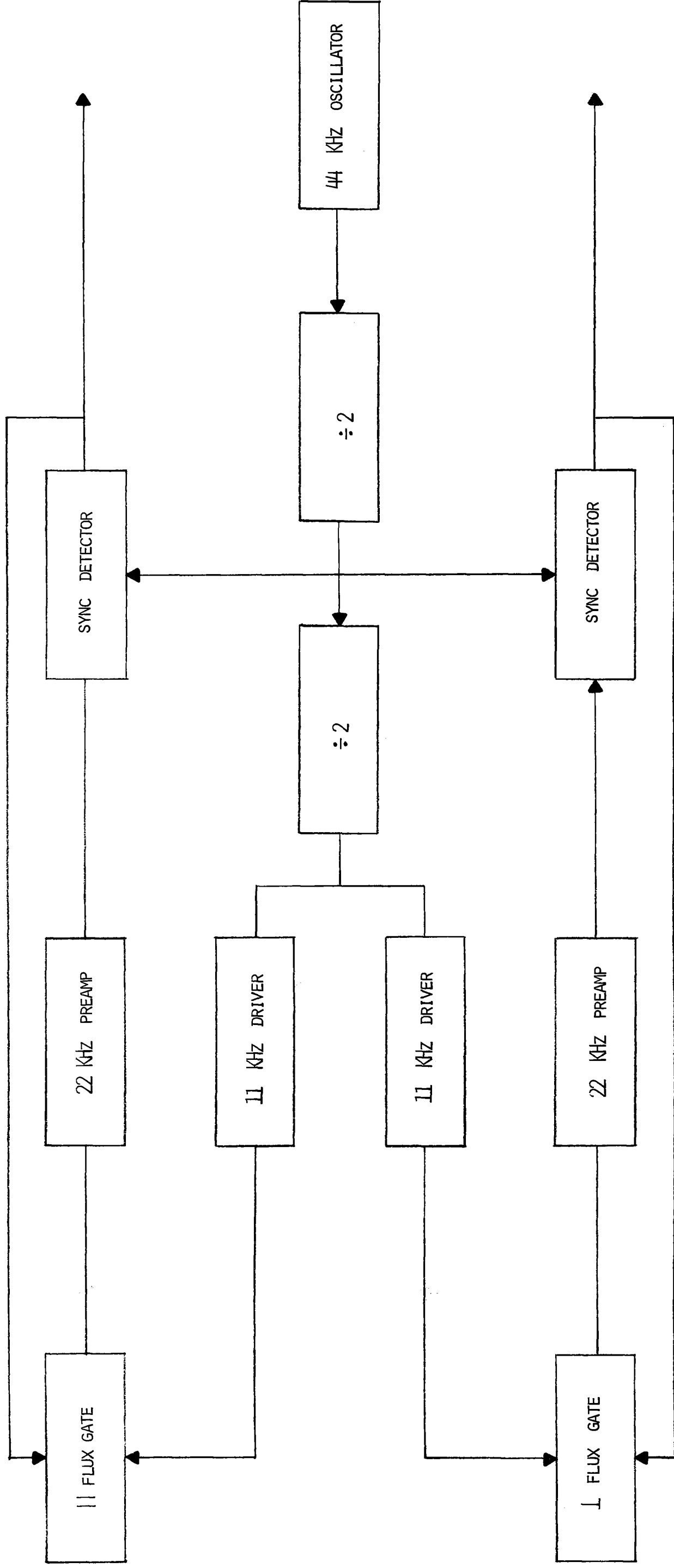


FIGURE 3

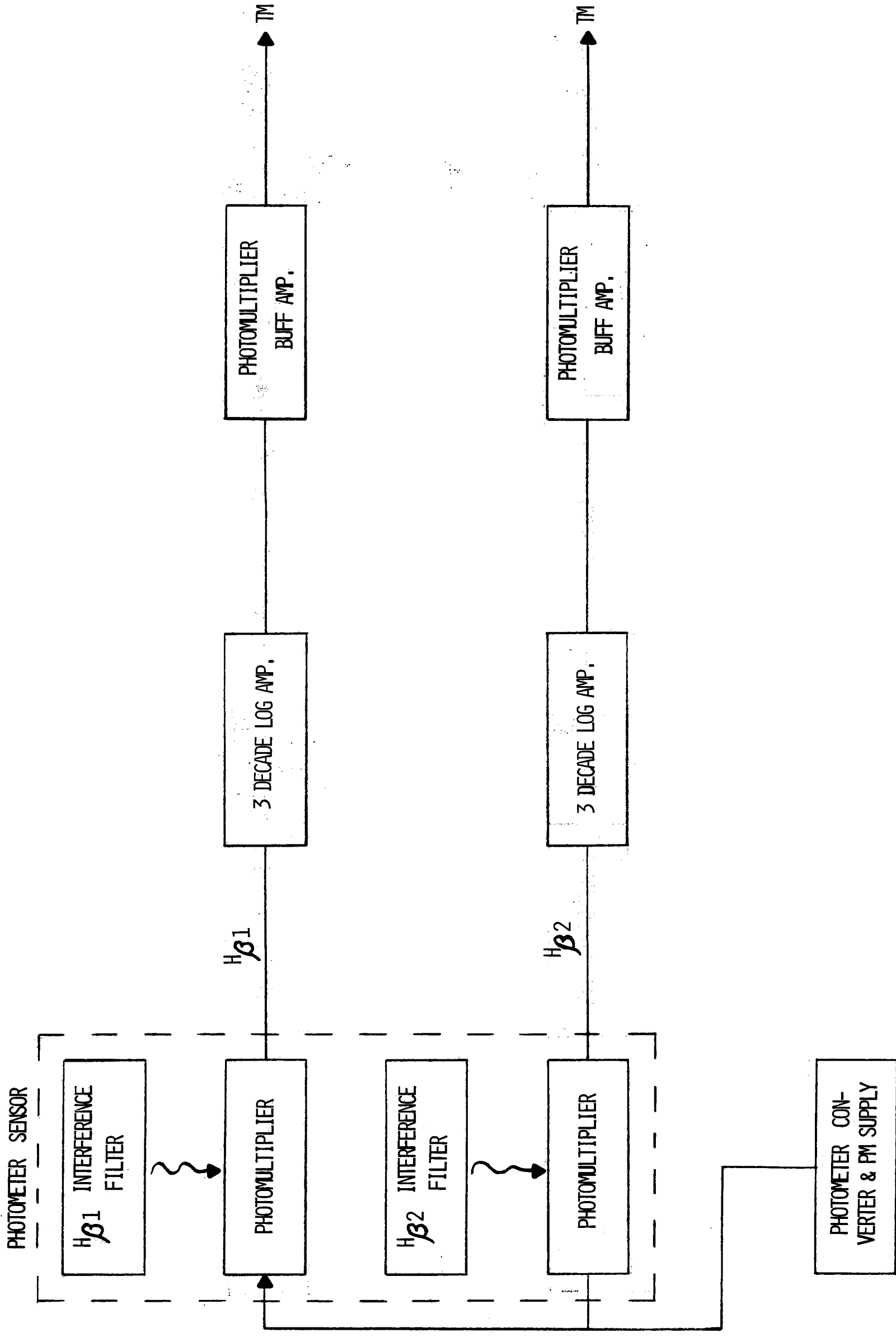


FIGURE 4

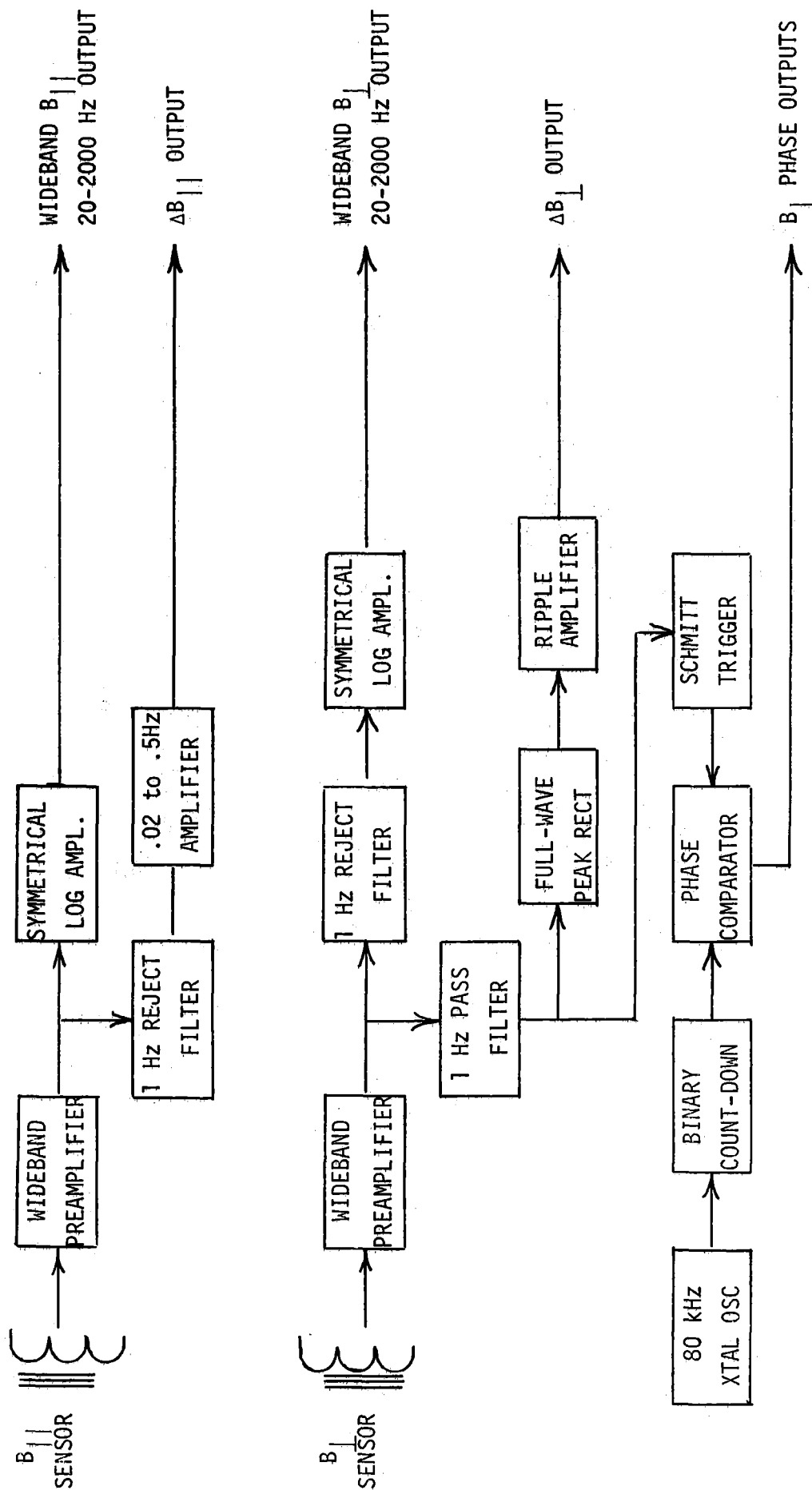


FIGURE 5

FIGURE 5

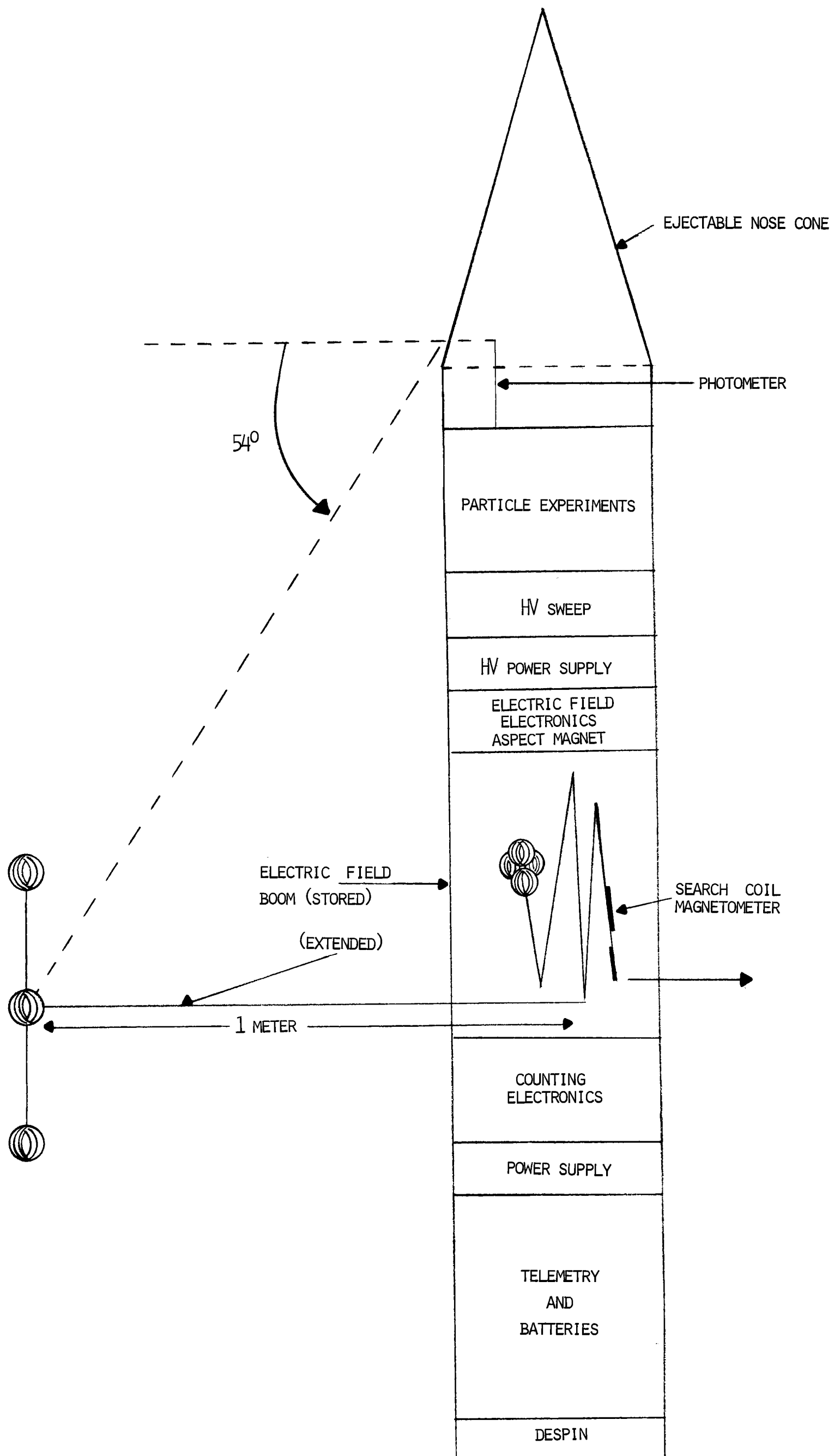


FIGURE 6

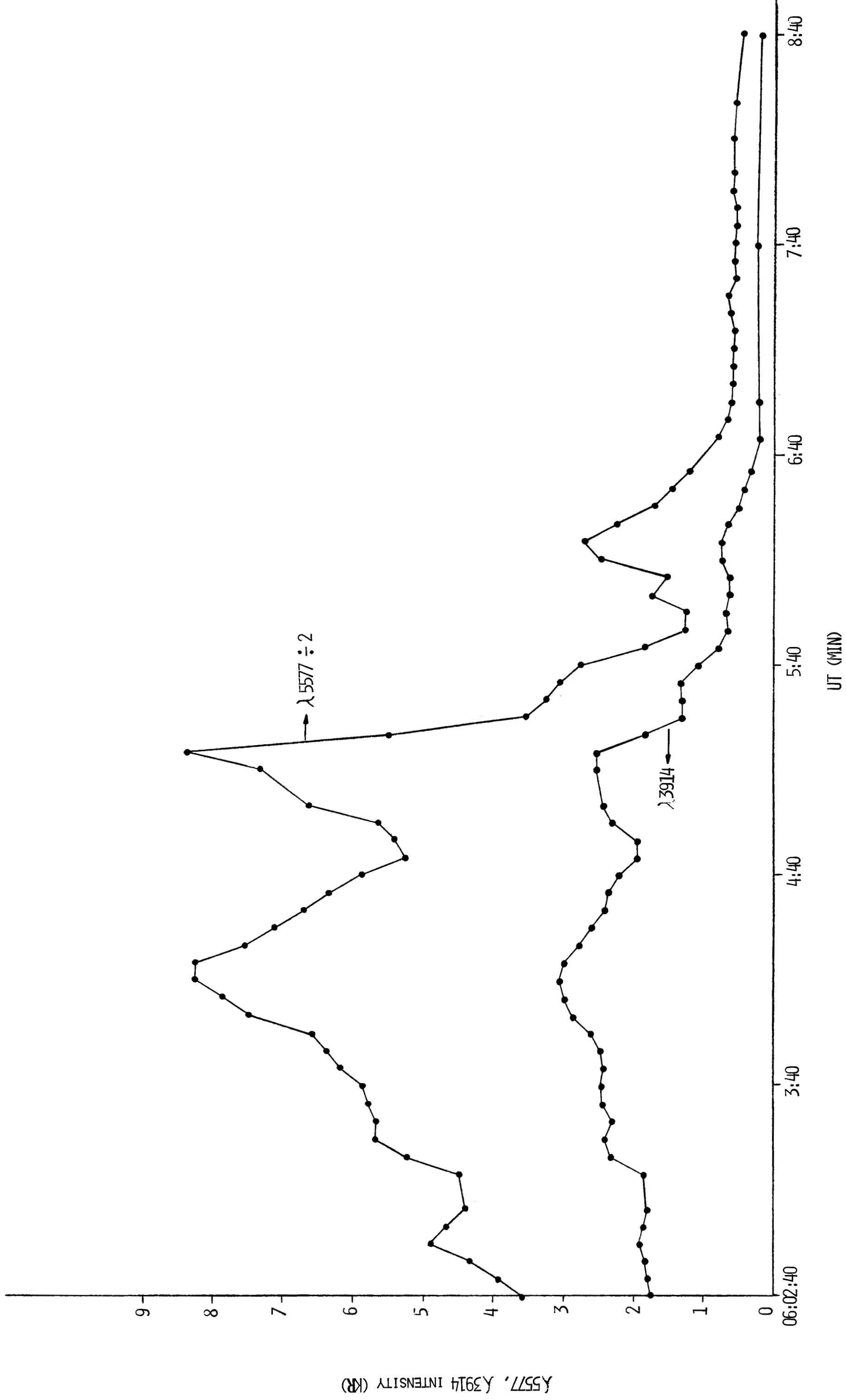


FIGURE 7A

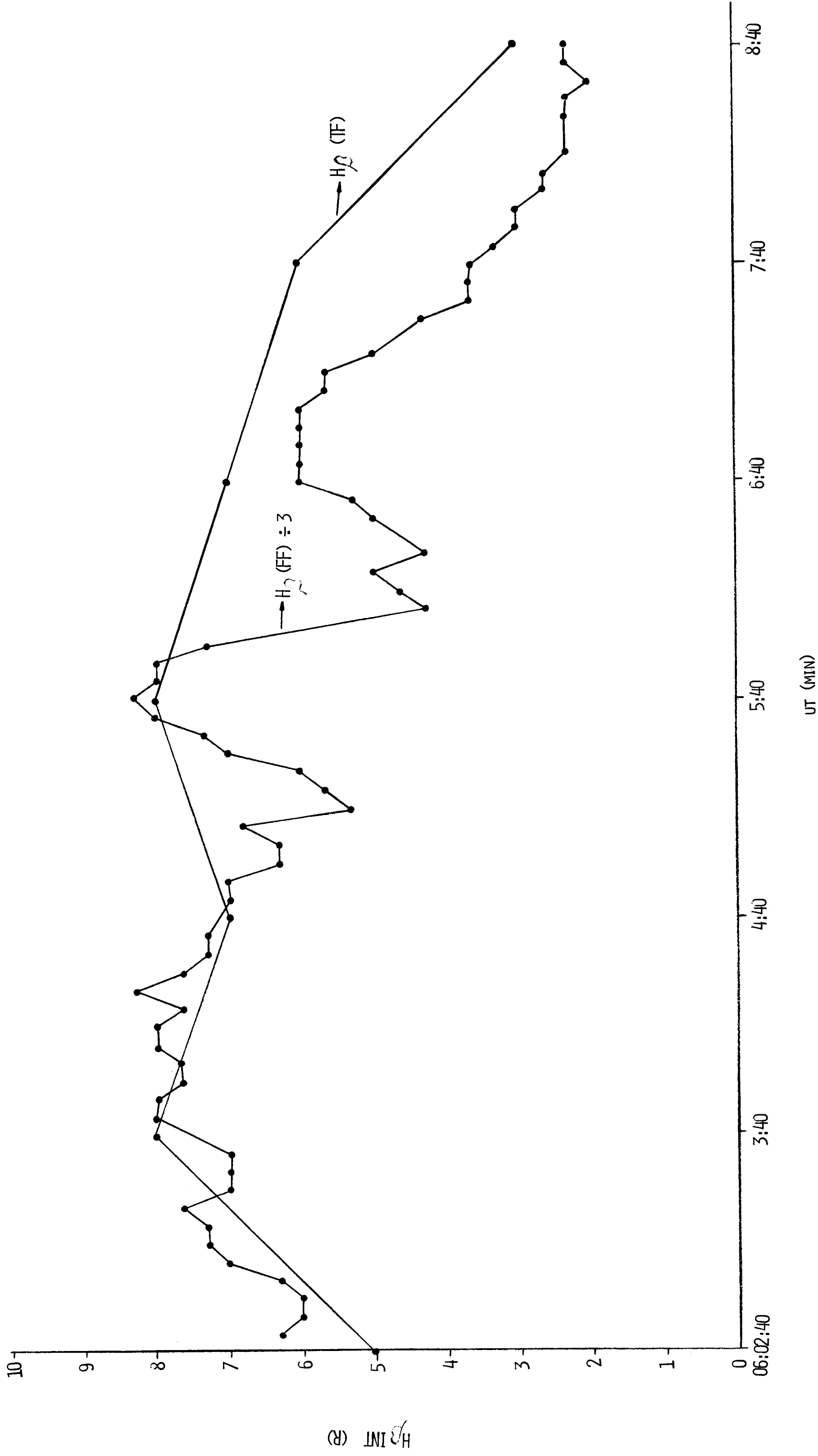


FIGURE 7B



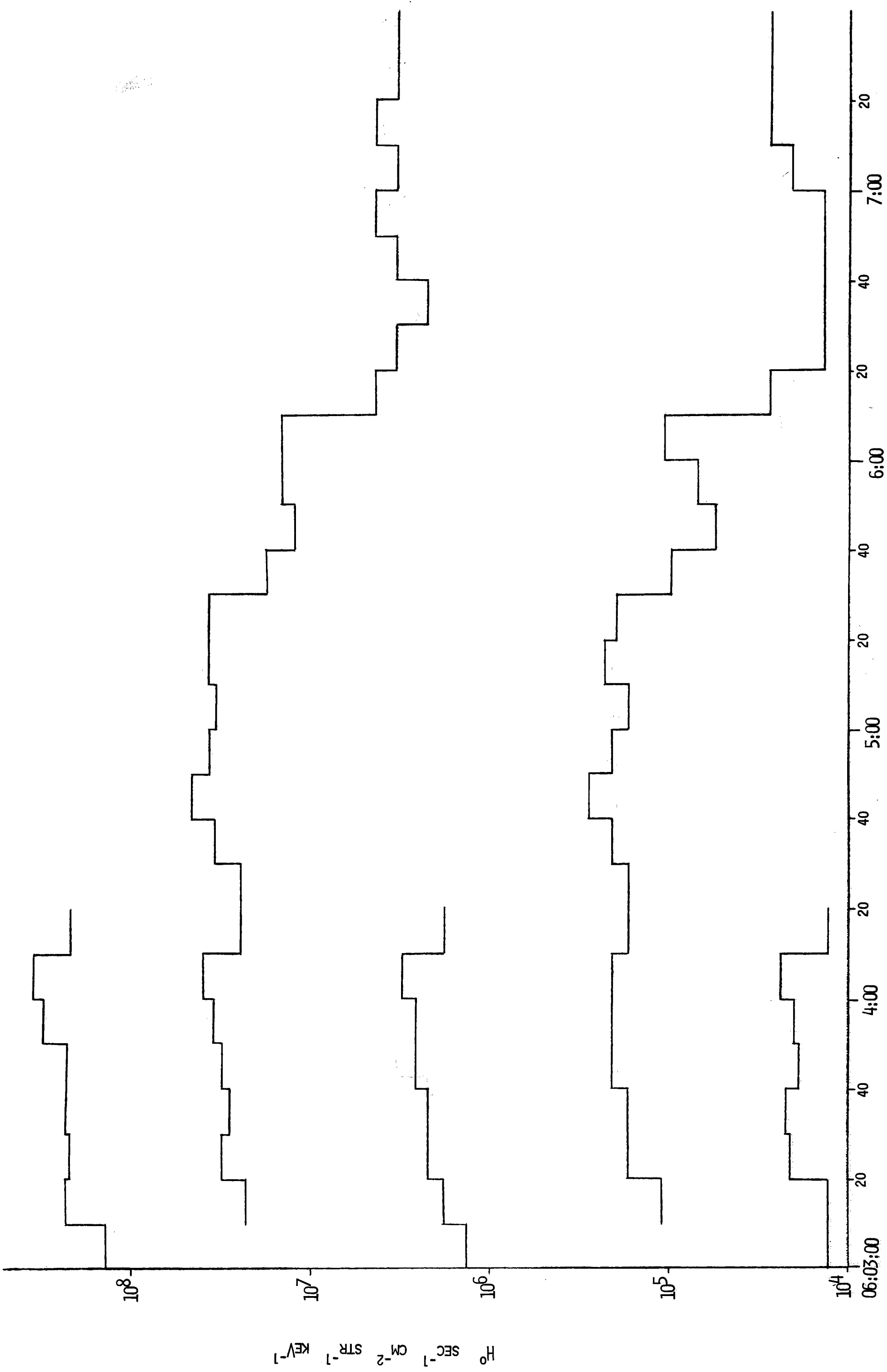


FIGURE 8

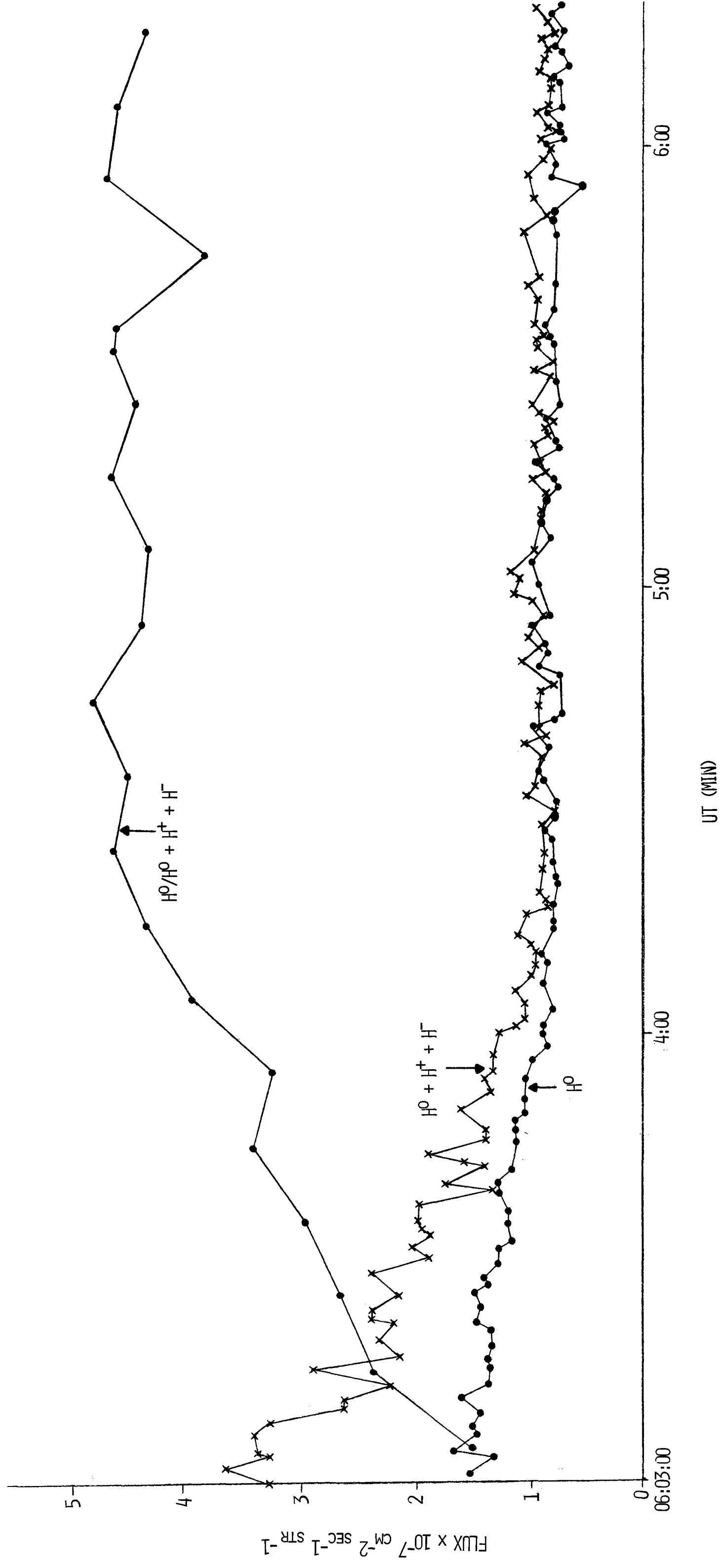


FIGURE 9

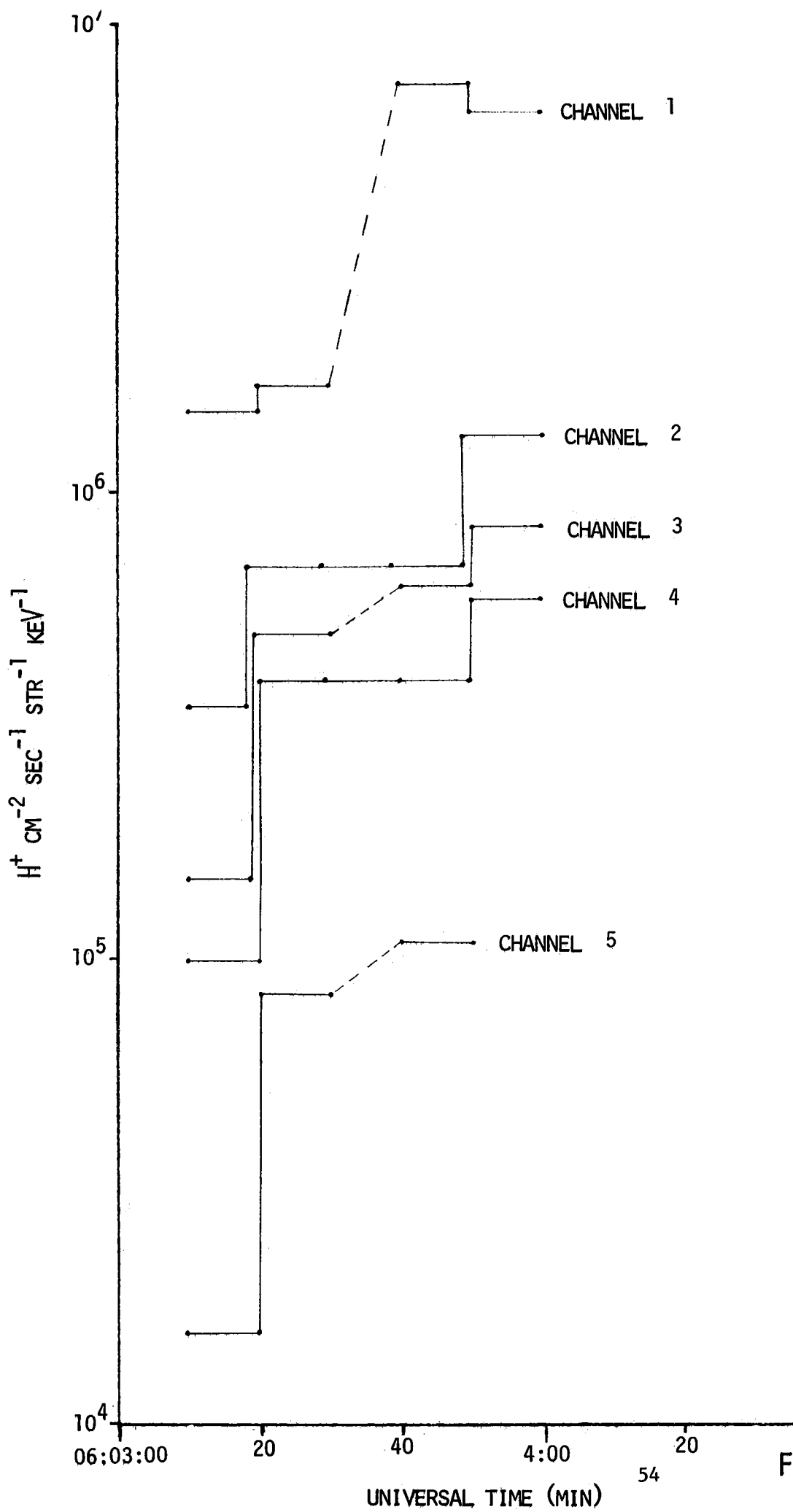


FIGURE 10

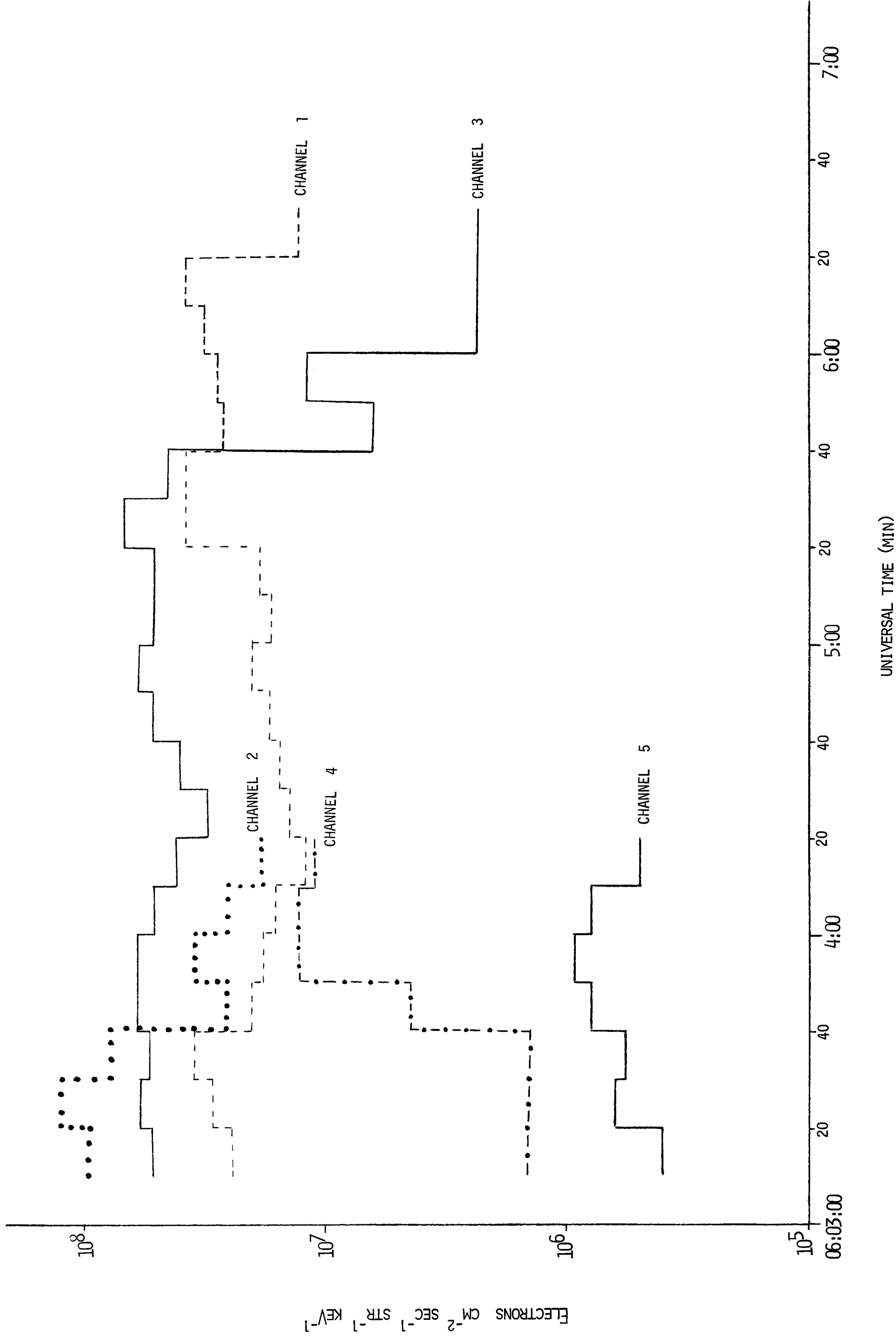
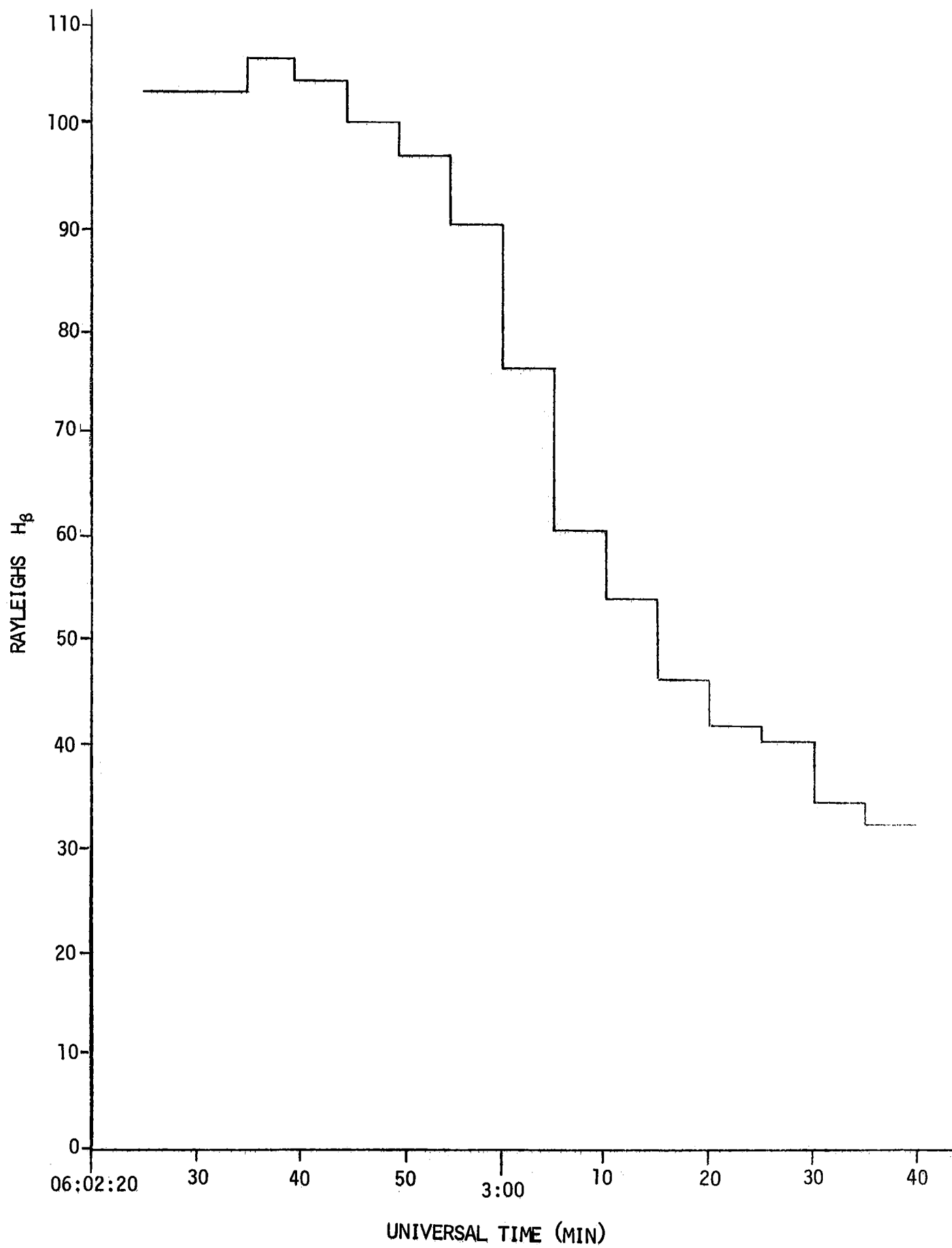


FIGURE 11



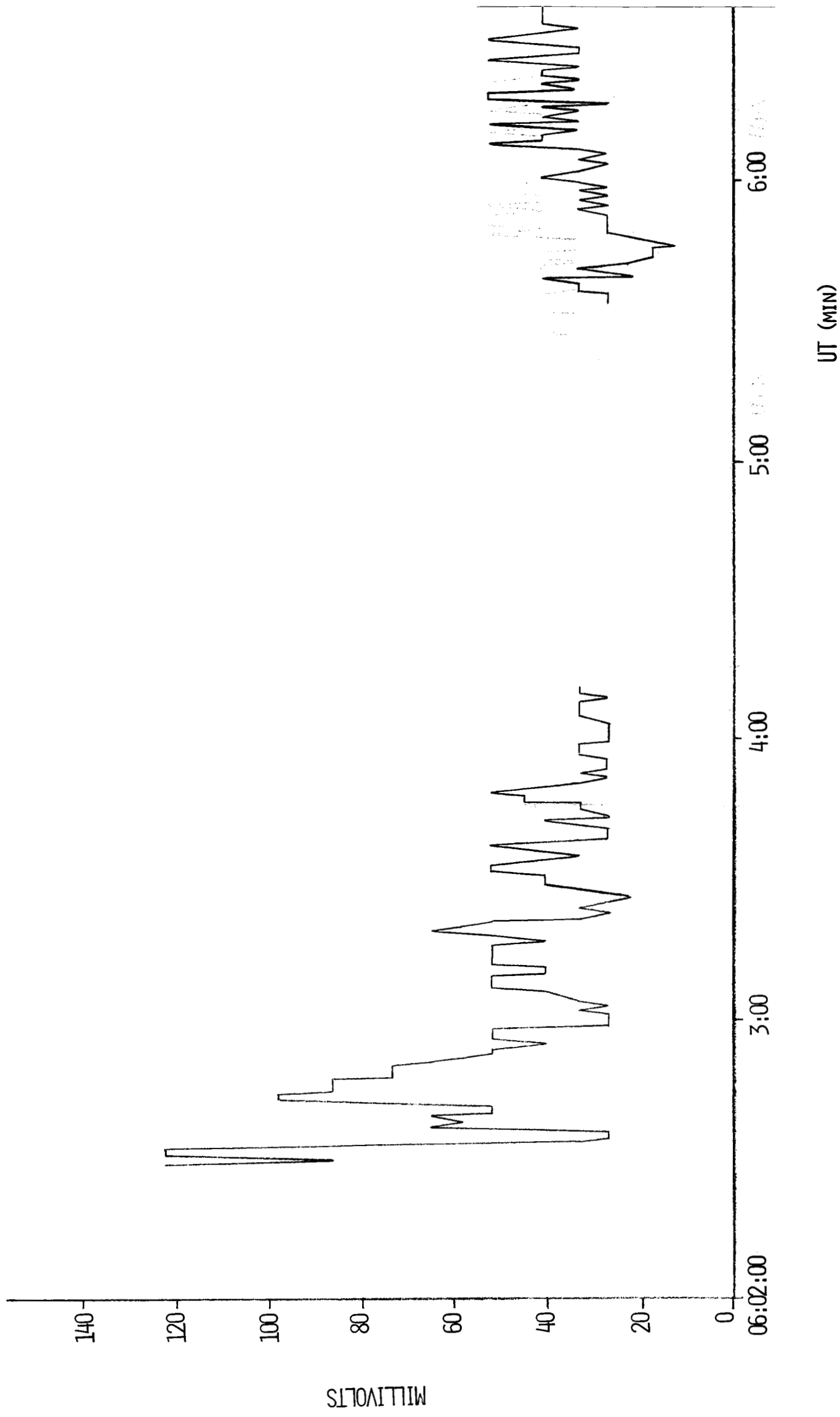
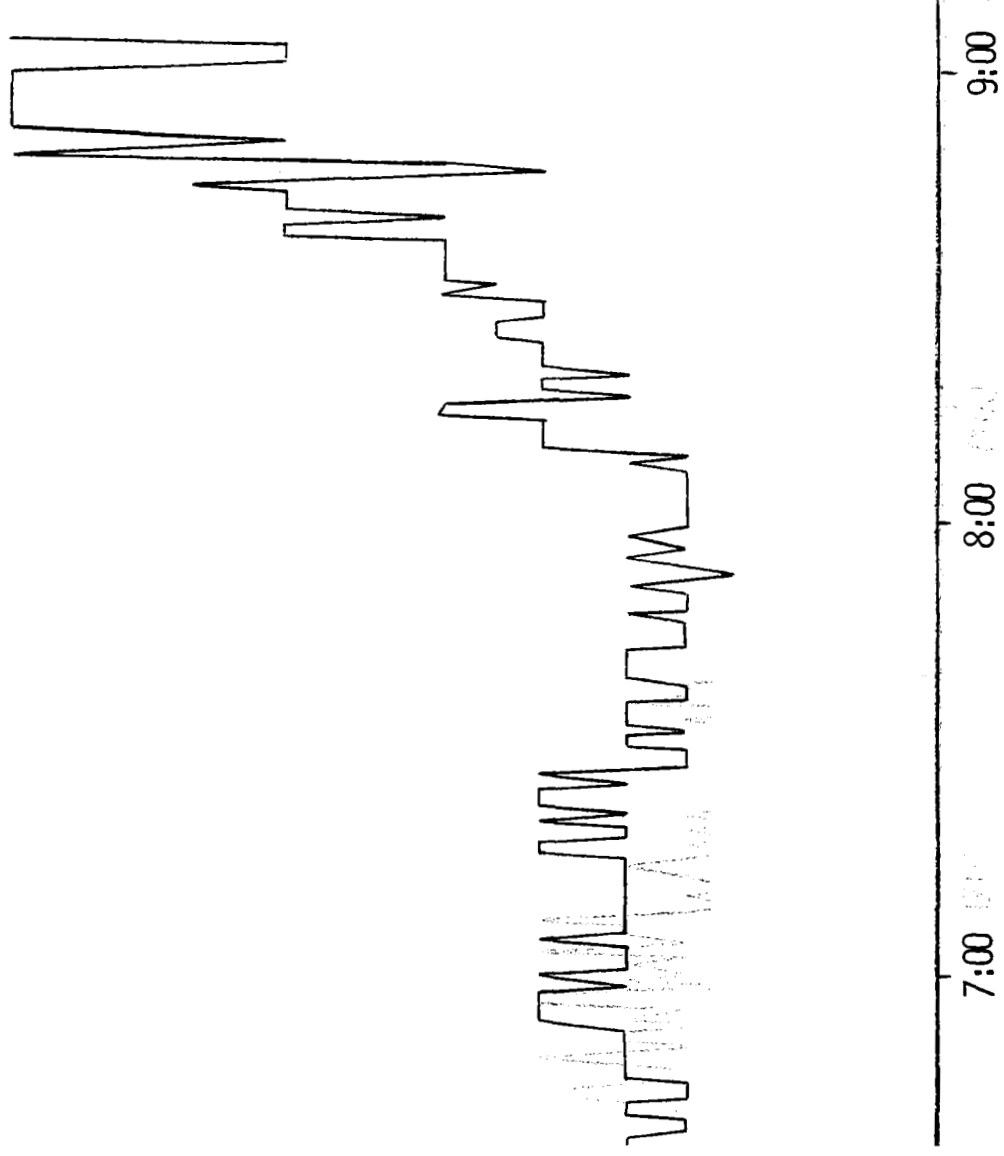


FIGURE 13

2



1

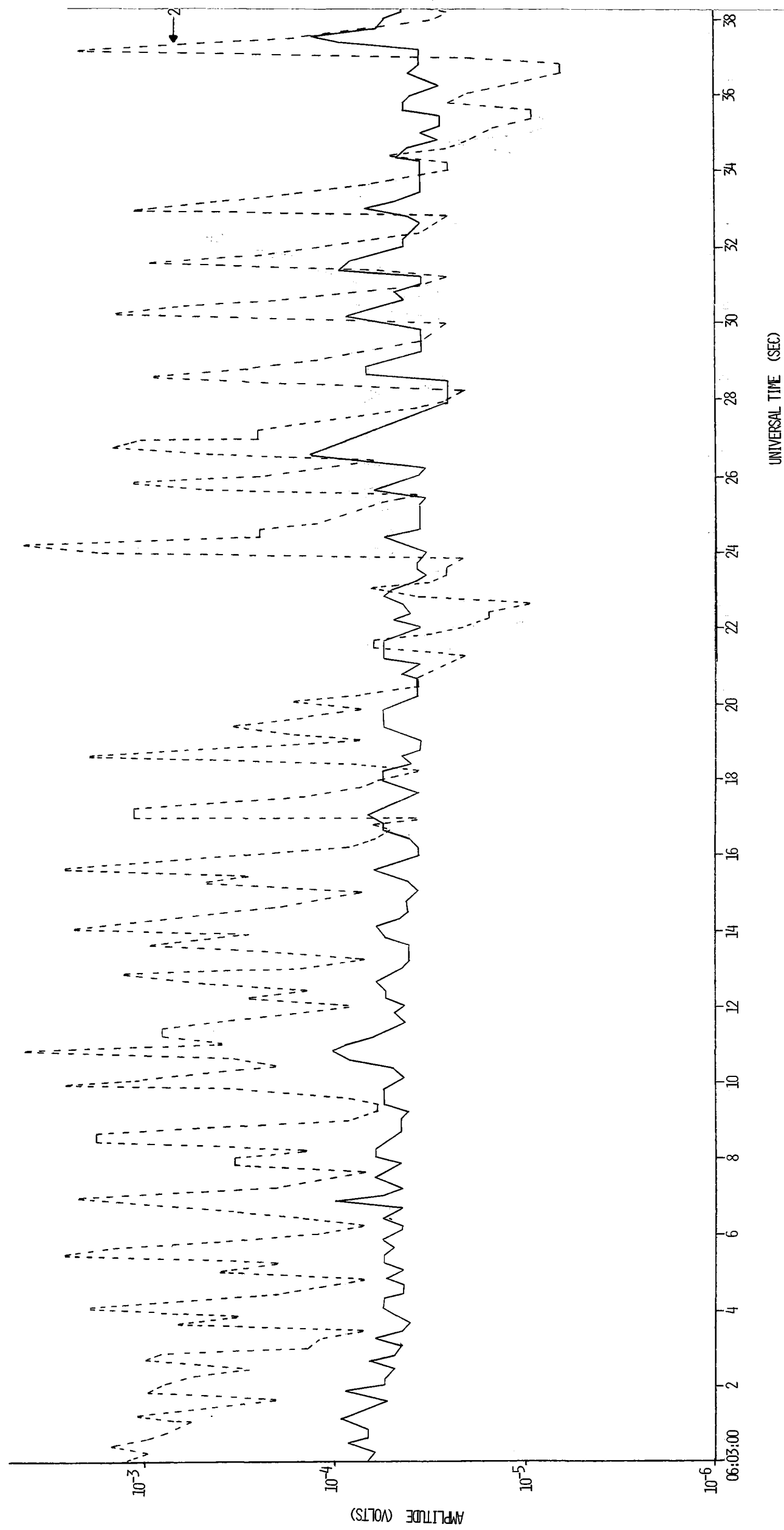
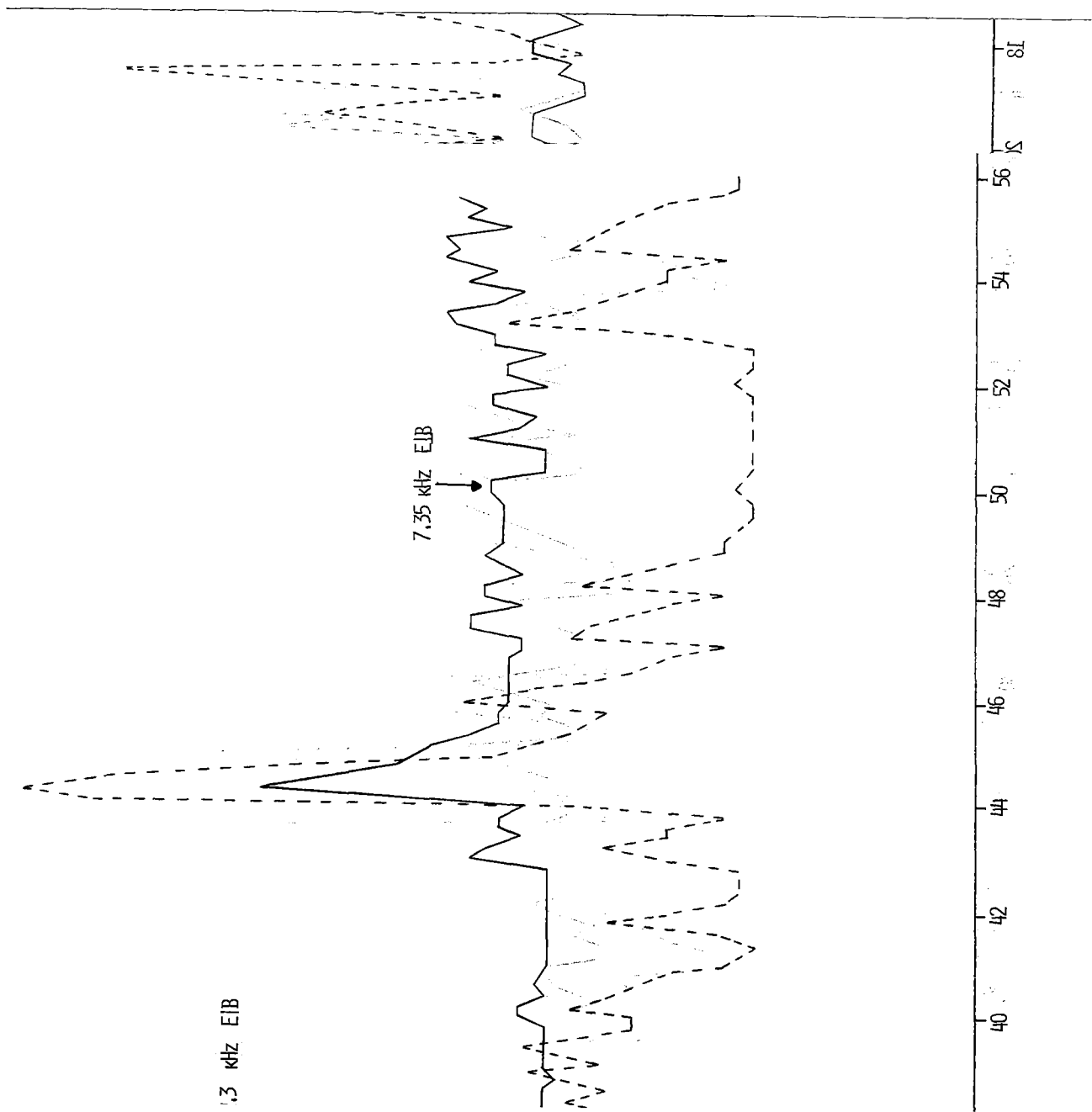


FIGURE 14A



-2-



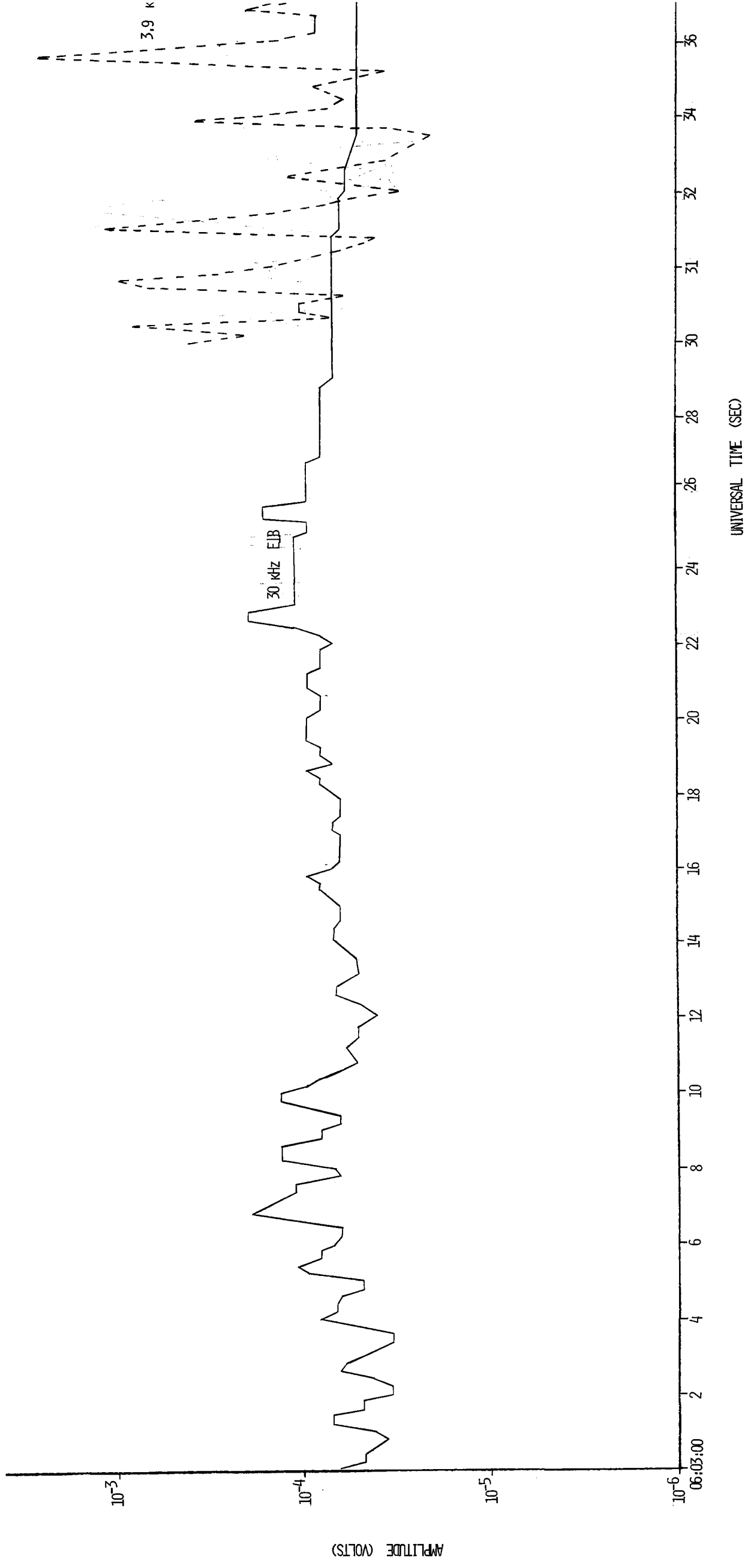
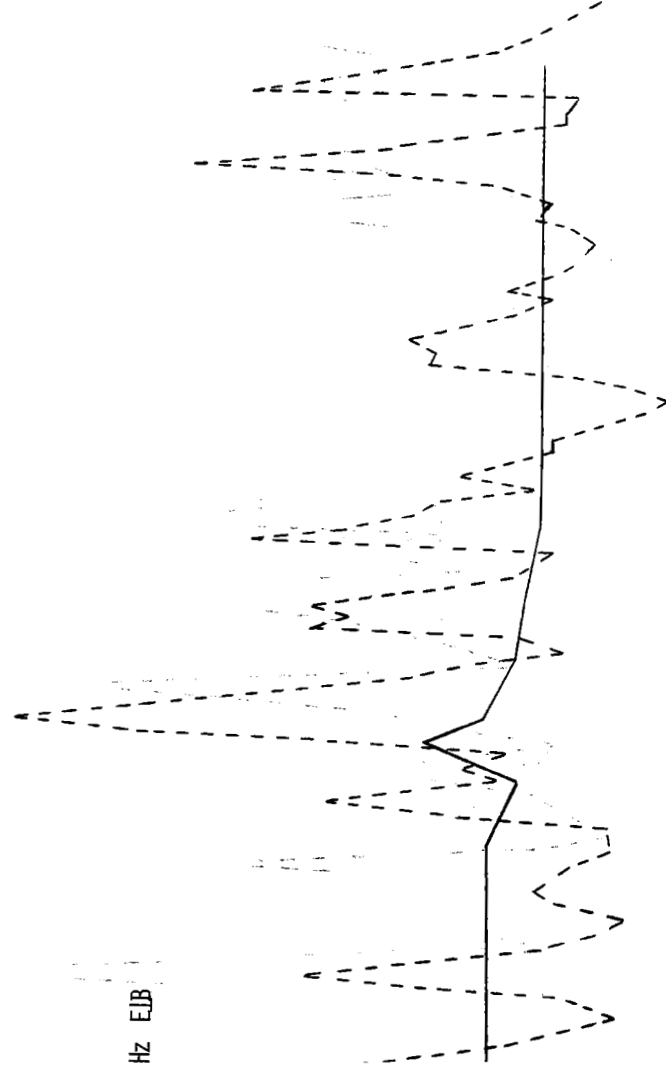
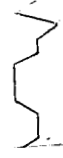


FIGURE 14B

2



Hz EJB



-1-

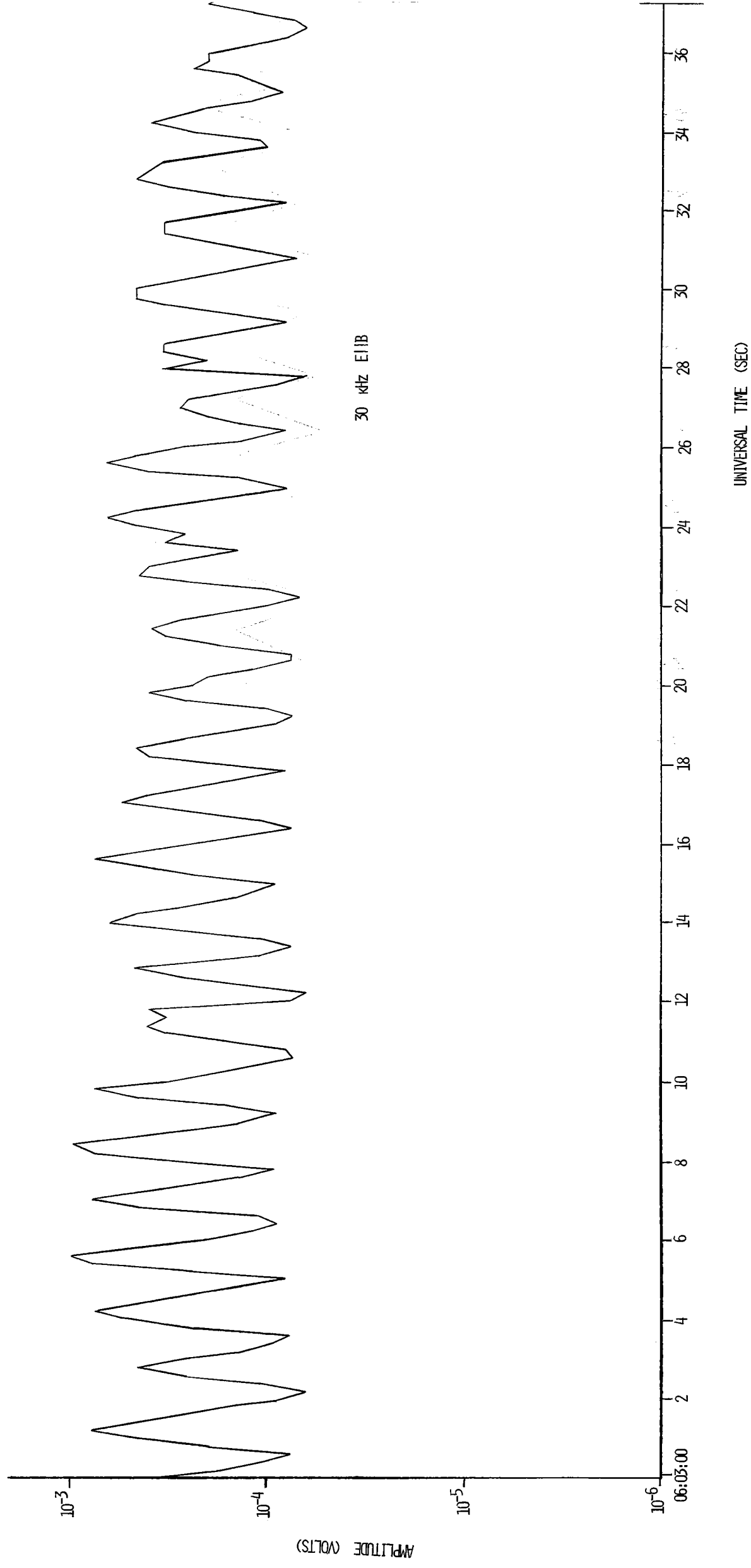
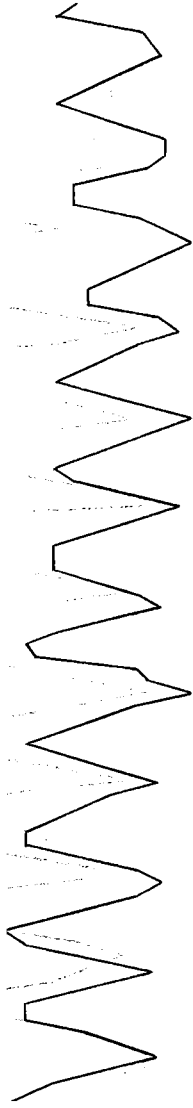


FIGURE 14C

12-



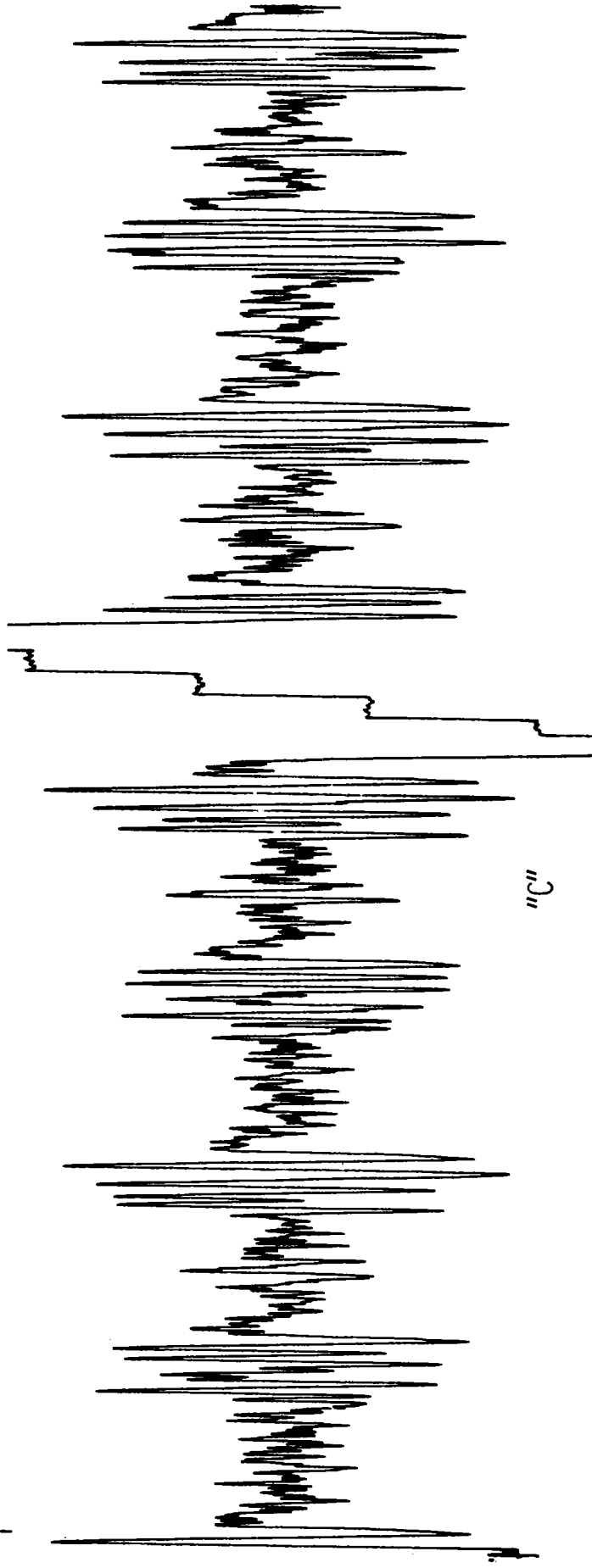
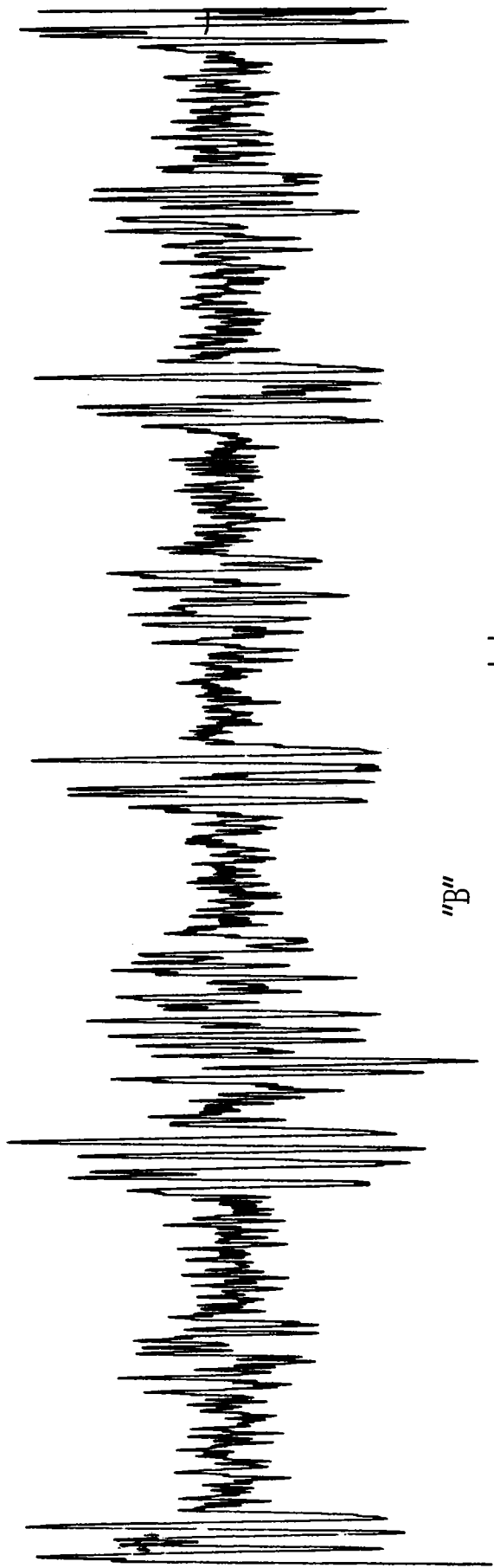
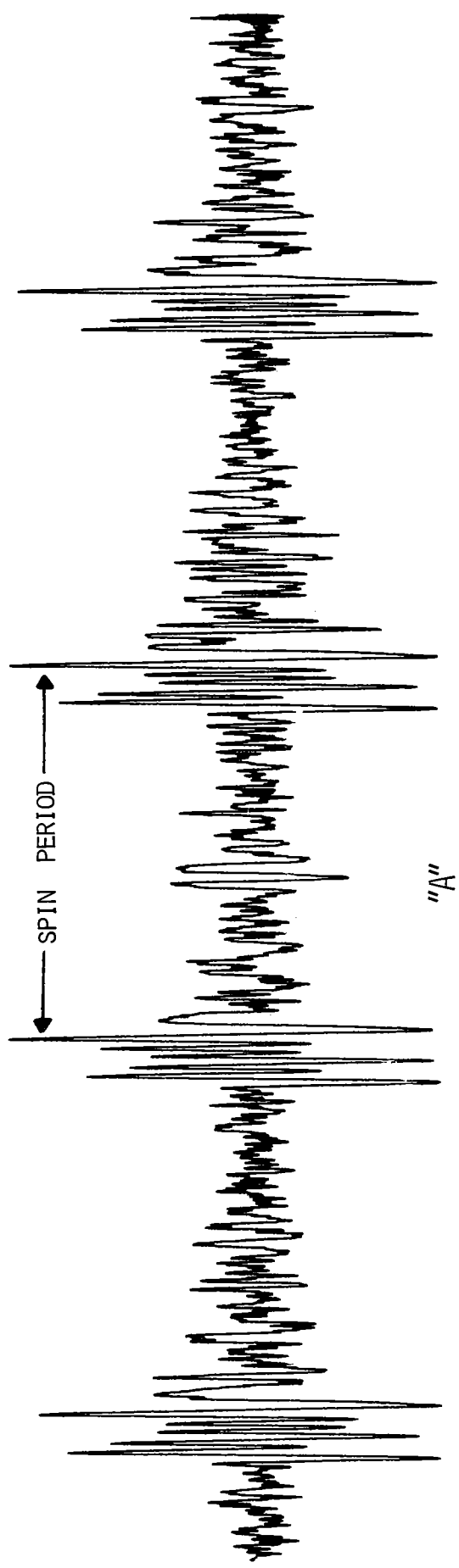


FIGURE 15 61

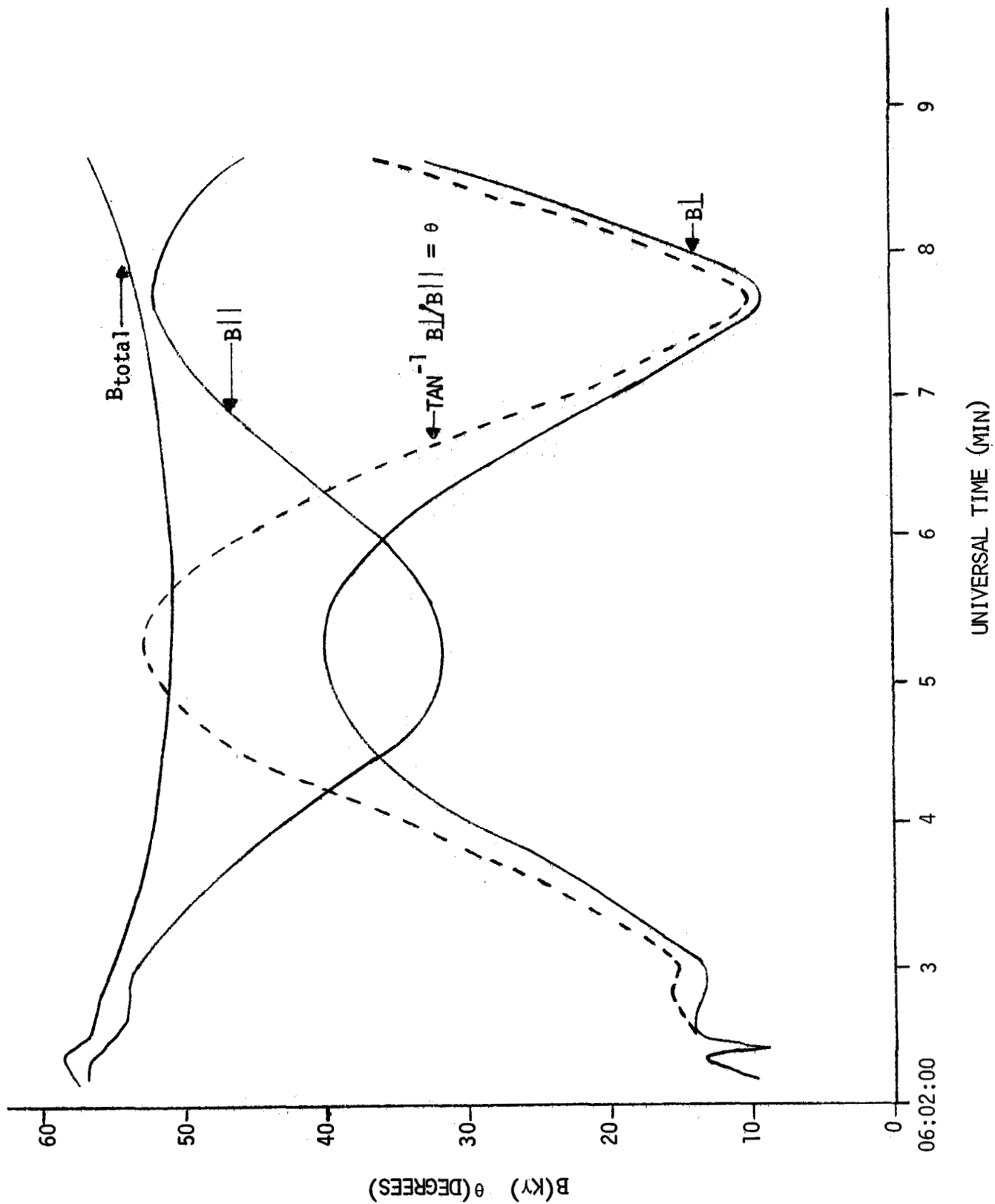


FIGURE 16

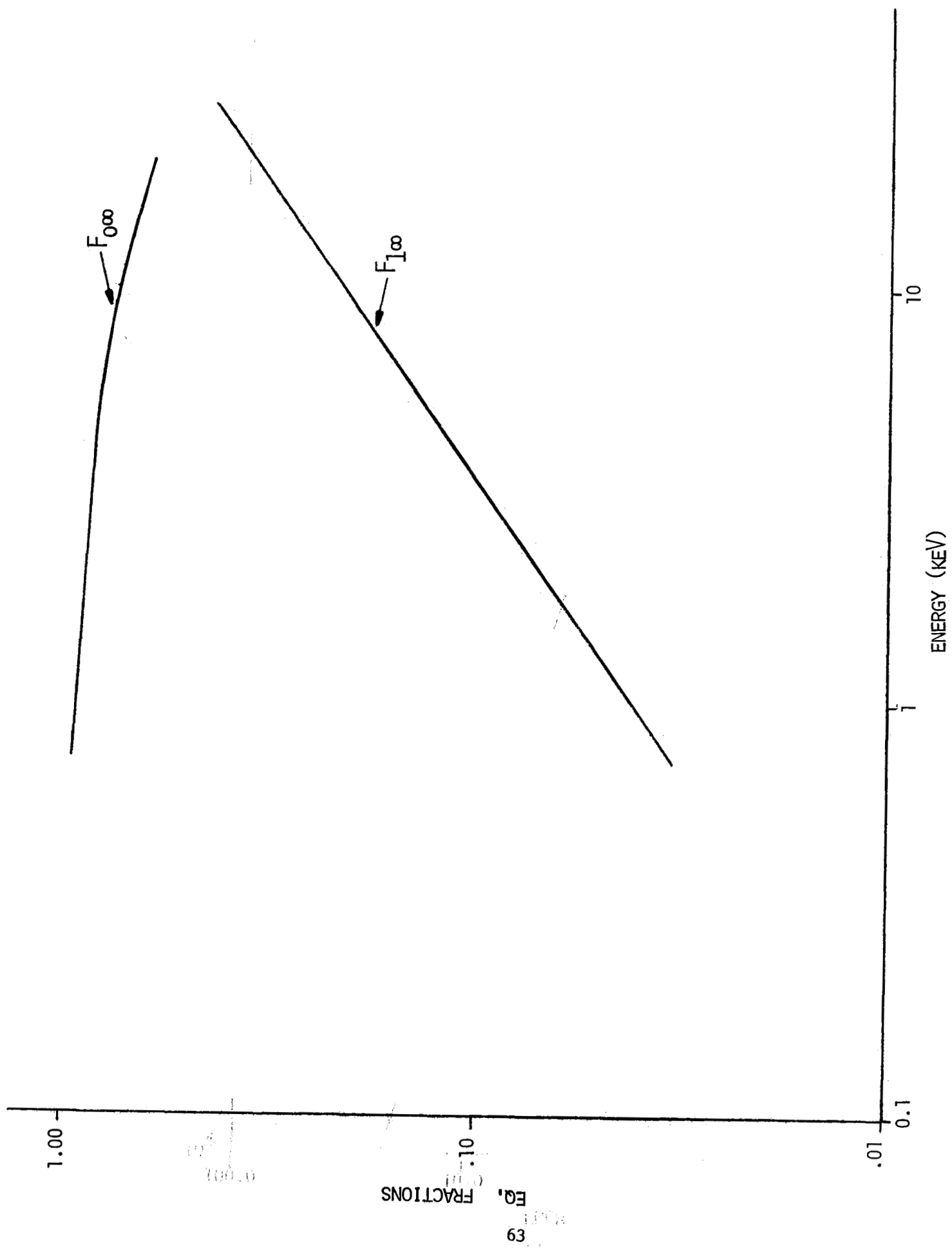
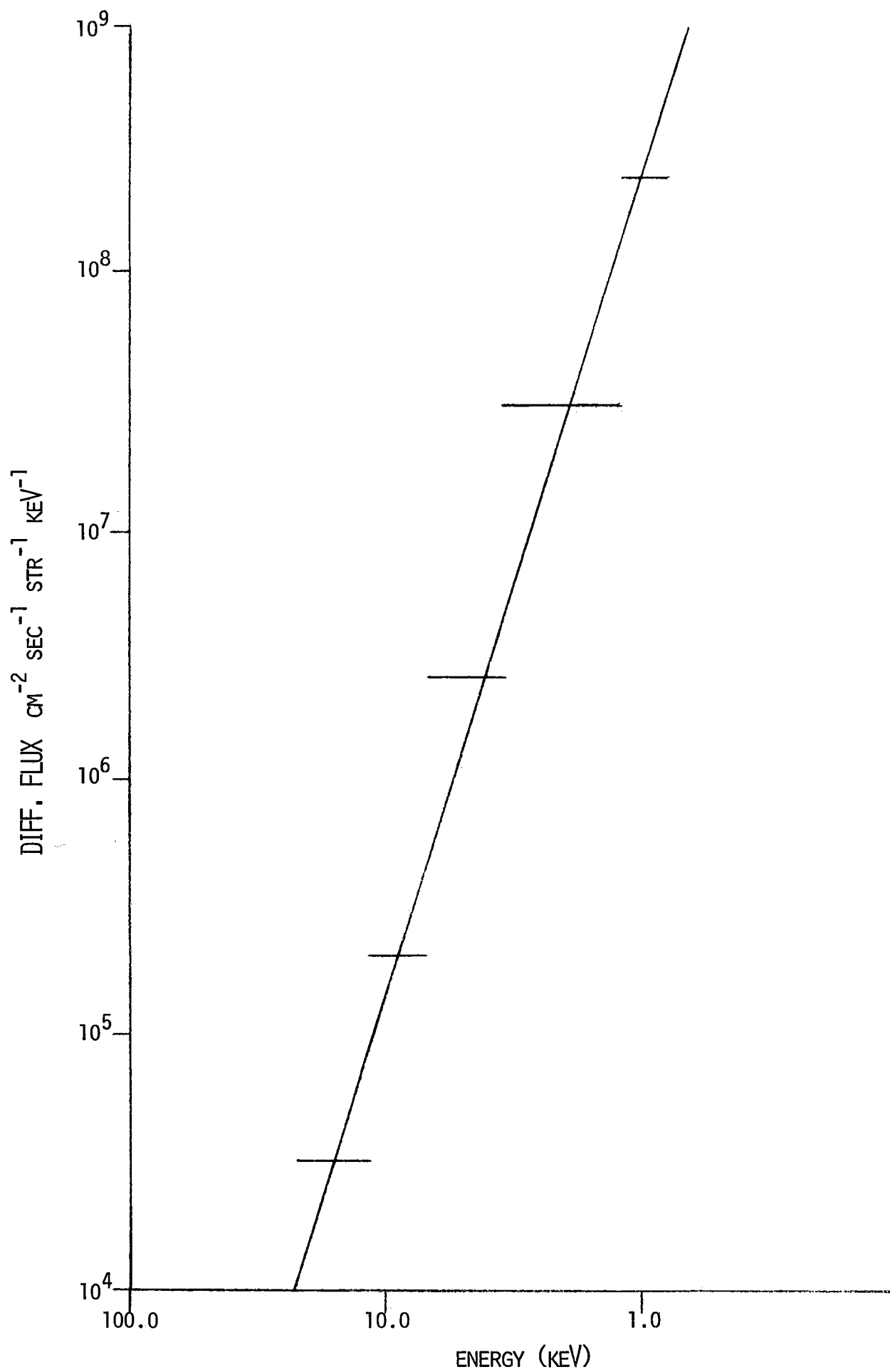


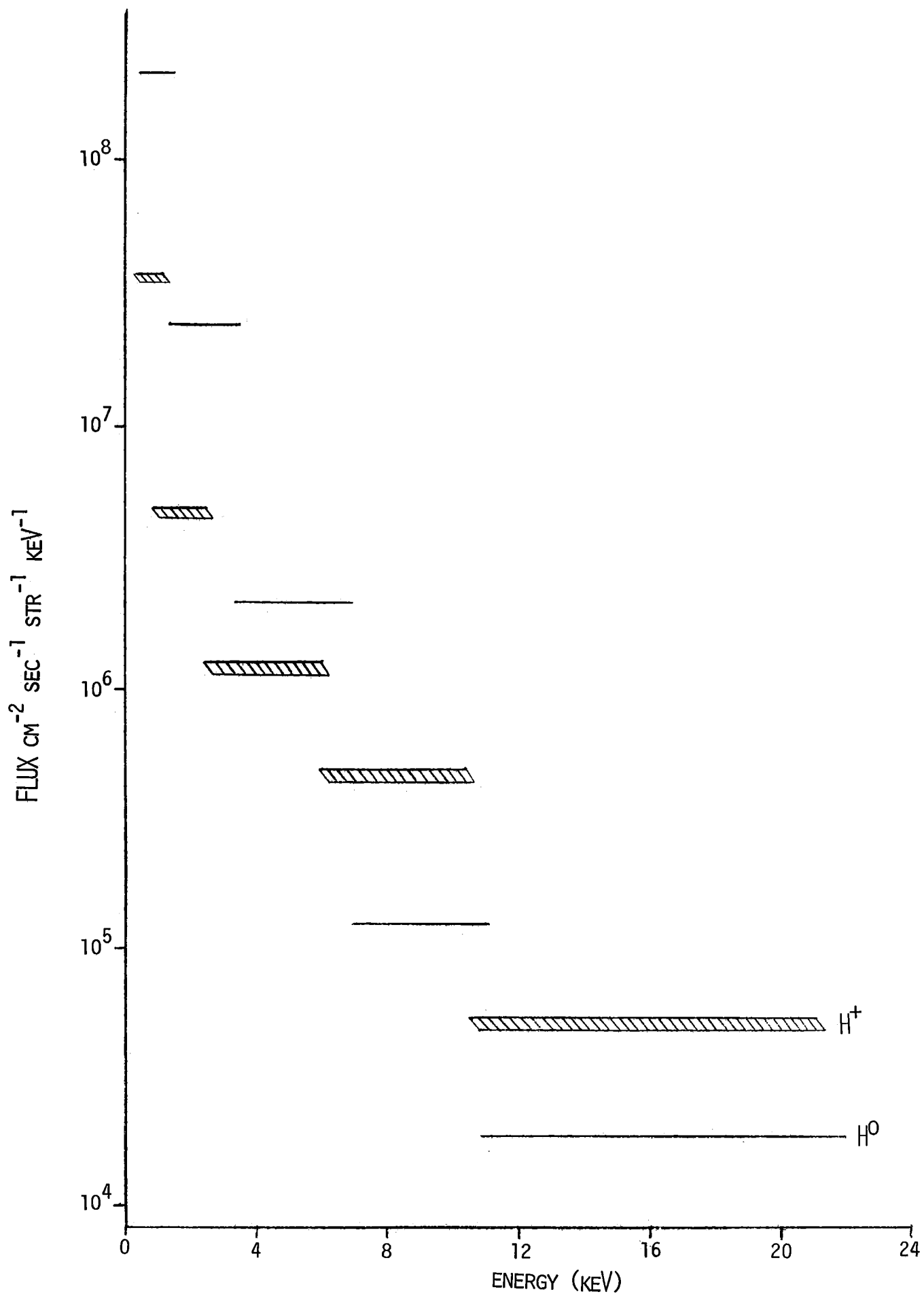
FIGURE 17

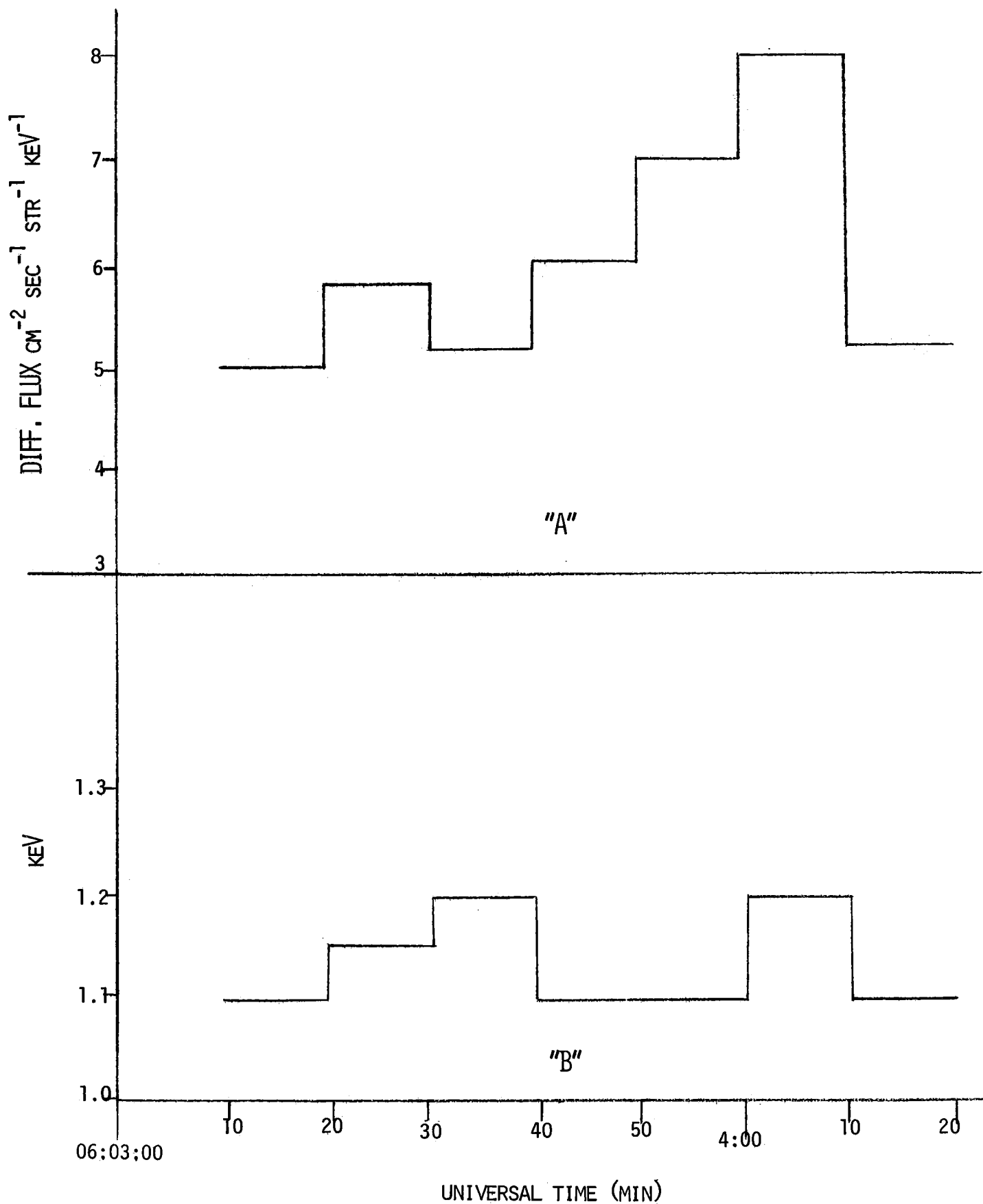




64

FIGURE 18





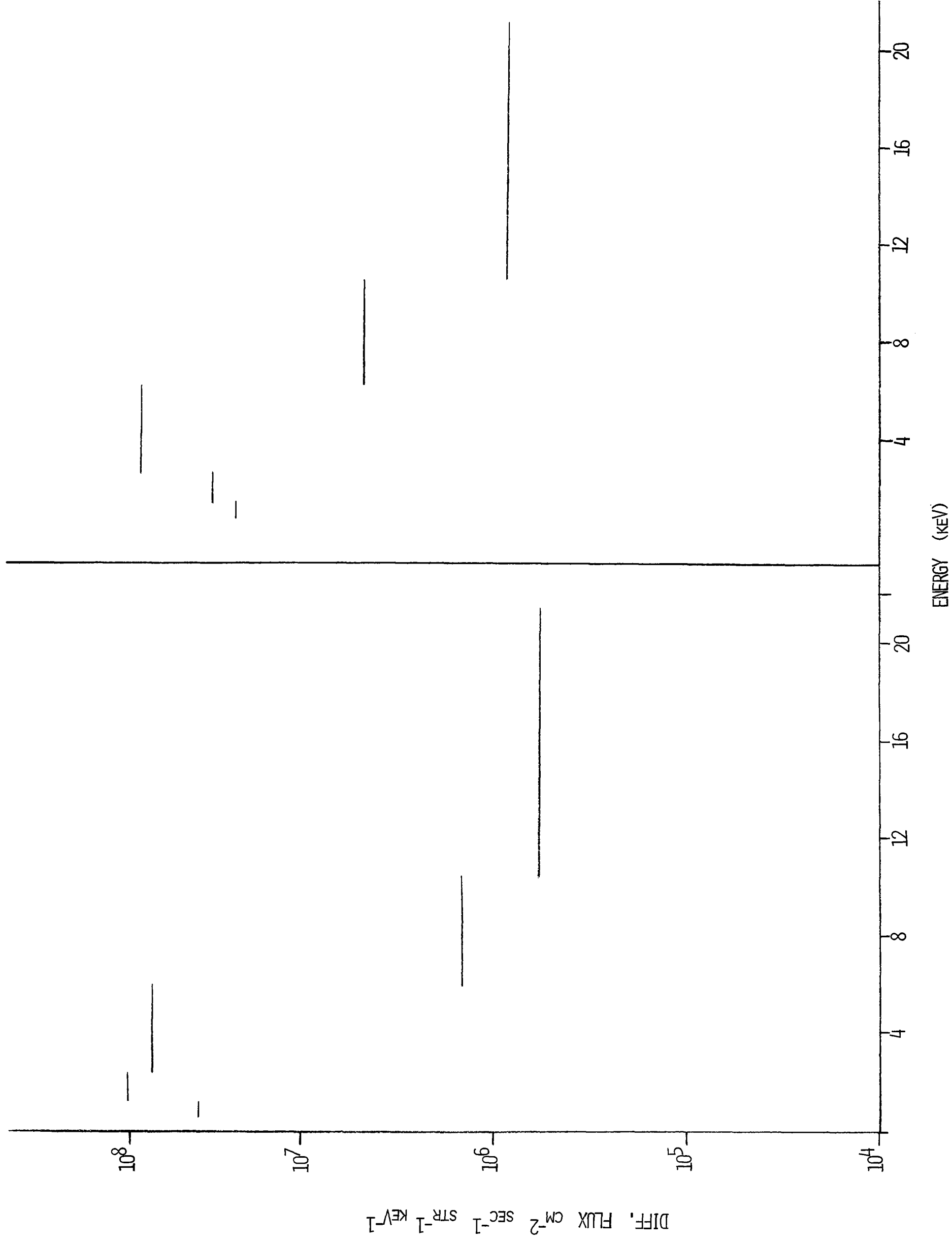
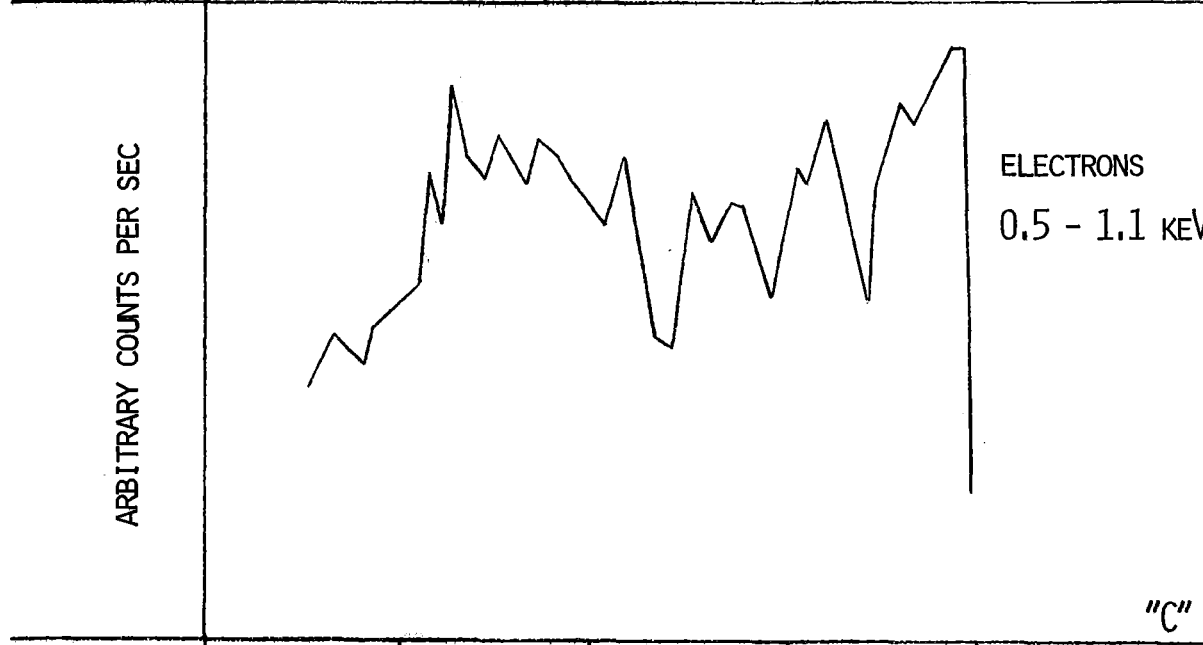
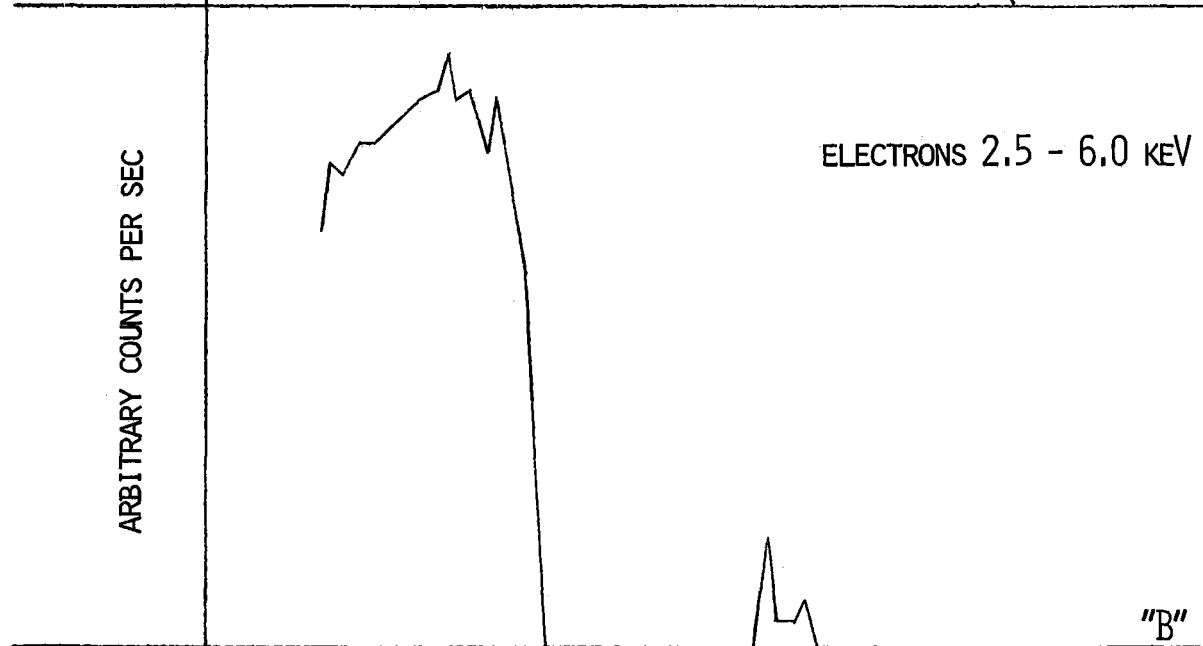


FIGURE 21



06:05:00

20

40

6:00

20

68

40

UNIVERSAL TIME (MIN)

FIGURE 22

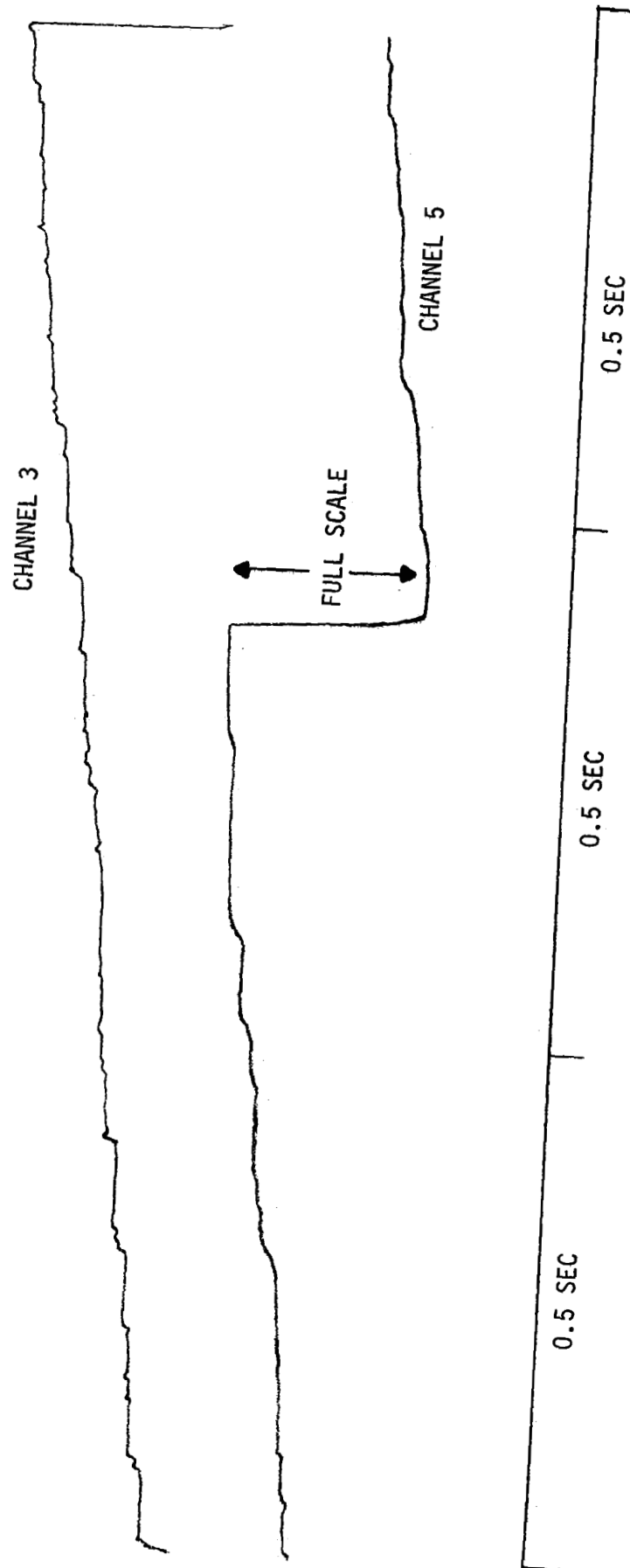
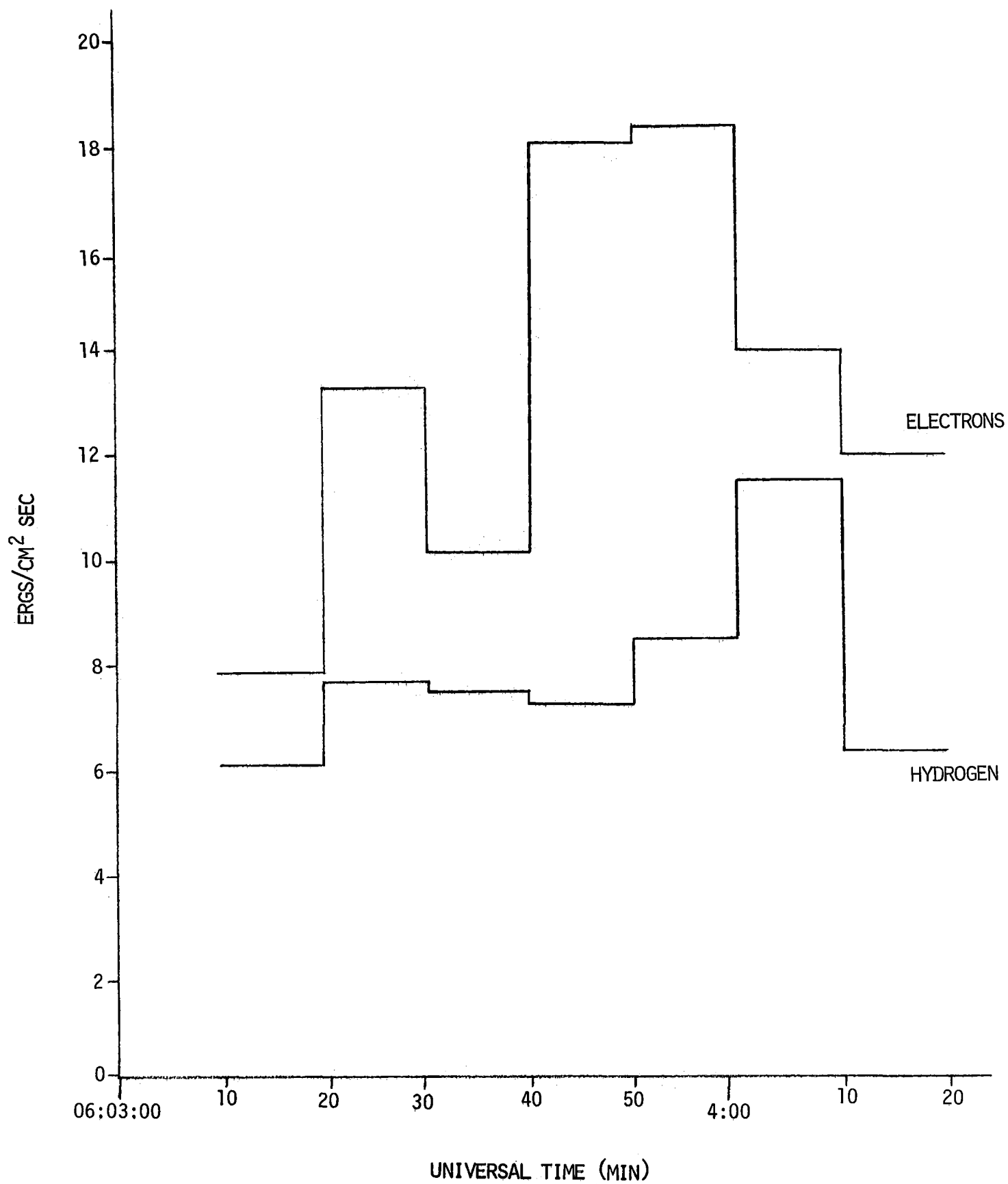
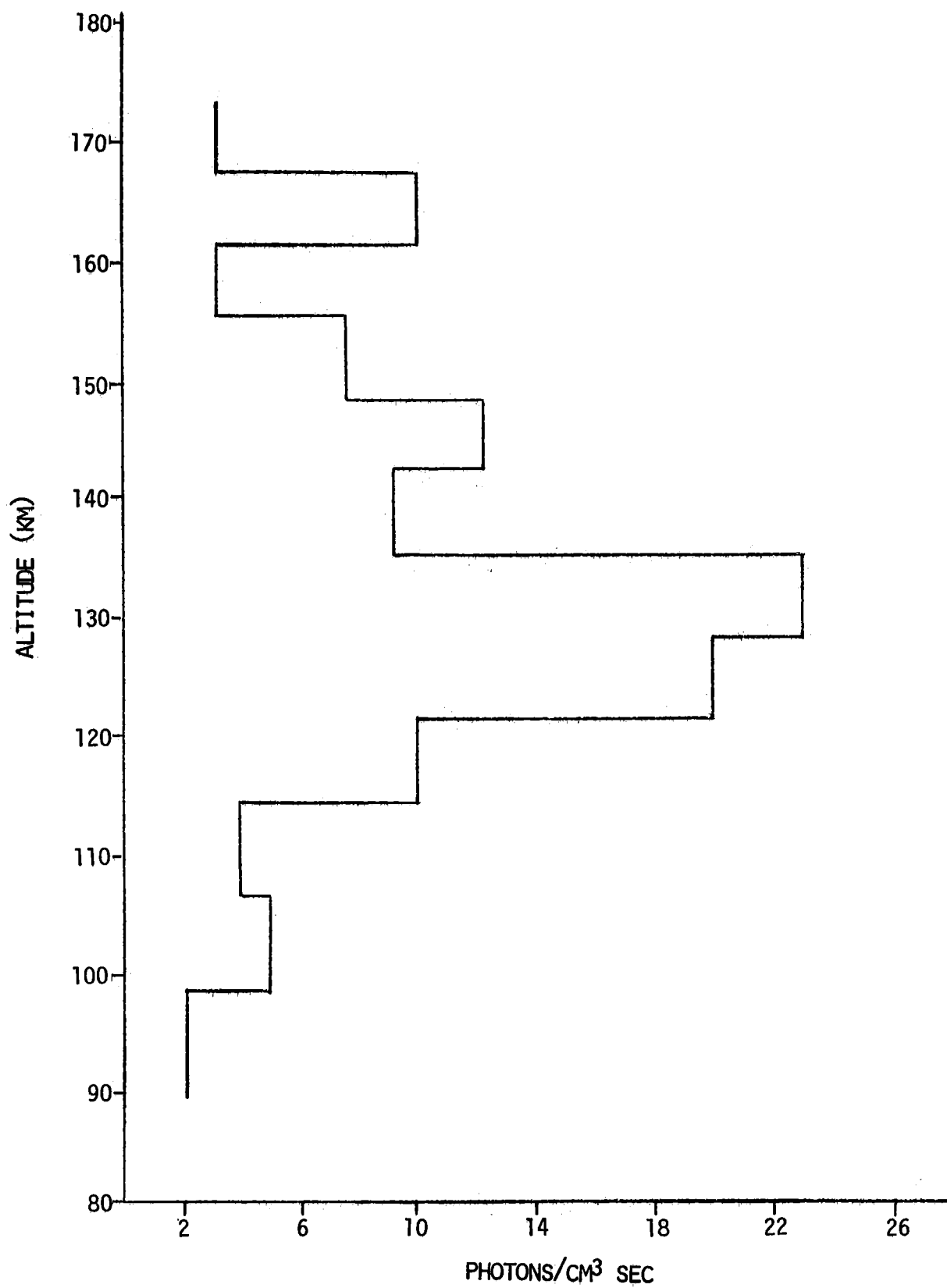


FIGURE 23







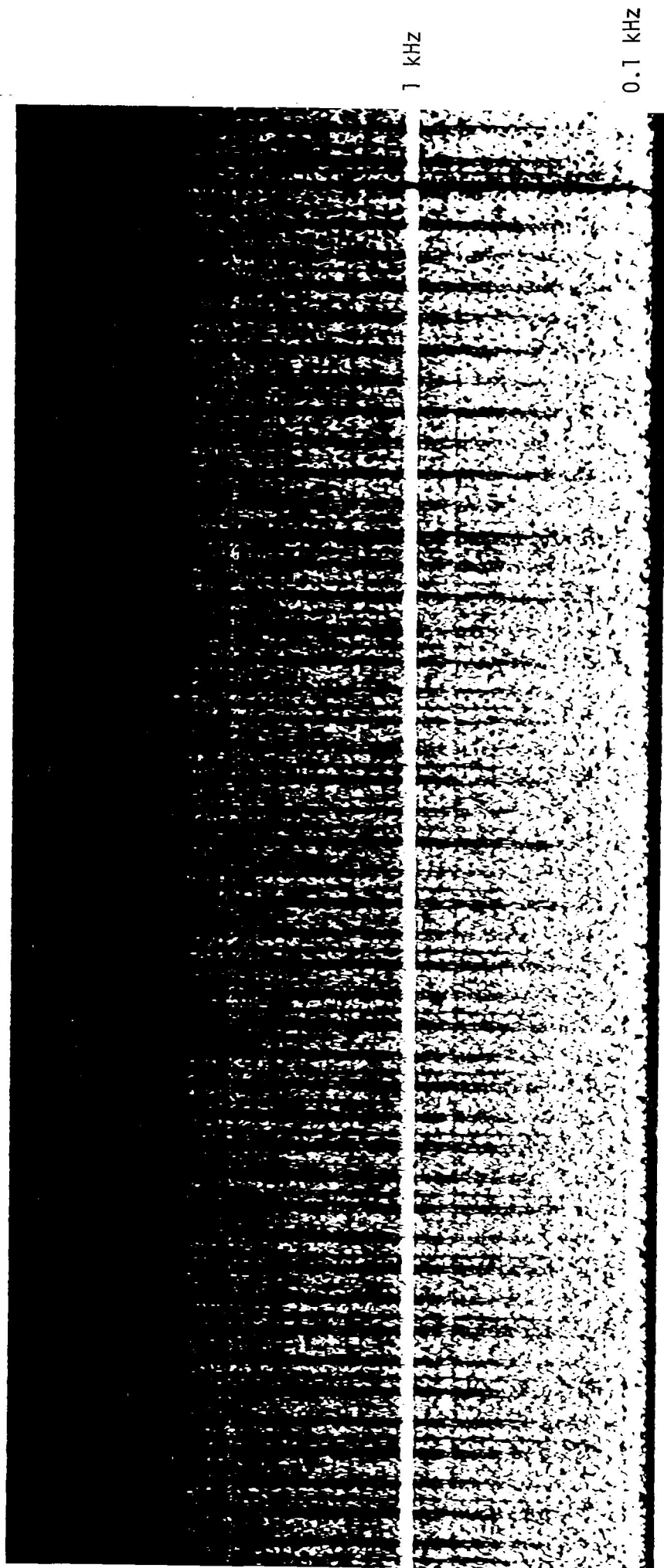


FIGURE 26

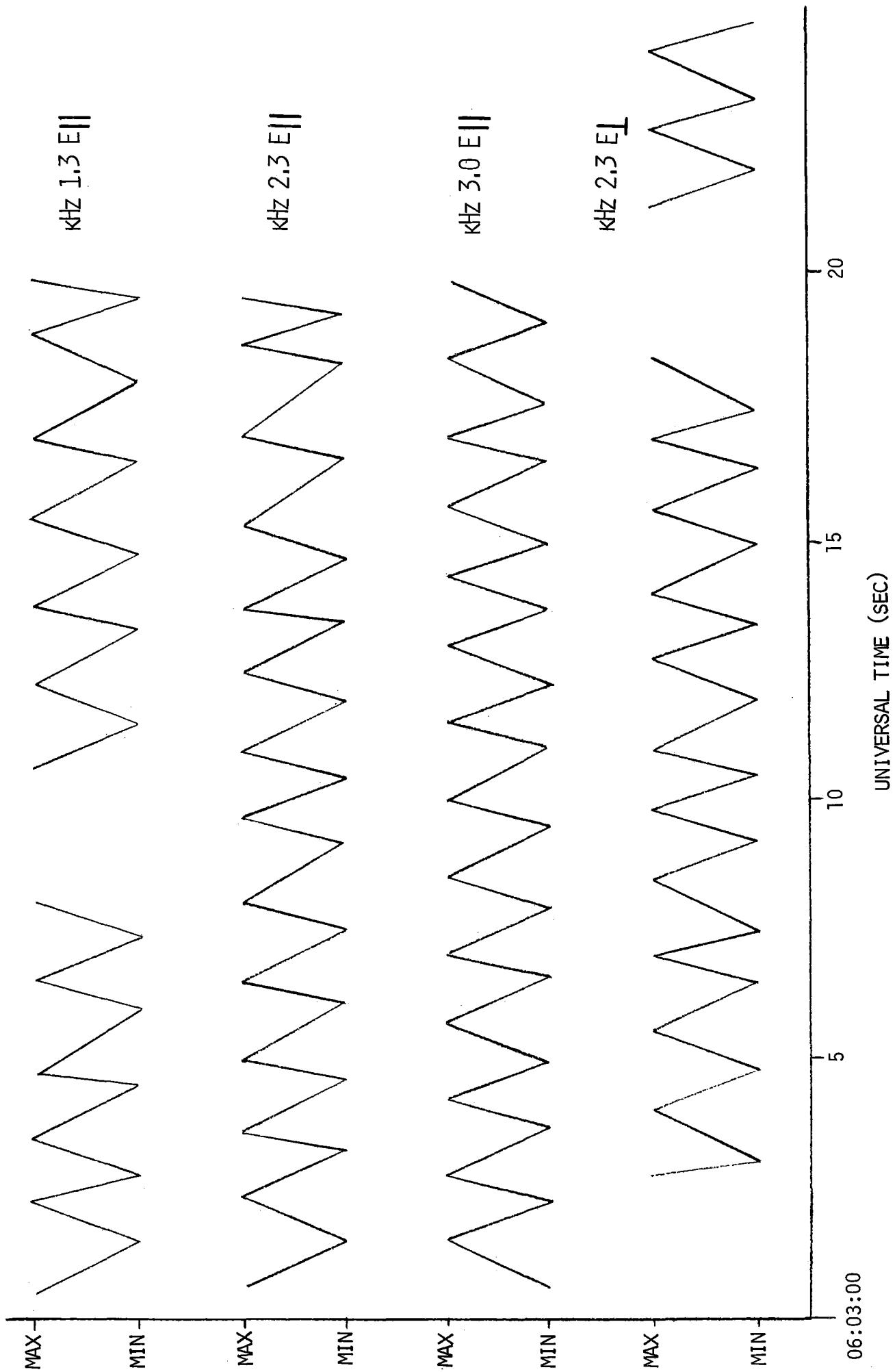


FIGURE 27

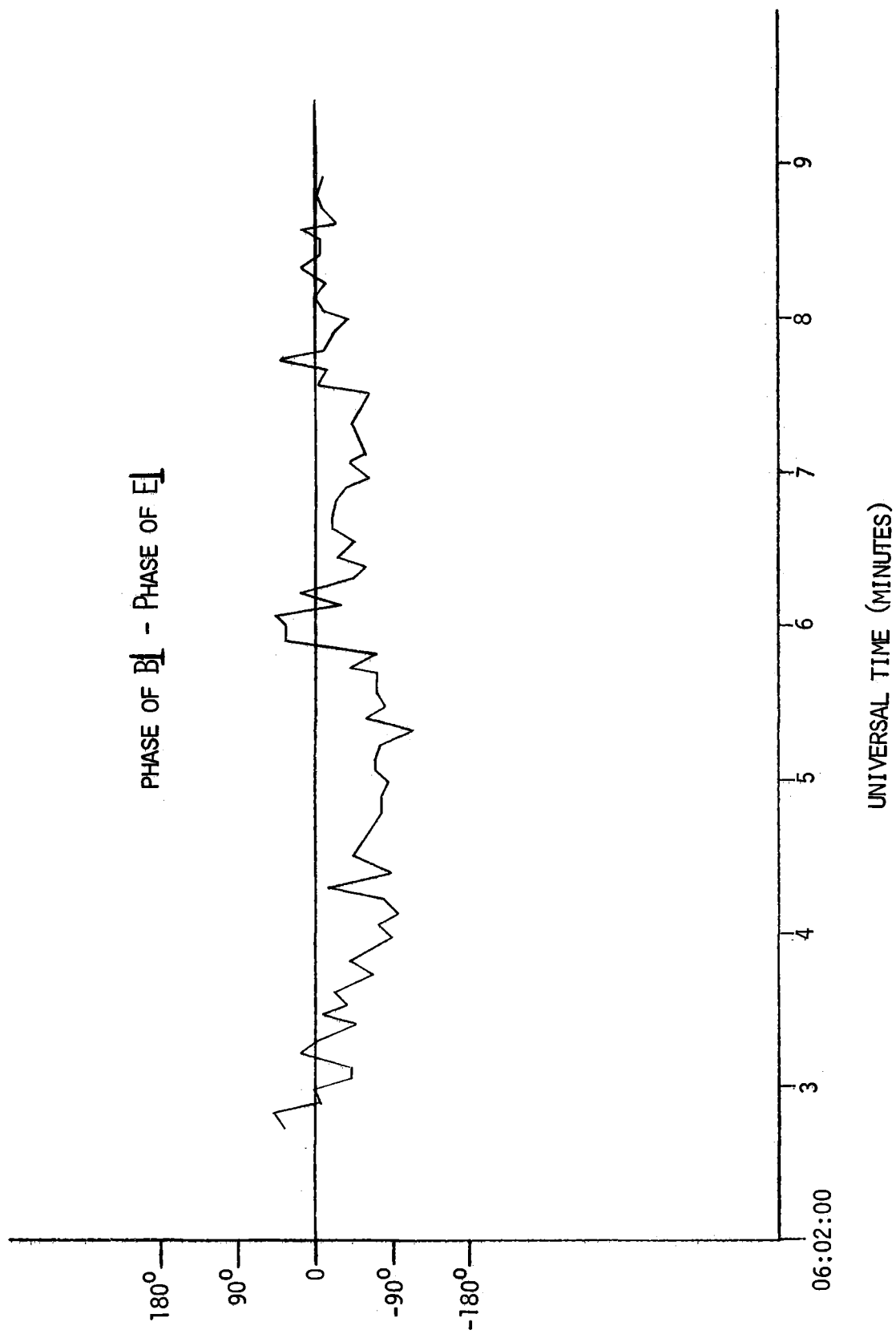
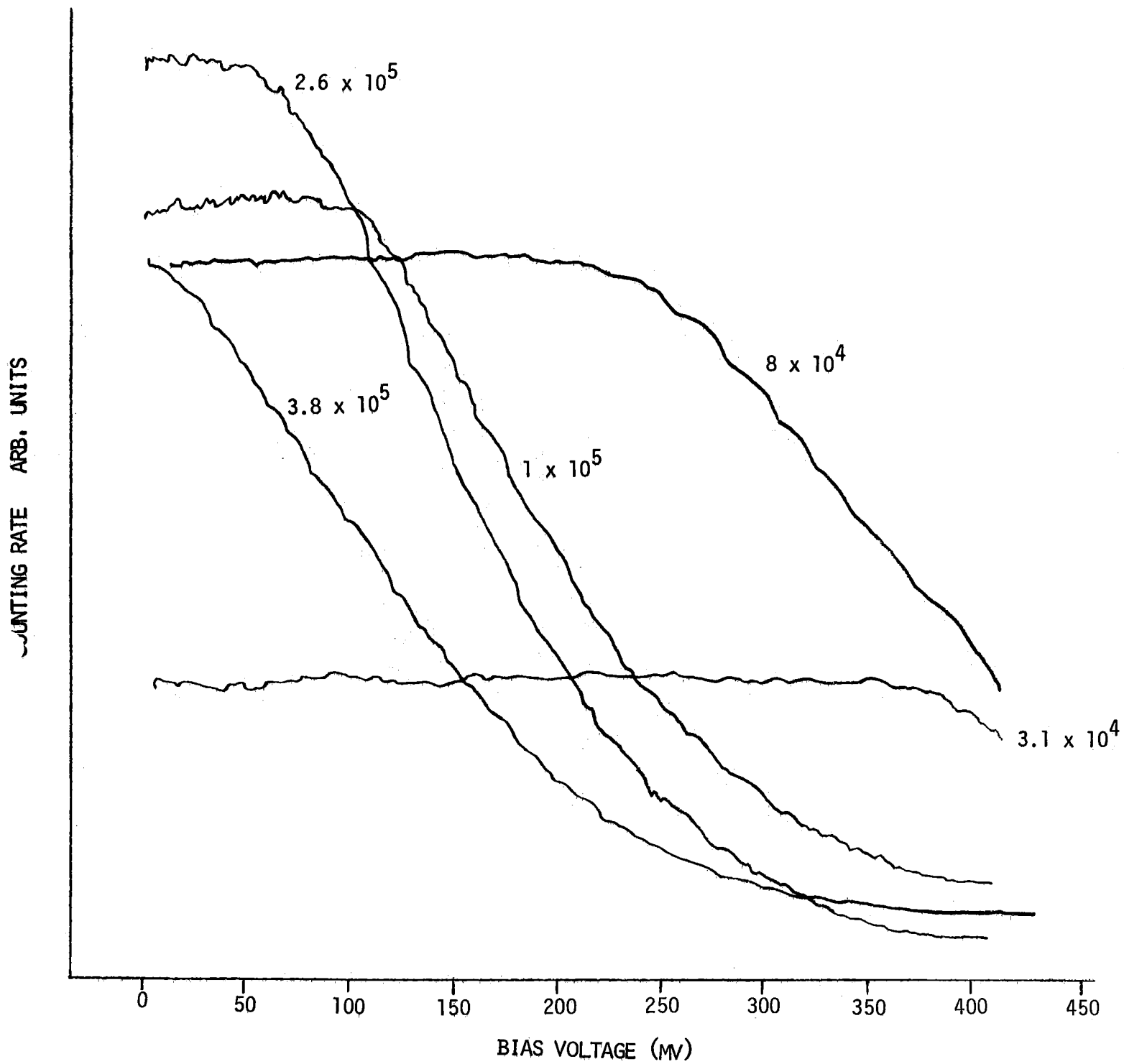
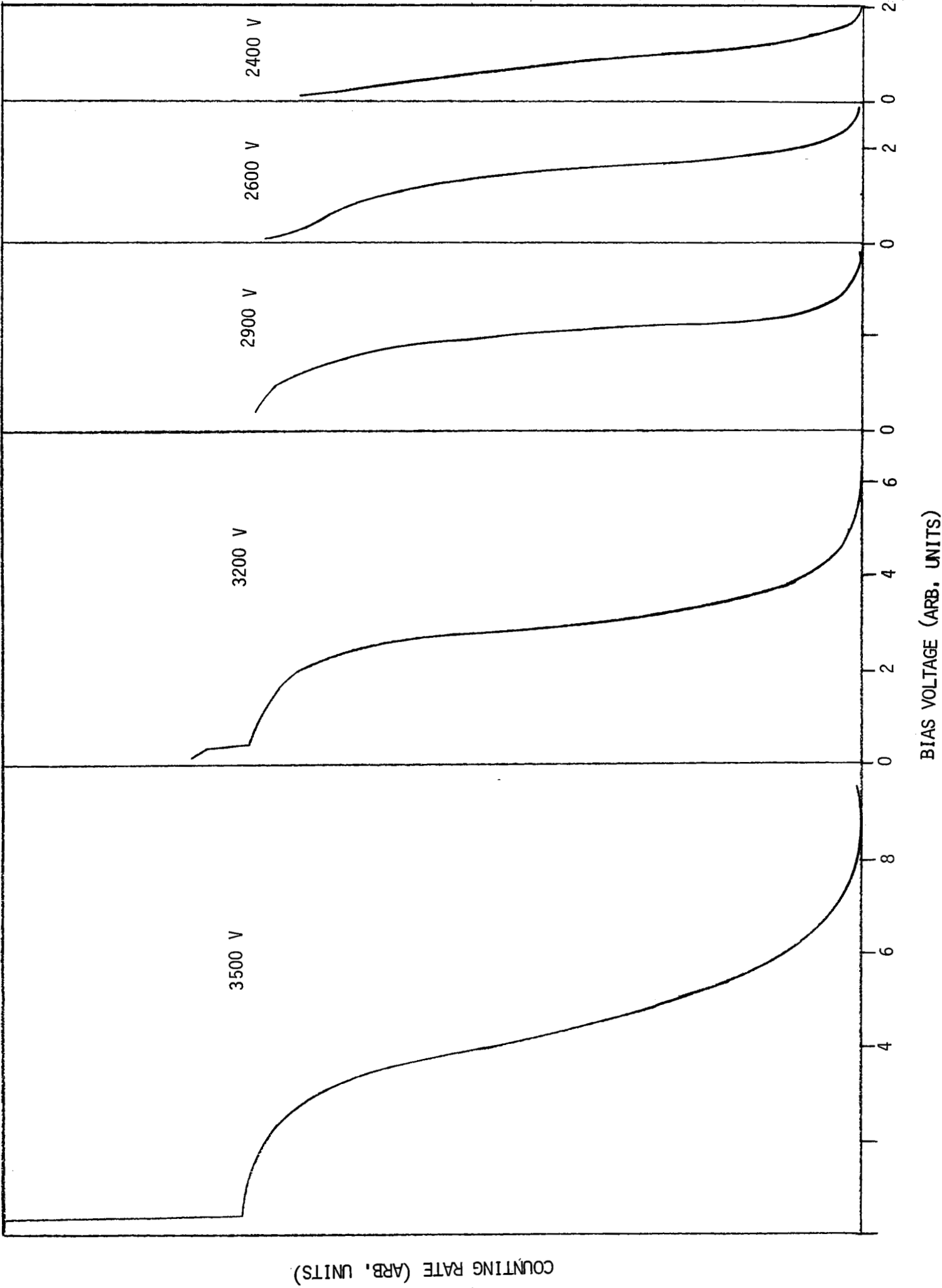


FIGURE 28



APPENDIX FIGURE 1



APPENDIX FIGURE 2

TABLE I

Condition	Time	Seconds from Launch	Measured Range	Measured Height (km)	Calculated Height (km)
Launch	1:45	0	0	0	-16
Computed	1:54	9	-	-	4
AOS-1	2:05	20	2.29	31.6	27
LOS-1	2:14	29	4.58	44.6	45
AOS-2	2:43	58	14.3	96.0	97
LOS-2	2:58	73	19.45	120.0	120
Computed	3:54	129	-	-	189
Computed Max H	5:31	226	-	-	235
Computed	7:14	329	-	-	183
Computed	8:48	423	-	-	45
Computed	8:54	429	-	-	32
AOS-3	9:45	480	127.8	10.30	-80
LOS-3	9:55	490	128.8	4.11	-107

An Energy Spectrometer for Energetic (1-20 keV)  
Neutral Hydrogen Atoms\*

W. Bernstein  
R. L. Wax  
G. T. Inouye  
N. L. Sanders

\*This work was supported by the  
National Aeronautics & Space  
Administration under contract  
NASW-1474

TRW SYSTEMS  
One Space Park  
Redondo Beach, Calif., USA

Although the presence of large fluxes ( $10^8/\text{cm}^2 \text{ sec}$ ) of energetic (1-20 keV) hydrogen atoms has been identified in auroral displays through observation of Doppler-shifted  $H_\alpha$  and  $H_\beta$  light emission (1), the direct measurement of these particles has not yet been attempted in flight experiments. The present paper describes an instrument primarily designed for flight on a Nike-Tomahawk sounding rocket to measure the energy spectrum of the energetic hydrogen associated with these proton auroras.

The measurement of the energetic  $H^0$  energy spectrum simultaneously with the  $H^+$  energy spectrum can provide an important diagnostic for auroral processes. If a long range electric field parallel to B does exist at rocket altitudes as proposed by Mozer and Bruston (6) and by Evans (7), then significant differences in the neutral and charged energy spectra will be observed because only the charged component is acted upon by the electric field. If we assume an incident proton energy distribution with an e-fold energy of 5-10 keV, it should be possible to identify electric fields as small as 20 millivolts/m if the field extends over distances  $> 30 \text{ Km}$ . This technique eliminates many of the difficulties encountered in the measurement of electric fields with electrostatic probes. It also removes the inherent space-time ambiguity associated with the derivation of electric field strengths from a measurement, with one vehicle, of the changes in energy spectrum or pitch angle distribution of a single class of particles.

Theoretical estimates of the interaction between precipitated protons and the upper atmosphere are based upon cross-sections determined in the laboratory (1). The vast difference in collision mean free paths between the laboratory and the upper atmosphere and also the presence of



other energy sources in the upper atmosphere can result in a significant change in the interaction probabilities. The in situ measurement of the energy dependence of the ratio  $H^+/H^0$  will indicate whether such inconsistencies do indeed exist.

The existence of energetic neutral hydrogen atoms in the interplanetary medium has also been proposed in several different contexts. Akasofu (2) has proposed that large fluxes ( $10^9/\text{cm}^2 \text{ sec}$  at the orbit of the earth) are emitted by the sun during periods of flare activity but subsequent estimates by Brandt and Hunter (3) and by Cloutier (4) have reduced these fluxes to  $\leq 10^5/\text{cm}^2 \text{ sec}$  because of UV and electron impact ionization in the outer corona. The observations of Doppler broadened Ly  $\alpha$  radiation from the interplanetary medium indicate the presence there of energetic hydrogen atoms (5). These atoms may be either an inwardly directed flux produced by charge exchange at the solar wind-interstellar magnetic field boundary, or an outward directed flux produced as a result of charge exchange between this inward neutral flux and solar wind protons. Current estimates of these fluxes are 0.1-1% of the solar wind flux ( $10^7 - 10^8/\text{cm}^2 \text{ sec}$ ) at the orbit of the earth. It should be noted that, with minor modifications, the described instrument would be adequate for interplanetary measurements under the minimal expected flux conditions.

In order to perform electrostatic energy measurements on neutral atoms, a fraction of the incident atoms must be ionized prior to analysis. The ionization technique employed in this instrument is to pass the incident neutral atoms through a  $2 \mu\text{g cm}^{-2}$  carbon foil (8). Scattering of the incident beam occurs during its transit of the foil; Table 1 shows the

energy dependence of the angle at which the half maximum intensity of the scattered distribution is observed. These angles show the expected  $E^{-1}$  dependence (9). For each energy the shape of the angular distributions appears to be intermediate between multiple and single scattering. The energy lost during transit of the foil is also given in Table 1, and shows the linear dependence on particle velocity predicted by the Fermi-Teller (10) low energy stopping power theory. To date, we have not specifically determined the ratio  $H^+/(H^+ + H^- + H^0)$  leaving the foil, because the magnitude of the  $H^+$  equilibrium fraction is included in the overall efficiency measurements described below. Qualitatively, the  $H^+$  equilibrium fraction decreases by about a factor of two between 10 keV and 4 keV (11). The techniques for neutral beam generation and the experimental arrangement for these measurements has been described by Wax and Bernstein (12).

Figure 1 is a schematic illustration of the analyzer, deflection plate, and detector arrangement. The energy analyzer is a pair of hemispherical plates which provide focussing in one dimension of the particles scattered by the foil. In the present instrument, the outer shell radius is 4.75 cm and the plate separation is 0.475 cm; the analyzer factor is 5.0 keV/kV. Two adjacent 0.5 cm radius foils are used for ionization and two adjacent 0.4 cm radius Bendix continuous channel multipliers, CCM, (13) are used as detectors. The CCM's are operated in the saturated mode with +3.5 kV on the collector and an electron retarding voltage of -30 V on the entrance aperture.

The energy resolution (FWHM) for incident hydrogen atoms is  $\sim 10\%$  and there is little evidence for straggling in the foil except at energies

below 3 keV. The overall efficiency of the instrument (defined as the number of detected events per atom incident on the foil) ranges from  $2 \times 10^{-3}$  at 2 keV to  $4 \times 10^{-2}$  at 10 keV; the complete tabulation of the efficiencies is also shown in Table 1.

The removal of incident protons prior to the foil is accomplished with a set of electrostatic deflection plates; an applied voltage of 3.5 KV removes incident protons with energy  $< 25$  keV. A 300 gauss magnetic field parallel to the electric field removes incident electrons with energies  $< 50$  keV. The deflection plates also serve to define the solid angle of the instrument. In the present configuration, the geometric factor is  $\sim 0.1 \text{ cm}^2$  ster for an isotropic incident flux. The analyzer plates have several small holes drilled through them in order to equalize the pressure on both sides of the foils during the rocket's ascent.

The present instrument is designed to operate over a counting rate range of 3 to  $3 \times 10^4$  counts/sec corresponding to precipitated fluxes of about  $3 \times 10^5 - 3 \times 10^9/\text{cm}^2$  sec. It can detect variations in both particle flux and energy spectrum in times as short as 10 milliseconds if the events recorded in this time interval are statistically significant; at lower counting rates, the detected events are time integrated to provide the desired statistical accuracy at the sacrifice of temporal resolution. For long integration times ( $\geq 1$  sec), this technique yields a very good time averaged energy spectrum.

Figure 2 shows the block diagram of the electronic system. Particles transmitted through the analyzer are detected by the pair of CCM's. The output pulses from each CCM, after a stage of amplification, drive a

noise rejecting discriminator which generates a standardized  $1 \mu$  sec output pulse. These pulses from each discriminator are then connected through an "OR" gate to turn on one of four fixed current sources for the duration of the  $1 \mu$  sec pulse. Thus each current source delivers a fixed charge per event to its own integrating capacitor.

The analyzer plate voltage is a not very linear  $-4$  kV peak sawtooth. The repetition rate is  $100$  Hz in order to satisfy the temporal resolution requirements, simplify power dissipation problems, and eliminate effects associated with the particle transit time through the analyzer. The control circuit divides each  $10$  millisecond sweep into four time intervals and a small reset interval as shown in an idealized representation in fig. 3. The control circuitry insures that all events detected during the first time interval are recorded by the first capacitor, those detected in the second time interval are recorded by the second capacitor, etc. Thus each time interval corresponds to an equivalent energy channel as shown and a four point differential energy spectrum can be obtained. This timing sequence is repeated for each sweep. The particular channel width pattern shown in fig. 3 is chosen as a compromise in view of the expected energy spectrum with a  $5$  keV e-folding energy above  $10$  keV and the possibility of even larger fluxes below  $10$  keV. In all cases, these energy intervals are large compared to the analyzer's resolution for mono-energetic particles.

Because of the wide dynamic range in counting rate required in auroral experiments, it is desirable that the capacitor voltage corresponding to a single count be identifiable above the telemetry noise level;

we have assumed that a 50 millivolt signal can be distinguished above this noise. Consequently, the discriminator pulse width, current source, and integrating capacitor are adjusted to yield increments of 50 millivolts per event. The minimum counting rate is therefore determined by the detector background counting rate, 1-2 counts/second.

In order to remain within the 5 volt limitation in the output voltage to the telemetry system, the integrating capacitors are reset to 0 volts once the 5 volt level is attained, i.e., 100 counts accumulated. The system is therefore equivalent to a scale factor of 100; the instantaneous capacitor voltage provides the interpolation between resets. At high counting rates, it is only necessary to count the number of resets. Figure 4 is a tracing of an oscilloscope photograph showing the simultaneous outputs to the telemetry of the four energy channels for an incident 6 keV  $H^0$  beam for a 5 second time period.

The low voltage, the CCM high voltage, and deflection plate high voltage supplies are conventional in nature and will not be described further. The total instrument weight is four pounds and the power consumption six watts. The  $2 \mu\text{gm cm}^{-2}$  carbon foils, which are mounted on an 80% transparent grid, have been successfully tested under Nike-Tomahawk vibration and g loading conditions.

We wish to acknowledge the important contributions of R. M. Alexander to the electronic design and of E. C. Offer to the construction and test of the instrument.

TABLE 1

Measured Scattering Angles, Energy Loss, and Detection  
Efficiency Over the Energy Range 2-10 keV

<u>Energy (keV)</u>	<u>Scattering Angle</u>	<u>Energy Loss (keV)</u>	<u>Efficiency</u>
2		0.75	$2.8 \times 10^{-3}$
3	18	0.95	$2.9 \times 10^{-3}$
4	14	1.0	$5.0 \times 10^{-3}$
5	11	1.15	
6		1.3	$1.7 \times 10^{-2}$
7		1.35	$2.5 \times 10^{-2}$
8	7	1.5	
9		1.65	$2.9 \times 10^{-2}$
10	5	1.55	$3.5 \times 10^{-2}$

## LIST OF REFERENCES

1. J. W. Chamberlain, "Physics of the Aurora and Airglow", Academic Press Inc., New York, 1961.
2. S. I. Akosofu, Planetary Space Science, 12, 905 (1964).
3. J. C. Brandt and D. M. Hunter, Planetary Space Science, 14, 95 (1966).
4. P. A. Cloutier, Planetary Space Science, 14, 809 (1966).
5. T. N. L. Patterson, F. S. Johnson, and W. B. Hanson, Planetary Space Science, 11, 767 (1963).
6. F. S. Mozer and P. Bruston, J. Geophys. Res., 72, 1109 (1967).
7. D. Evans, J. Geophys. Res., 72, 4281 (1967).
8. Purchased from the Yisum Research Development Co., Jerusalem, Israel.
9. S. K. Allison, Rev. Mod. Phys., 30, 1137 (1958).
10. J. D. Jackson, "Classical Electrodynamics", (John Wiley & Sons Inc., New York, 1962).
11. E. Fermi and E. Teller, Phys. Rev., 72, 399 (1947).
12. R. L. Wax and W. Bernstein, Rev. Sci. Instr., 38, 1612 (1967).
13. See for example, D. S. Evans, Rev. Sci. Instr., 36, 375 (1965).

**FIGURE CAPTIONS**

**Figure 1.** Schematic representation of the electrostatic analyzer, charged particle deflection arrangement, and detectors.

**Figure 2.** Block diagram of the electronic system.

**Figure 3.** Idealized representation of the method used to define the four energy channels. The "On" times of the channels are indicated by the shaded areas.

**Figure 4.** Tracing of the outputs of the four energy channels to the telemetry system for an incident 6 keV  $H^O$  beam. The duration of this data sample is 5 seconds.



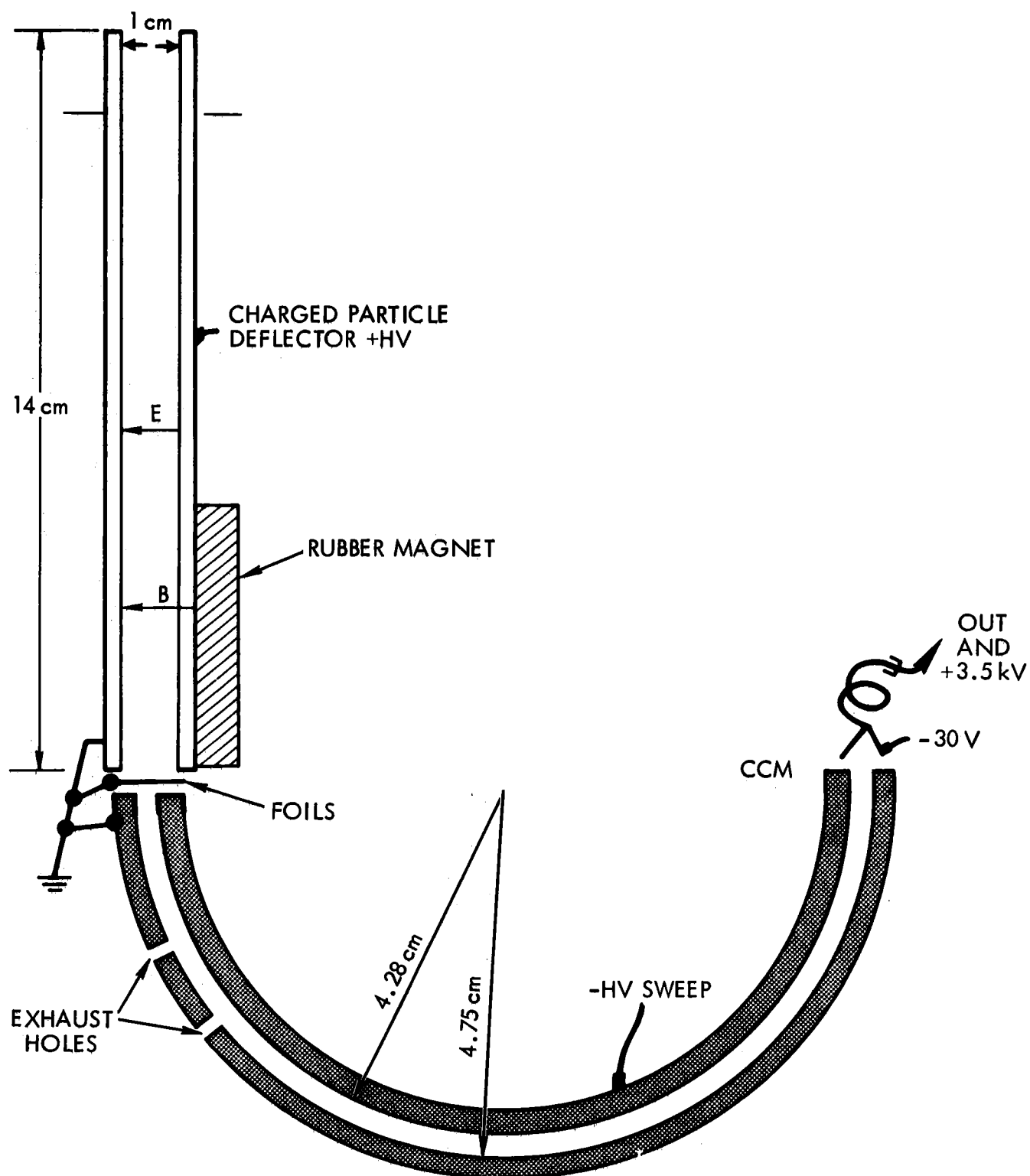


Figure 1. Schematic representation of the electrostatic analyzer, charged particle deflection arrangement, and detectors.

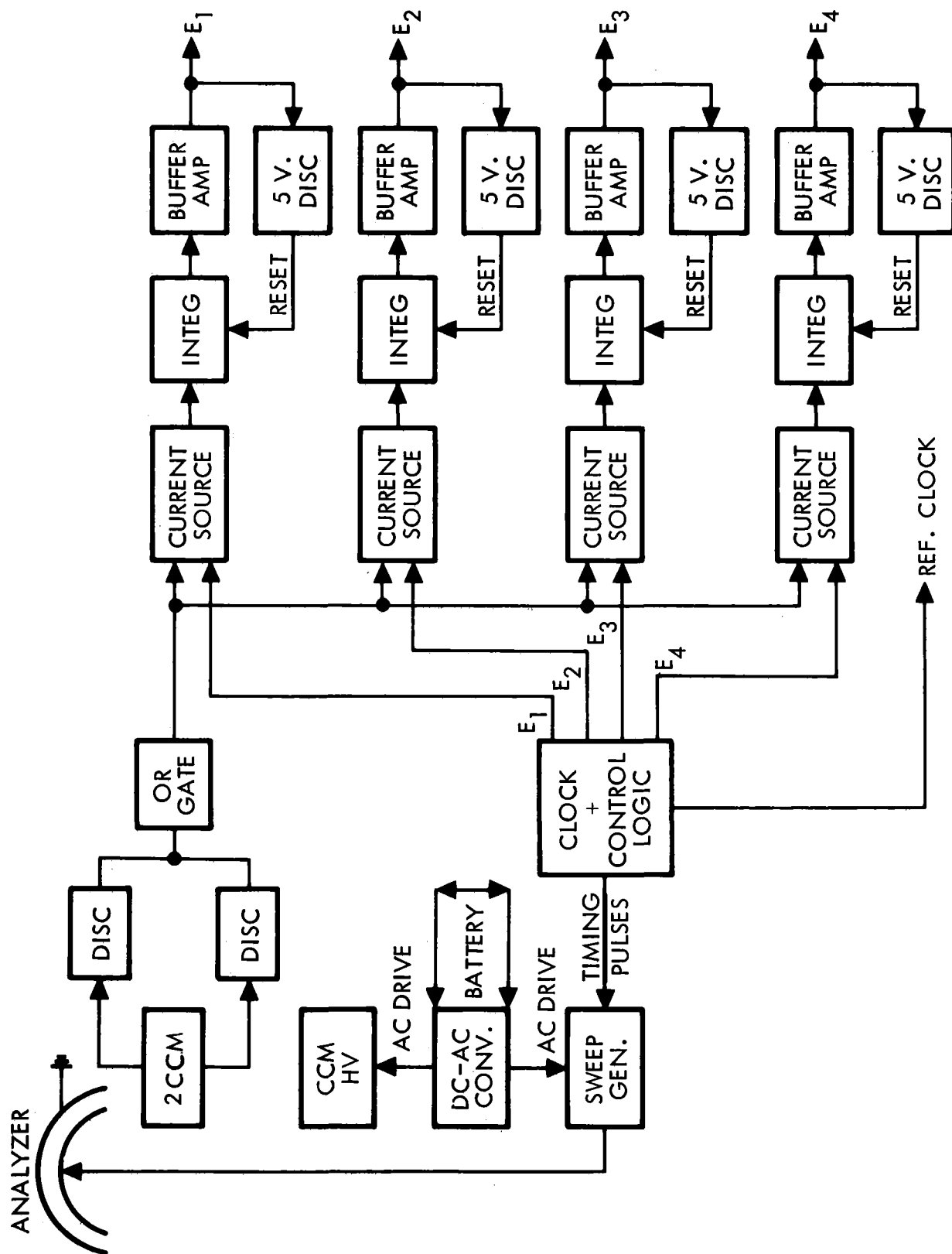


Figure 2. Block diagram of the electronic system.

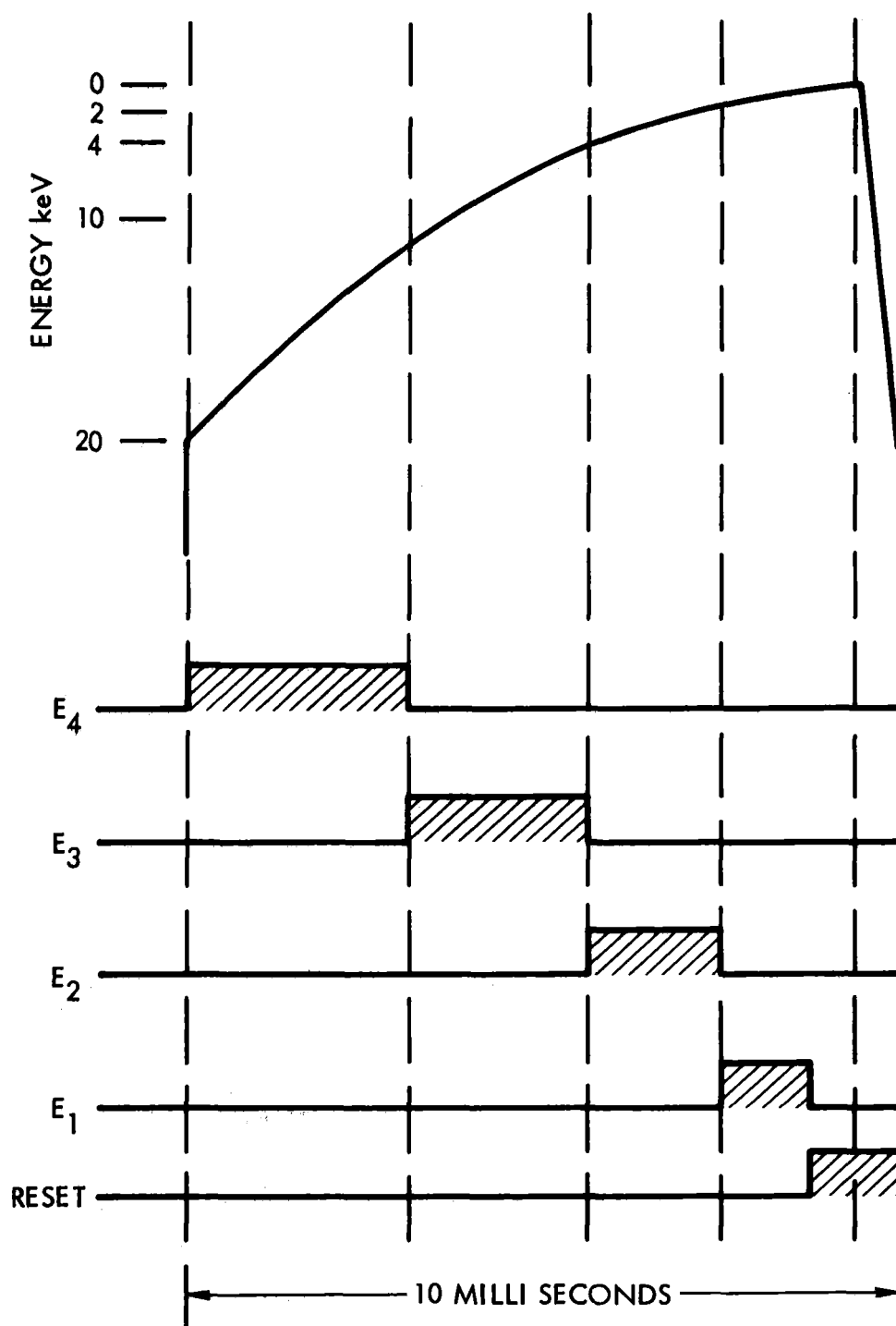


Figure 3. Idealized representation of the method used to define the four energy channels. The "On" times of the channels are indicated by the shaded areas.

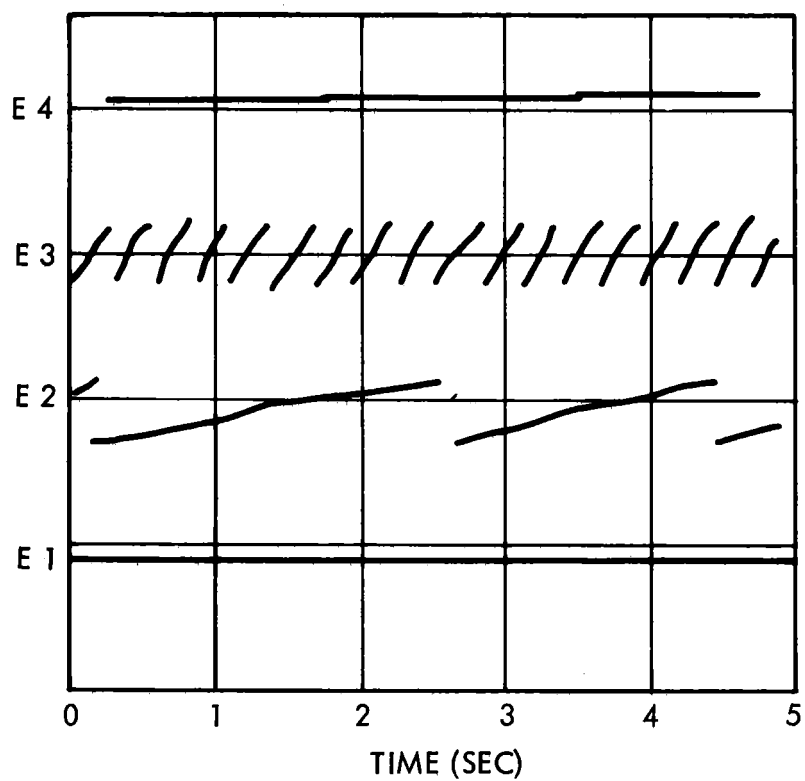


Figure 4. Tracing of the outputs of the four energy channels to the telemetry system for an incident 6 keV  $H^O$  beam. The duration of this data sample is 5 seconds.

## Energy-Independent Detector for Total Hydrogen Fluxes in the Range 1-10 keV for Space and Laboratory Applications\*

R. L. WAX AND W. BERNSTEIN

TRW Systems Inc., Redondo Beach, California 90278

(Received 9 June 1967)

An energy-independent instrument capable of detecting total hydrogen fluxes (either  $H^0$  or  $H^0+H^+$ ) in the energy range 1-10 keV has been developed. Low extreme ultraviolet sensitivity has been achieved by scattering of the incident particles in a thin carbon foil to a detector located in an off-axis position. Energetic electrons are removed by a magnetic field. Measurements of the ratio of the neutral to total fluxes leaving the foil, the angular distribution of the scattered particles, and the energy lost in transit of the foil are presented. The instrument has an efficiency for energetic hydrogen of 0.7%, an euv sensitivity of  $2 \times 10^{-3}\%$ , and a geometrical factor of  $0.06 \text{ cm}^2 \text{ sr}$ .

To date, the direct measurement of energetic (1-10 keV) hydrogen atoms has not been attempted in space experiments. The presence of large fluxes ( $10^8/\text{cm}^2 \text{ sec}$ ) of these particles has been identified in auroral displays through observation of Doppler-shifted  $H\alpha$  and  $H\beta$  light emission.<sup>1</sup> Akasofu<sup>2</sup> has proposed that large fluxes ( $10^9/\text{cm}^2 \text{ sec}$ ) of these particles are emitted by the sun during periods of flare activity in order to account for specific geomagnetic phenomena. Subsequent estimates by Brandt and Hunter<sup>3</sup> and by Cloutier<sup>4</sup> have reduced these flux estimates to  $\sim 10^8/\text{cm}^2 \text{ sec}$  because of uv and electron impact ionization in the solar corona. Although the geomagnetic phenomena can no longer be explained at these lower flux levels, the measurement of neutral atom fluxes still may provide a useful diagnostic of solar processes. Lastly, the observation of Doppler-broadened  $Ly_\alpha$  radiation from the interplanetary medium indicates the existence there of energetic  $H^0$  atoms. Patterson *et al.*<sup>5</sup> have suggested that these particles are produced at the shock interface between the solar wind and the interstellar magnetic field; they estimate this return flux to be  $\sim 1\%$  of the solar wind proton flux at the orbit of the earth.

The characteristics required for a useful flight instrument for total flux measurements include (1) high efficiency and sensitivity, (2) extreme ultraviolet (euv) and visible light rejection, (3) vacuum operation, (4) energy independence, (5) the ability to measure with equal efficiency  $H^0$  and  $(H^0+H^+)$ , and (6) the instrument must meet the typical constraints of flight instruments including survival, life, power, size, and weight. An instrument which can satisfy these requirements would also be useful in laboratory high energy plasma experiments.

A variety of techniques are employed for the measurement of fluxes of energetic  $H^0$  atoms produced in high energy plasmas. These include solid state detectors, CsI scintillators, Faraday cups, and proportional counters.<sup>6</sup> None of these techniques satisfy all the listed requirements.

One technique for the reduction of euv sensitivity relative to the particle sensitivity is by scattering of the particles during their transit of thin foils so that the detector need no longer be in the direct light path, because it does not appear possible to produce a detector of 1-10 keV atoms which is insensitive to euv over the range 300-1500 Å. Scattering of particles to off-axis points is required because sufficiently thin foils opaque over the entire uv spectrum are nonexistent and the problem of pin holes would always be present. Since most of the particles that leave the foil are neutral,<sup>7</sup> the detection system employed must be independent of the charge state. On the other hand, a fraction of the incident neutral atoms is charged on exit from the foil; therefore, energy analysis of this fraction is possible.

In the following sections, measurements of the charged and neutral fractions leaving the foil, the scattering angular distribution, and the energy loss for the energy range 1-10 keV are described for an  $\sim 2 \mu\text{g}/\text{cm}^2$  carbon foil.<sup>8</sup> The atomic and ionic beams used in this experiment are produced in a bombardment source; velocity and energy analyzers select monoenergetic  $H^+$  or  $H_2^+$  ions. These are then passed through a water vapor cell to produce selected beams of  $H_2^0$ ,  $H^0$ ,  $H^+$ , or  $H^-$ . For an  $H_2O$  vapor pressure of  $2 \times 10^{-2} \text{ mm Hg}$  and 5 cm cell length, the energy lost by the particles in transit of the cell is about 50 eV. Beam fluxes as high as  $10^{11}/\text{cm}^2 \text{ sec}$  are obtained.

### CHARGED TO NEUTRAL RATIOS

The ratio  $H^0/(H^0+H^+)$  is determined by using an electrostatic deflection system to remove the charged com-

\* This work was initiated under the TRW Independent Research program and was subsequently supported by NASA under contract number NASW-1474.

<sup>1</sup> J. W. Chamberlain, *Physics of the Aurora and Airglow* (Academic Press Inc., New York, 1961).

<sup>2</sup> S. I. Akasofu, *Planetary Space Sci.* **12**, 905 (1964).

<sup>3</sup> J. C. Brandt and D. M. Hunter, *Planetary Space Sci.* **14**, 95 (1966).

<sup>4</sup> P. A. Cloutier, *Planetary Space Sci.* **14**, 809 (1966).

<sup>5</sup> T. N. L. Patterson, F. S. Johnson, and W. B. Hanson, *Planetary Space Sci.* **11**, 767 (1963).

<sup>6</sup> G. W. McClure and D. L. Allensworth, *Rev. Sci. Instr.* **37**, 1511 (1966).

<sup>7</sup> S. K. Allison, *Rev. Mod. Phys.* **30**, 1137 (1958).

<sup>8</sup> Purchased from The Yissum Research Development Co., Jerusalem, Israel.

TABLE I. Ratio of  $H^0$  to total flux at various energies for thin carbon and aluminum foils.

Energy	Carbon	Aluminum*
2 keV	$0.86 \pm 0.01$	—
3	0.85	—
4	0.84	0.856
5	0.85	—
6	0.83	—
7	—	0.840
8	0.80	—
10	0.78	0.818

\* Values for a clean aluminum foil from Allison.<sup>7</sup>

ponent of the emergent beam prior to detection. In Table I, the ratio of the  $H^0$  to the total flux is given as a function of incident particle energy. Of the charged fraction, approximately one third appears as  $H^-$ . Although Allison<sup>7</sup> does not tabulate data for carbon foils, these results appear to be consistent with the tabulated values for other foil materials. His values for a clean aluminum foil are given in Table I.

### ANGULAR DISTRIBUTIONS

The angular distributions resulting from scattering of a pencil beam of monoenergetic  $H^0$  atoms during transit of the  $2 \mu\text{g}/\text{cm}^2$  carbon foil are measured by placing a  $1 \text{ cm}^2$  detector approximately 6 cm behind the foil and moving it in a plane perpendicular to the foil. Figure 1 shows the dependence on incident energy of the half angle of the scattered distribution. The observed  $1/E$  dependence of the half angle is in agreement with classical scattering theory.<sup>9</sup>

The theoretical angular distribution of the flux leaving the foil is gaussian at small angles and varies as  $\theta^{-3}$  at large angles, where  $\theta$  is the angle between the beam axis and

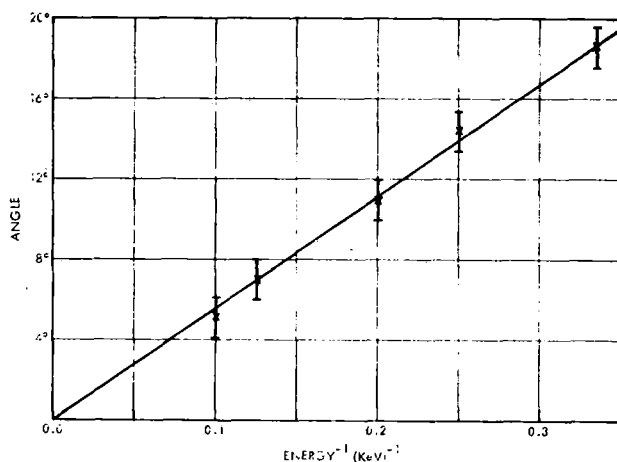


FIG. 1. The half angle at half maximum of the angular distributions for incident neutral hydrogen beams scattered by an  $\sim 2 \mu\text{g}/\text{cm}^2$  carbon foil plotted as a function of incident energy.

\* J. D. Jackson, *Classical Electrodynamics* (John Wiley & Sons, Inc., New York, 1962).

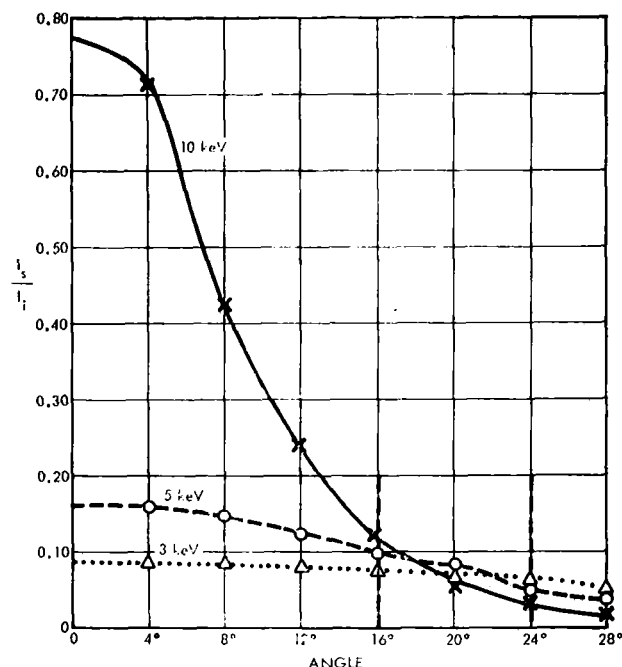


FIG. 2. The ratio of the scattered flux to the total incident flux at 3, 5, and 10 keV given as a function of the angle from the axis of the incident beam for a thin pencil beam of neutral hydrogen incident on an  $\sim 2 \mu\text{g}/\text{cm}^2$  carbon foil.

the detector. Because a foil thickness of  $2 \mu\text{g}/\text{cm}^2$  represents only about 10 collision mean free paths, the angle at which the distribution passes from a gaussian to an inverse cubic is smaller than that predicted by simple classical theory, which assumes many collisions. The value of the half angle at 10 keV calculated for a gaussian distribution is 0.179 rad, whereas the value for an inverse cubic dependence is 0.081 rad. At 10 keV, the measured

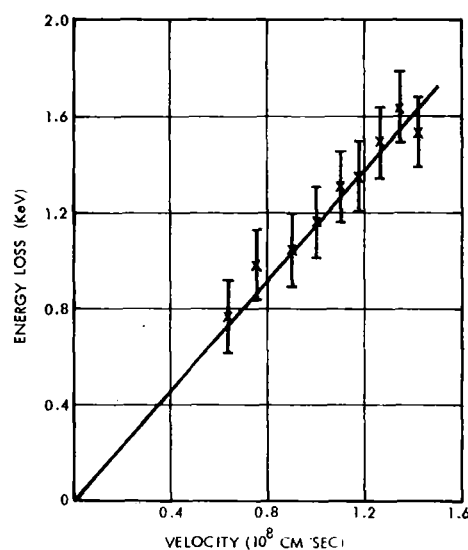


FIG. 3. A plot of the energy lost by a neutral hydrogen particle traversing an  $\sim 2 \mu\text{g}/\text{cm}^2$  foil as a function of the incident velocity of the atom.

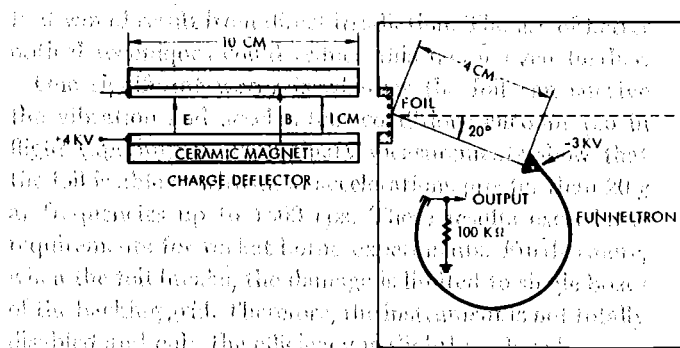


FIG. 4. A schematic diagram of the total hydrogen flux detector. The half angle is 0.089 rad, and therefore the inverse cubic distribution is dominant even at angles as small as the half angle.

In Fig. 2, plots of the angular distributions for three energies (10, 5, and 3 keV) are given. The ordinate is the ratio of the observed scattered intensity at a given angle to the total beam intensity incident upon the foil; this ratio therefore represents the efficiency of the detection arrangement. At a detector angle of  $\sim 20^\circ$ , the observed efficiency is seen to be nearly independent of energy and to be  $\sim 7\%$ . A variation of the detector area or its distance from the foil only produces a change in the efficiency. Thus, at a detector angle of  $20^\circ$ , it is possible to achieve energy independence over at least the energy range 3–10 keV. At this  $20^\circ$  angle, the detector is no longer in the direct particle or light path, and the only photons which can reach the detector also must be scattered.

### ENERGY LOSS

A hemispherical electrostatic analyzer is used to measure the energy distribution of the charged particles leaving the foil. Because of the charge exchange and stripping reactions occurring in the foil, only  $\sim 10\%$  of the emergent particles are charged and available for analysis. The dependence of the energy loss on incident velocity for both protons and neutral atoms is the same and is given in Fig. 3. These data extend the experimental measurements of Wilcox<sup>10</sup> and of Warshaw<sup>11</sup> into the 1–10 keV range. The energy loss is a linear function of the particle's velocity in agreement with the theoretical predictions of Fermi and Teller.<sup>12</sup> In addition, the observed energy loss of 1.6 keV at 10 keV compares favorably with the value of 1.5 keV as calculated from the simplest Fermi-Teller model for a  $2 \mu\text{g}/\text{cm}^2$  carbon foil. The energy loss data indicate that protons and hydrogen atoms with energies as low as 1 keV can easily pass through the foil. An energy spectrometer for energetic neutral atoms has been built using this energy loss data to obtain the incident spectrum.

<sup>10</sup> H. A. Wilcox, Phys. Rev. **74**, 1743 (1948).

<sup>11</sup> S. D. Warshaw, Phys. Rev. **76**, 1759 (1949).

<sup>12</sup> E. Fermi and E. Teller, Phys. Rev. **72**, 399 (1947).

### DESCRIPTION OF THE INSTRUMENT

A schematic illustration of the  $\text{H}^0$  total flux detector is shown in Fig. 4. The transverse magnetic field, 200 G produced by rubber magnets, removes incident omnidirectional electrons with energies as high as 100 keV. The electrostatic deflection plates with an applied voltage of 4 kV remove incident omnidirectional protons with energies up to 28 keV. Thus, when the instrument is operated with and without the electrostatic deflection voltage, it is capable of measuring  $\text{H}^0$  alone and ( $\text{H}^0 + \text{H}^+$ ) without interference from electrons over at least the energy range 1–10 keV. The  $2 \mu\text{g}/\text{cm}^2$  foil is mounted on a 0.5 mm mesh nickel wire grid with a transparency of  $\sim 80\%$  to provide mechanical support. The detector, which is placed 4 cm behind the foil and at an angle of  $20^\circ$  to the middle of the foil, is a Bendix funnel-type channeltron<sup>13</sup> with a circular sensitive area of  $0.19 \text{ cm}^2$ . Preliminary calibration data show that the detection efficiency of the funneltron for incident  $\text{H}_2^+$ ,  $\text{H}^+$ , and  $\text{H}^0$  is at least 50% and is relatively independent of energy over the range 1–10 keV. The funneltron normally is operated with a negative voltage of 3 kV applied to the entrance and a  $100 \text{ k}\Omega$  load resistor attached to the collector. A pressure of less than  $5 \times 10^{-4} \text{ mm Hg}$  is required for satisfactory operation of the detector.

In Table II, the observed efficiency is given over the energy range 1–10 keV. If incident  $\text{H}_2$  is considered to be a single particle, the resulting efficiencies over the entire energy range are twice those for an incident  $\text{H}^0$  beam. These efficiencies are lower than those shown in Fig. 2 primarily because of the reduced detector area. Increased efficiency can be obtained by use of several funneltrons to increase the detecting area.

The euv sensitivity at 1188 Å is determined with a vacuum uv source; the incident euv flux is calibrated with a CuBe electron multiplier. With Hinteregger's data<sup>14</sup> for the photoelectric efficiency of Be (Weissler<sup>15</sup> suggests that these data are valid for oil-contaminated Be such as is used in this experiment), an euv efficiency of  $2 \times 10^{-5}$  counts/photon is obtained for the  $\text{H}^0$  detector. Thus, operation at an angle of  $20^\circ$  decreases the ratio of the euv sensitivity to the  $\text{H}^0$  sensitivity by a factor of about  $10^2$  from the ratio

TABLE II. Efficiency of the total detector at various energies.

Energy	Efficiency
2 keV	$7.3 \pm 2.2 \times 10^{-3}$
4	$7.1 \pm 1.8$
6	$8.2 \pm 2.8$
8	$6.2 \pm 1.2$
10	$6.4 \pm 0.8$

<sup>13</sup> See, for example, D. S. Evans, Rev. Sci. Instr. **36**, 375 (1965).

<sup>14</sup> H. Hinteregger, Phys. Rev. **96**, 538 (1954).

<sup>15</sup> G. L. Weissler, *Encyclopedia of Physics*, S. Flugge, Ed. (Springer-Verlag, Berlin, 1958), Vol. 21, p. 352.

that would result from direct irradiation. The use of better optical techniques could reduce this factor even further.

One significant worry is whether the foil can survive the vibration and acceleration conditions encountered in flight experiments. Preliminary measurements show that the foil is able to withstand accelerations greater than 20 *g* at frequencies up to 1500 cps. These results exceed the requirements for rocket-borne experiments. Furthermore, when the foil breaks, the damage is limited to single boxes of the backing grid. Therefore, the instrument is not totally disabled and only the efficiency is slightly reduced.

The described instrument appears to be adequate for measurement of the neutral hydrogen fluxes expected in proton auroras and for the return flux expected in the interplanetary medium. The characteristics of the instru-

ment include an acceptance geometrical factor of 0.06 cm<sup>2</sup> ster, an H<sup>0</sup> efficiency of 0.7%, and an euv efficiency of  $2 \times 10^{-3}$  %. The instrument is extremely simple and rugged; the power, weight, volume, and survival characteristics are consistent with the requirements of flight experiments.

#### ACKNOWLEDGMENTS

We wish to thank N. L. Sanders for helpful discussions. A. L. Berg mounted the foils and together with R. Alexander performed the foil vibration tests; D. Judge conducted the euv efficiency tests. We are particularly indebted to E. Offer for construction of the instrument and maintenance of the experimental apparatus.



## Technique for the Generation of Quasi-isotropic 1-10 keV Proton Fluxes\*

W. BERNSTEIN, N. L. SANDERS, AND R. L. WAX

TRW Systems Inc., Redondo Beach, California 90278

(Received 9 June 1967)

**I**SOTROPIC proton fluxes in the energy range 1-20 keV are encountered in the earth's magnetosphere and other regions of space. These fluxes usually are small compared to those encountered in the laboratory and therefore instruments with relatively large acceptance angles ( $15^\circ$  half angle) are required.<sup>1</sup> The typical method for determining the resolution and geometrical factor for these instruments is to use a monoenergetic pencil beam and to carry out a large number of measurements over many angles and positions.

A new technique for performing these measurements is described. A pencil beam of mono-energetic protons, which impinges upon an  $\sim 2 \mu\text{g}/\text{cm}^2$  carbon foil placed at the entrance of a detector, generates a quasi-isotropic flux of particles simulating the conditions under which the instruments are employed. Figure 1 shows the angular distribution of a scattered 3 keV proton beam emerging from the foil. As can be seen, the half angle of this distribution is  $27^\circ$ . Because a static beam represents only a point source, it is necessary to sweep the pencil beam across an area of foil larger than the entrance aperture of the detector to produce quasi-isotropic fluxes. Sweeping of the pencil beam is accomplished by electrostatic deflection plates. The frequency of the sweep should be fast compared with the sampling time of the instruments. At 3 keV this scattered flux is isotropic to within  $\sim 3\%$  over an angular spread of  $10^\circ$ . The energy loss in the foil at 3 keV is 900 eV. The dependence on energy of the angu-

lar distribution, energy loss, and charged fraction of the scattered beam are described elsewhere.<sup>2</sup>

As an example of this technique, Fig. 2 shows the dependence of resolution on energy of a  $90^\circ$  cylindrical electrostatic analyzer having a calculated full width at one half maximum of 11% for an isotropic beam and an acceptance half angle of  $3.5^\circ$ . Significant straggling is seen only at incident beam energies below 6 keV and correction for this effect can be made easily. A resolution of 6% is

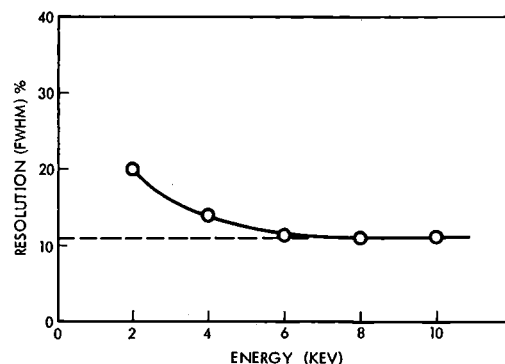


FIG. 2. A plot of the measured resolution of a  $90^\circ$  cylindrical electrostatic analyzer vs incident energy obtained by using the quasi-isotropic flux from a carbon foil (solid line). The dashed line gives the calculated resolution (full width at one half maximum) for isotropic fluxes.

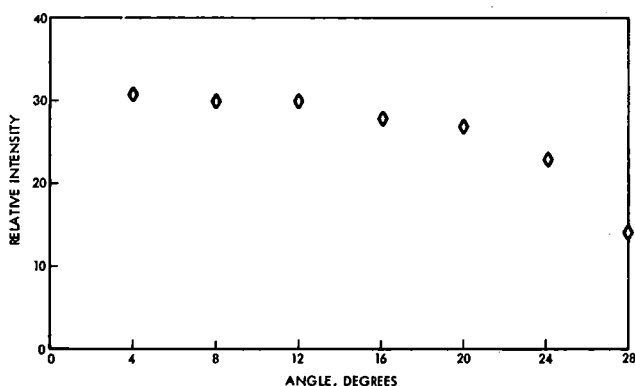


FIG. 1. A plot of the scattered intensity as a function of angle for a 3 keV proton beam incident on an  $\sim 2 \mu\text{g}/\text{cm}^2$  carbon foil.

obtained when a mono-energetic pencil beam is used to measure the resolution at the center of the aperture; therefore, the resolution is significantly different for isotropic fluxes. By using a Faraday cup to determine the total beam flux, the omnidirectional geometrical factor is measured in one step and without involved calculations. For this  $90^\circ$  analyzer the calculated omnidirectional geometrical factor is  $1 \times 10^{-4} \text{ cm}^2$  and the measured value is  $(1.7 \pm 0.5) \times 10^{-4} \text{ cm}^2$ . While the measured values of resolution and geometrical factor for this instrument agree well with the calculated values, it is still generally desirable to calibrate any instrument with the type of beam it is designed to measure.

\* This work was supported by NASA under Contract No. NASW-1474.

<sup>1</sup> L. A. Frank, J. Geophys. Res. **72**, 185 (1967).

<sup>2</sup> R. L. Wax and W. Bernstein, Rev. Sci. Instr. (to be published in Nov. 1967).

## Preliminary Report on Detection of Electrostatic Ion Waves in the Magnetosphere

F. I. SCARF, G. M. CROOK, AND R. W. FREDRICKS

*TRW Space Technology Laboratories, Redondo Beach, California*

**Abstract.** The Lockheed-Aerospace P11 satellite (1964-45A) launched into a polar eccentric orbit on August 15, 1964, included in its payload a VLF electric field experiment supplied by TRW Space Technology Laboratories. Measurements in the frequency range 1.7 to 14.5 kc/s reveal that the indicated background rarely falls below  $10^{-3}$  volt/m and that sustained field enhancements with  $E \simeq 20$ –100 mv/m are generally detected in regions where energetic electrons are precipitated from the Van Allen belts. The experiment is described; some early results are presented; and an interpretation in terms of electrostatic ion waves is given. The possibility that large-amplitude ion waves cause diffusion across  $L$  shells and magnetospheric electron acceleration is also discussed.

### INTRODUCTION

In 1962, one of the authors (G. M. Crook) was invited to supply a VLF electric field experiment for a Lockheed-Aerospace satellite to be placed in orbit during an Air Force launch. A charge-sensitive ac electrometer was designed, and on August 15, 1964, the P11 satellite, 1964-45A, was launched into a near polar eccentric orbit (apogee 3720 km, perigee 268 km, inclination  $96^\circ$ ). In this note we describe the experiment, present some early data, and suggest an interpretation in terms of electrostatic oscillations in the magnetospheric plasma.

The fields are measured in four VLF channels ranging from 1.7 to 14.5 kc/s, and the main results for orbits near the 2 o'clock meridian may be summarized as follows: (1) the indicated background field levels are generally in the range of 1–2 mv/m with occasional dips to 600–800  $\mu$ v/m; (2) frequent persistent enhancements (duration of the order of 3–10 minutes) are found on the night side of the earth with average fields generally from 20 to 100 mv/m and occasional maximums in the volt per meter range; (3) these night-side enhancements are strongly correlated with the characteristics of precipitating energetic electrons as determined by Aerospace Corporation particle detectors on the same spacecraft. The broad peaks also tend to fall near certain  $L$ -shell bands.

The indicated electric field strengths are considerably higher than those that would be con-

sistent with whistler background and peak values derived from VLF magnetic measurements, and it is therefore most tempting to try to interpret the data in terms of electrostatic or longitudinal plasma oscillations. In section 2 some general properties of ion waves are discussed and the anticipated theoretical background and peak field strengths for the upper ionosphere ( $h \simeq 500$ –600 km) and the transition region are given. Section 3 contains a brief description of earlier attempts to measure VLF electric fields above the ionosphere, and the TRW/STL experiment is discussed in section 4. In section 5, P11 data for fairly typical orbits (47, 85) are presented and correlated with ephemeris parameters and response of the Aerospace Corporation solid-state particle detector. The physical significance of these findings is discussed in section 6, and some estimates of sheath effects are given in the Appendix.

### GENERAL PROPERTIES OF ION WAVES

In a collisionless magnetized plasma, three distinct modes of wave propagation are possible. They may be classified as transverse Alfvén waves, fast or magnetosonic oscillations, and longitudinal or electrostatic modes. The last represents density irregularities, and the associated fluctuating electric fields have

$$\mathbf{E} = -\nabla\phi \quad \phi = \phi_0 \cos(\mathbf{k} \cdot \mathbf{r} - \omega t) \quad (1)$$

There are two spectral regions in which electrostatic waves have sizable intensities; for  $\mathbf{k}$  parallel to the applied field,  $\mathbf{B}_0$ , the high-fre-

quency branch (electron plasma oscillations) has

$$\omega^2 \simeq \omega_p^2 + 3k^2 a^2/2 + \dots \quad 0 < k < k_D \quad (2)$$

and the dispersion relation for the low-frequency branch (ion waves) is approximately

$$\frac{1}{\omega^2} \simeq \frac{M}{k^2 \kappa T_e} + \frac{1}{\Omega_p^2} + \dots \quad 0 < k < K_D \quad (3)$$

Here  $\omega_p$  and  $\Omega_p$  are the electron and ion plasma frequencies,  $k_D$ ,  $K_D$  are the Debye wave numbers  $(4\pi N e^2 / \kappa T_e)^{1/2}$ , and  $\kappa T_e = \frac{1}{2} m a^2$ ,  $\kappa T_i = \frac{1}{2} M v^2$ . For  $\mathbf{k} \times \mathbf{B}_0 \neq 0$ , the dispersion relations are considerably more complex. At frequencies well below the ion cyclotron frequency,  $\Omega_i$ , the approximate generalization of equation 3 for finite angles is [Stix, 1962, p. 221]

$$\frac{1}{\omega^2} \simeq \frac{M}{k_{\parallel}^2 \kappa T_e} + \frac{1}{\Omega_p^2} + \frac{k_{\perp}^2}{k_{\parallel}^2} \frac{1}{\Omega_e^2} \quad (4)$$

and this reveals that waves with arbitrary angles between  $\mathbf{k}$  and  $\mathbf{B}_0$  (and hence  $\mathbf{E}$  and  $\mathbf{B}_0$ ) are allowed, but equation 4 can also be used to show that the group velocity remains quite close to the  $\mathbf{B}_0$  axis, as in whistler propagation.

Since ion waves are electrostatic, the only magnetic fields associated with these oscillations arise from the relative motion between the observer and the waves. If we attempt to detect an ion acoustic wave with a magnetic loop on a spacecraft moving with velocity  $\mathbf{V}$ , then

$$\Delta \mathbf{B} \simeq -\left(\mathbf{V} + \frac{\omega}{k^2} \mathbf{k}\right) \times \mathbf{E}/c^2 \quad (5)$$

This magnetic disturbance is generally many orders of magnitude smaller than  $nE/c$ , the value that would be associated with a VLF transverse wave (a whistler) having the same electric field strength. Thus, an electric field antenna must be used to detect ion waves, but an associated magnetic loop should be available to distinguish between electrostatic waves and occasional very large amplitude whistlers.

Ion waves are heavily damped if the plasma is in thermal equilibrium ( $T_e \approx T_i$ ) with negligible currents, gradients, and anisotropies. Nevertheless, the thermal or equilibrium amplitude for these waves in the magnetosphere is already extremely large in comparison with the natural

background for whistlers. Rostoker [1961] has shown that in the absence of any growth mechanisms the ion wave background is given by

$$\frac{E_n^2}{8\pi} \sim \frac{1}{(2\pi)^3} \int d^3k \frac{\kappa T_e}{2} \frac{K_D^2}{k^2 + K_D^2} \quad (6)$$

where the last factor in the integrand represents the Landau damping. In a typical application of equation 6, the output from an electric field antenna on a spacecraft might be passed through a narrow bandpass filter. If the filter is centered at  $f_0 = \omega_0/2\pi$ , with fractional half-width  $\delta$ , and if  $(\omega/k)_{\omega_0} \ll V$ , the spacecraft speed, the Doppler shift puts essentially the entire ion wave spectrum into the filter channel for  $\mathbf{k}$  parallel to  $\mathbf{V}$  while the integration in equation 6 runs approximately from  $k_0(1 - \delta/2)$  to  $k_0(1 + \delta/2)$  for  $\mathbf{k}$  perpendicular to  $\mathbf{V}$  [ $k_0 = k_0(\omega_0)$ ]. With these approximations, equation 6 yields

$$\begin{aligned} \langle E_n^2(\omega_0, \delta) \rangle &\simeq \kappa T_e K_D^3 [(u_+ + 1)^{1/2} \\ &\quad - (u_- + 1)^{1/2}] \\ u_{\pm} &= (k_0^2/K_D^2)(1 \pm \delta/2)^2 \end{aligned} \quad (7)$$

for  $\omega \ll \Omega_p$ . If  $\delta$  is small and  $k_0 \ll K_D$ , equation 7 becomes

$$\langle E_n^2 \rangle \simeq \kappa T_e K_D k_0^2 \delta \quad (8)$$

As an example of the application of equations 3, 7, 8 we consider the background amplitude expected with  $f_0 = \omega_0/2\pi = 1.7$  kc/s and  $\delta \simeq 0.15$  at an altitude of 500–600 km. Here  $T_e \simeq 1500^\circ\text{K}$ ,  $T_i \simeq 1000^\circ\text{K}$ ,  $M_i \simeq 5M_p$ , and  $N_e \simeq 5 \times 10^4 \text{ cm}^{-3}$ , so that  $f_{pi} = \Omega_p/2\pi = 21$  kc/s,  $K_D^{-1} = 0.98 \text{ cm}$ ,  $(\kappa T_e/M_i)^{1/2} = 1.56 \times 10^8 \text{ cm/sec}$ , and  $\lambda_0 (1.7 \text{ kc}) = 0.92 \text{ meter}$ . Thus,  $f_0 \ll f_{pi}$ ,  $k_0 \ll K_D$ ,  $(\omega/k)_{k_0} \ll V$ , and equation 8 should be valid; it gives

$$(E_n)_{\text{rms}} \simeq \begin{cases} 1.2 \times 10^{-8} \text{ statvolt/cm} \\ 360 \text{ } \mu\text{V/m} \end{cases} \quad (9)$$

At this altitude the VLF background seen by a magnetic loop is certainly less than  $10^{-3} \gamma$  [Gurnett and O'Brien, 1964]. For a typical geomagnetic field value of 0.3 gauss, the 1.7-kc/s whistler index of refraction is

$$n \simeq [f_p^2(e)/f_c(e)]^{1/2} \simeq 54$$

and the electric field amplitude for the 1.7-kc/s whistler background is then less than  $5.5 \text{ } \mu\text{V/m}$ .

Thus, the background ion wave field amplitude at  $h \simeq 500$ – $600$  km is already at least a factor of 60 larger than the VLF background for transverse waves (similar calculations may be carried out for higher altitudes and lower frequencies; equation 6 is valid wherever the plasma is in equilibrium, but the simplified expressions of equations 7 and 8 may be used only if  $\omega \ll \Omega_p$ ,  $\omega/k \ll V$ ).

However, ion wave field amplitudes in the magnetosphere and transition region should rarely be as small as the theoretical background level for an equilibrium plasma, e.g., the value predicted using equations 6 to 8. This is so because a variety of natural magnetospheric phenomena can serve to reduce the Landau damping and, in fact, to stimulate growing ion waves.

The particular instability that has been examined in the greatest detail is the drift or current instability that occurs when the ions and electrons have a finite relative velocity. The threshold velocity depends on the electron and proton temperatures, and a curve based on computations by Jackson [1960] and Fried and Gould [1961] for Maxwellian distributions is shown in Figure 1. At  $h \simeq 500$ – $600$  km,  $T_e/T_i \sim 1$ – $2$ , so that electron plasma oscillations and ion waves will both be stimulated by protons with  $\frac{1}{2}mv_p^2 > \kappa T_e$  or  $E_p$  (drift)  $> 200$ – $300$  ev. Near the subsolar transition region,  $T_e \simeq 1$ – $2 \times 10^7$  °K [Bame et al., 1964] and  $T_i \sim 10^6$  °K [Wolfe and Silva, 1964]; in this case  $T_e/T_i \gg 1$ , and protons with  $E_p$  (drift)  $\geq 1$  kev will generate ion waves but no electron plasma oscillations. Since large fluxes of streaming protons have been detected at low altitudes [Freeman, 1962] as well as in the transition region [Wolfe and Silva, 1964; Strong et al., 1964], it seems very likely that current instabilities do trigger growing ion waves throughout the magnetosphere and transition region. Ion wave instabilities are also associated with inhomogeneities [Krall and Rosenbluth, 1963] and with anisotropic velocity distributions [Harris, 1961].

For overstable (i.e., growing) ion waves, various nonlinearities become significant and lead to upper bounds for the potential amplitude,  $\phi_0(\text{max}) = \phi_M$ , and electric field,  $E(\text{max}) = E_M$ . No rigorous evaluations of these bounds are available, but several theoretical estimates based on analytic models [Klimontovich and Silin, 1961], physical arguments involving particle

trapping [Stix, 1964], and numerical experiments [Buneman, 1959; Dawson, 1959, 1962; Smith and Dawson, 1963] are all in fair agreement. These yield

$$\phi_0 \leq \phi_M \sim \kappa T_e / e \quad E \leq K_0 \phi_M \quad (10)$$

so that

$$E^2/8\pi \leq E_M^2/8\pi \approx \frac{1}{2} N \kappa T_e \quad (11)$$

At an altitude of 500–600 km,  $N \kappa T_e \simeq 10^4$  erg/cm<sup>3</sup>, and thus the absolute maximum ion wave field strength is of the order of 10 volts/m: although such extreme fields would be expected to occur rarely, if ever, at these very low altitudes, it is noteworthy that the motional magnetic field associated with such an enhancement might be just large enough to be detected by a VLF detector like that on Injun 3.

In the transition region,  $N \simeq 10$  electrons/cm<sup>3</sup> and  $T_e \simeq 2 \times 10^7$  °K, so that  $E_M$  is again of the order of 10 volts/m. Near the stagnation point, however, the solar wind itself should stimulate a more or less continuous beam-plasma overinstability [Bernstein et al., 1964; Kellogg, 1964; Scarf et al., 1965; Fredricks et al., 1965], and the peak field strength should remain close to the maximum. It is also important to note that, in this region, equation 10 predicts peak potential amplitudes of the order of hundreds of volts.

### 3. EARLY MEASUREMENTS OF MAGNETOSPHERIC ELECTRIC FIELDS

Various rockets and probes have carried instruments designed to measure dc and VLF electric fields in the ionosphere. Since recent theories [Farley, 1963; Buneman, 1963] suggest that even within the ionosphere a collision-dominated plasma instability involving neutrals, ions, and electrons will produce large-amplitude ion waves, it is of interest to reexamine the results of these low-altitude measurements. There is no direct relation between the theories applicable for wave production in the essentially collisionless plasma above 500–600 km and the collisional production mechanisms that appear to be valid within the ionosphere, but, since slow, short-wavelength, large-amplitude VLF electric oscillations are expected to be present in both regions, similar detection techniques should be successful or unsuccessful in the magnetosphere and ionosphere. In particular, low-frequency

electrostatic waves with  $\omega/k \lesssim V$  can be Doppler-shifted so that they are detected with a dc-type electrometer on a moving probe. The dc instruments may also pick up low-frequency electric field noise *directly* if the signal is demodulated by a bridge circuit designed to process a modulated dc input, since synchronous detectors of this type have essentially no ability to reject true noise of comparable amplitude. This is especially significant if instabilities allow ion wave fields to grow to their maximum values; a hypothetical steady-state plasma sheath surrounding the vehicle has a voltage drop of the order of

$$\phi_{\text{sheath}} \simeq \kappa T_e / 2e \ln T_e M / T_i m \quad (12)$$

in a distance of the order of a Debye length, but this sheath would be *violently* disturbed by electrostatic oscillations with fields of the order of  $k_D \kappa T_e / e$  (see equation 10).

The most extensive ionospheric field measurements in the altitude range  $125 \text{ km} < h < 450 \text{ km}$  were made by means of pairs of electrostatic fluxmeters on Soviet rockets [Gdalevich, 1964; Imyanitov *et al.*, 1964], and Sputnik 3 with apogee near 1850 km had similar instrumentation [Imyanitov and Shvarts, 1964]. A rotating screen converts the field strength at the pickup to 900-cps alternating voltage, which is filtered, amplified, and fed to a synchronous demodulator. Separate instruments are placed at two different positions on each flight in an attempt to distinguish between external electrostatic fields and those associated with the spacecraft potential and sheath.

On these flights, both fluxmeters generally indicated the presence of large-amplitude fields (of the order of 1–3 volts/cm). This would suggest an average spacecraft-plasma potential difference of several volts. Using the measured instantaneous potential difference between the two fluxmeters, however, it was argued that ionospheric or external electric fields with strengths ranging from 100 mv/m to 10 volts/m were also frequently encountered. These external fields generally varied rapidly and chaotically during the flights, and since synchronous demodulators were used it is reasonable to speculate that the Soviet instruments were in fact responding to electrostatic VLF (ion wave) noise rather than to true dc fields. (It should be noted that some Faraday cup plasma probes

have circuits similar to the electrostatic fluxmeters and may also be sensitive to ion waves.) Kavadas and Johnson [1964] used different techniques (perturbation of a VCO frequency) to determine field strengths in the *E* layer directly. They also found very large amplitudes ( $E \simeq 10\text{--}90 \text{ mv/m}$ ) during travel of the probe through a subvisual auroral display, and the values varied rapidly from point to point over distances of a few hundred meters or less, indicating passage through a region with sizable density irregularities.

Some properties of ionospheric VLF electric fields associated with density irregularities were apparently measured by Storey *et al.* [1964] during the flights of the FR-1 program rocket experiments in October 1963. The electric and magnetic field vectors in the wave fields of special 22.3-kc/s transmissions from NSS were carefully measured (amplitude, phase, and direction) during flights extending up to 170–190 km. The impedance of the electric field antenna was also determined. It was found that the VLF magnetic field behaved as expected, but that the VLF electric field sometimes did not. It was concluded that these electric field anomalies were associated with small-scale irregularities in the medium, and the measurements of wave propagation direction, magnetic field intensity, and power flux also indicated that larger-scale irregularities were present.

A VLF experiment designed to measure electric field strengths at  $15.5 \pm 0.05 \text{ kc/s}$  (NSS transmissions plus ambient noise) was provided for Explorer 6 by Stanford University. The signal received in a 108-Mc/s telemetry antenna was sent to a preamplifier-receiver system with a sensitivity of  $2 \mu\text{v/m}$  and a dynamic range of about 80 db. Between launch and passage through the *D* layer ( $h \simeq 67 \text{ km}$ ) the NSS transmission and atmospheric noise were received [Helliwell, 1960], although the solar paddles were then folded over the VLF antenna, reducing sensitivity by an estimated 30 db; this reduction apparently accounted for an absence of signal between the *D* layer and the first passage over the horizon at  $h \simeq 140 \text{ km}$ . The solar paddles were erected beyond sight of the tracking station, but in subsequent orbits (apogee  $\sim 7.5R_e$ ) no *strong* VLF signals were found, whereas interference from a local payload noise source became significant. No generally ac-

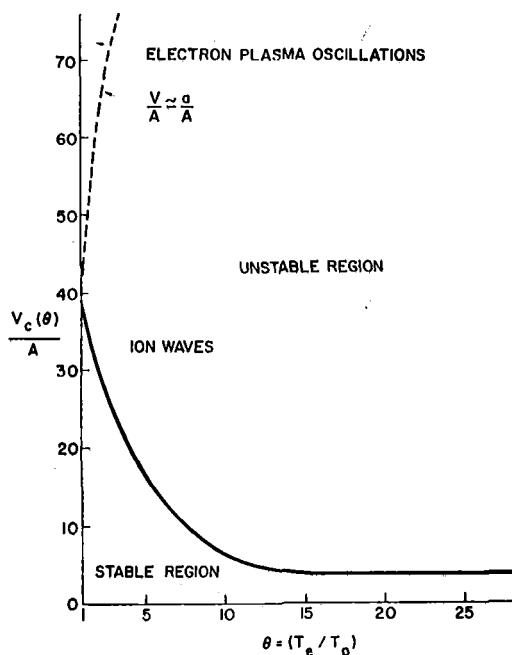


Fig. 1. The critical drift velocity  $V_c$  as a function of the electron-proton temperature ratio  $\theta$ . Here  $ma^2 = 2kT_e$ ,  $MA^2 = 2kT_p$ , and, for a given  $\theta$ , any velocity above the heavy line represents an unstable configuration. For a detailed discussion see Bernstein *et al.* [1964].

cepted explanation for this response has been given (Helliwell, private communication), but it is of interest that the extreme fading and scintillation of the Explorer 6 100-Mc/s telemetry signal could indicate the presence of large density irregularities with  $\lambda$  near 3 meters.

Electric field VLF measurements in the range 400 cps to 10 kc/s are also made on Alouette 1 at an altitude of 1000 km. The ambient signal from one of the long dipole sounder antennas (tip-to-tip lengths of 46 and 23 meters, respectively) is occasionally connected to a VLF receiver with an AGC loop which holds the output constant to within 3 db for an input variation of 60 db; the time constant is 0.2 second [Barrington *et al.*, 1963]. There appears to be little capability for precise measurements of VLF signal amplitude, but preliminary reports seem to indicate that the AGC system operates so that only relatively large-amplitude whistlers are detected. When no large-amplitude whistlers are present, 500-cps to 2-kc/s noise signals are commonly recorded. They could be associated with

ion waves, but since  $l_{\text{antenna}} \gg \lambda_{\text{ion wave}}$  the experiment is obviously not an optimum one for detection of short-wavelength electrostatic plasma oscillations.

Finally, it should be noted that ground-based radar backscatter is affected by density fluctuations in the plasma. Temperature-dependent corrections are needed, because the electromagnetic wave is scattered by an ion oscillation having approximately the same wavelength and an amplitude that depends on  $T_e/T_i$  through equation 6 (we are indebted to O. Buneman for pointing out this connection). Thus, a radar backscatter determination of  $T_e/T_i \approx 1.5$  at  $h \approx 500$ –600 km [Evans, 1964] ensures that above the transmitter the ion waves do have the appropriate thermal level indicated in equation 8.

#### 4. DESCRIPTION OF THE P11 VLF EXPERIMENT

This instrument was designed to measure VLF electric field amplitudes as efficiently and accurately as possible under somewhat unfavorable conditions of weight, power, telemetry, and antenna assignments. The experiment consists of a noise-measuring instrument with four filtered bandpass channels, and as high a threshold sensitivity and as wide a dynamic range as possible. At the time of design in late 1962, the only known published field intensity data on exospheric VLF phenomena were those of Cain *et al.* [1962] concerning the whistler signals observed with the Vanguard 3 magnetometer. The fact that the levels of the signals ranged from  $10^{-8}$  to 5  $\gamma$  indicated that occasional large-amplitude whistler signals might be encountered, justifying the need for a wide dynamic range.

Figure 2 shows a block diagram of the experiment. In addition to the four bandpass channels there was an 'overcounter.' This circuit is merely a count rate meter with a threshold fixed at the saturation level of the linear system so that when these circuits are overloaded the frequency of the overloading signal will be measured. The nominal trigger threshold value is 1 volt/m. Although the frequency of a continuous coherent signal would be indicated, if the signal were of short duration it would simply produce an output to signify that the signal had been received. The noise threshold of

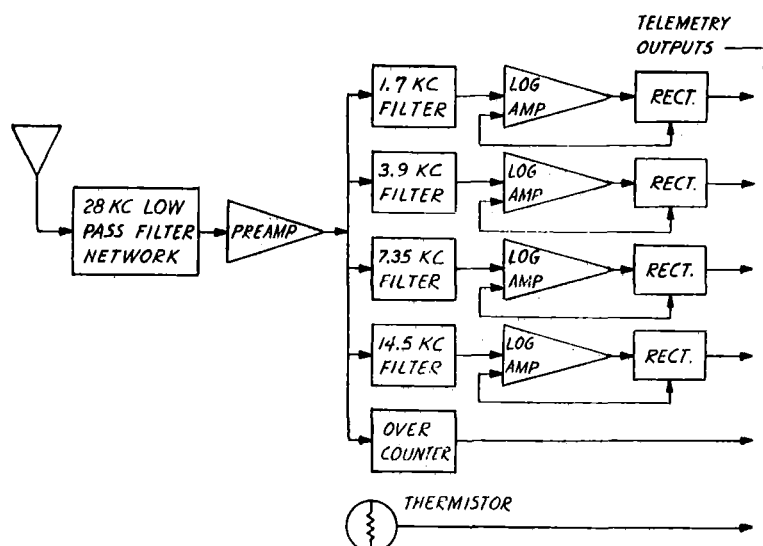


Fig. 2. Block diagram for the TRW/STL VLF electric field experiment on 1964-45A.

the experiment ranged from 300 to 600  $\mu\text{V}/\text{m}$ , and the dynamic range was greater than 70 db. The filters chosen for the experiment have center frequencies of 1.7, 3.9, 7.35, and 14.5 kc/s, with a bandwidth of 15% of center frequency.

Figure 3 shows a composite frequency response of the four bandpass channels from an automatic plot. The amplitudes are relative, because of the method of combining them. For convenience, all calibrations are referred to free-space values. Appropriate adjustments in values can be made for orbital position (see appendix).

One of the most serious considerations in the design of this experiment was the designing of the input circuit. The antenna assigned to the experiment is a standard telemetry antenna 18 inches long and  $\frac{3}{8}$  inch in diameter, with a calculated capacity of 5.3 picofarads. This capacity is the predominant component of the antenna output impedance. Extensive previous experience had shown that, if the input circuit of a noise detector of this general type contained elements that could be shock-excited so that they would 'ring,' serious errors in measurement could be made. To prevent ringing, all inductive circuits were critically damped or properly terminated.

Matching the highly reactive antenna impedance into an amplifier while maintaining damping and controlling frequency response presents quite a problem. Because the charac-

teristics of the antenna under various orbit conditions are variable and sometimes difficult to determine [Storey, 1963], it was decided that the purposes of the experiment would be better served by making the instrument appear capacitive, and thus a capacitive voltage divider consisting of the antenna capacity and the input capacitance of the preamplifier was formed. The resulting instrument is actually a charge-sensitive VLF electrometer rather than a receiver. As an electrometer, the instrument has a threshold sensitivity of the order of  $10^{-10}$  coulomb. It can therefore detect an equivalent excess charge of about 625 electrons on the antenna.

The experiment was assigned ten subcommutator points separated by 1 second, each point to be sampled once per 1.068 minutes. It was thought that, by arranging the points so that the frequency of the channel sampled increased and then decreased, it might be easier to recognize phenomena like whistlers and hiss. It is doubtful that such a simple system as this would allow the differentiation of chorus or other complicated forms of phenomena usually identified with the aid of an  $f-t$  analysis.

It was recognized at the outset that this instrument is far from an ideal sensor for whistlers and related phenomena, since the poor time resolution and threshold sensitivity are both limiting factors. Even in 1962, however, the ex-

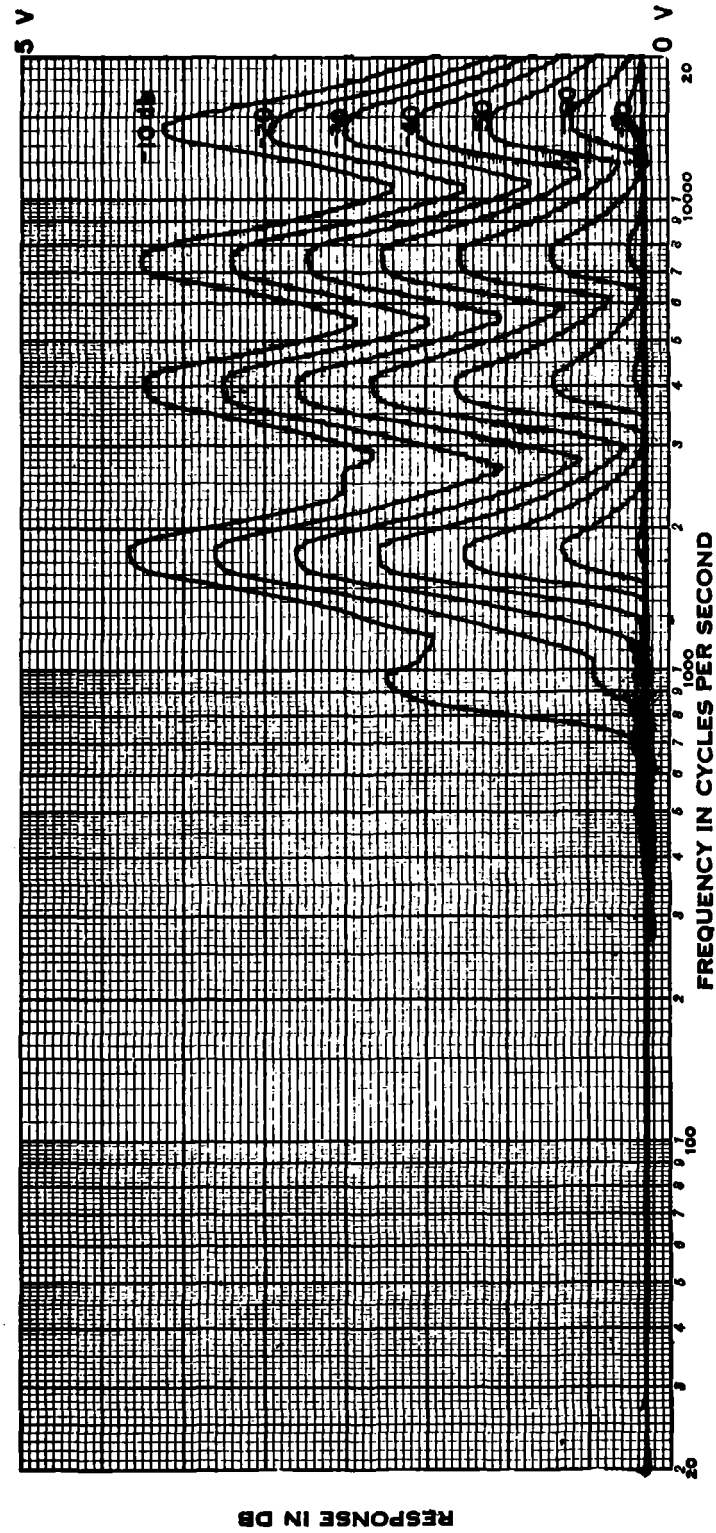


Fig. 3. Combined calibration curve for the TRW/STL VLF electric field experiment on 1964-45A. All channels  $\pm 30^\circ$ F. Attenuation in decibels is the calibration input value below 1 volt.



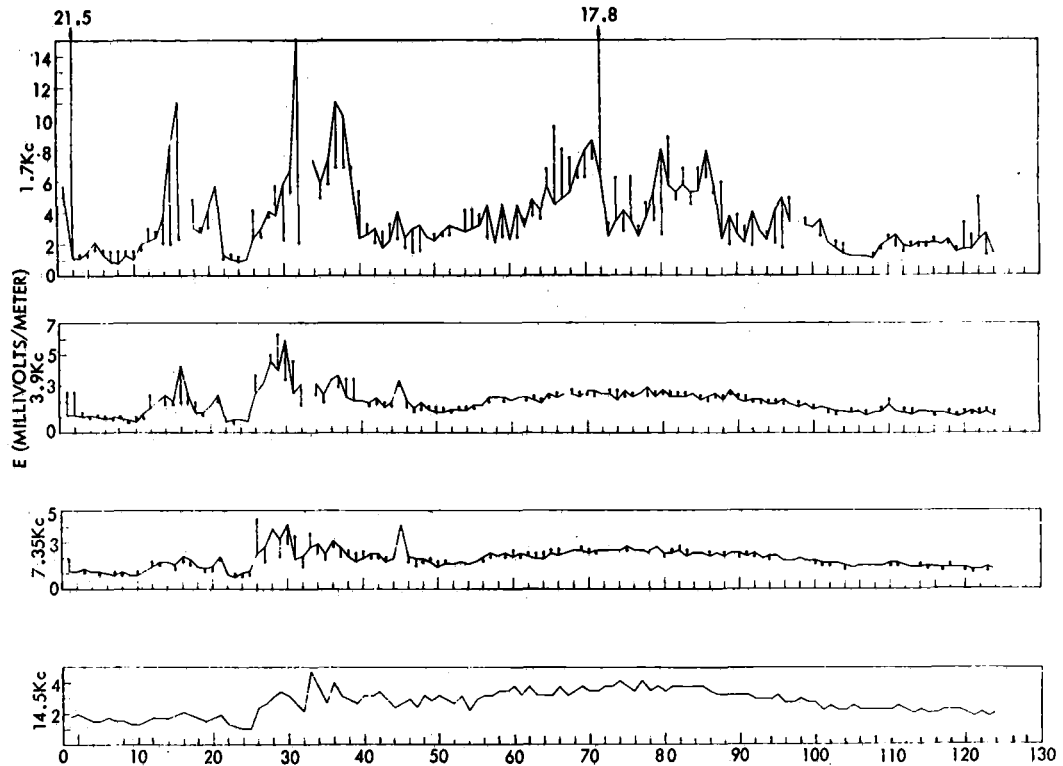


Fig. 4. VLF electric fields measured on orbit 47. The continuous lines connect samples measured once every 1.068 minutes. On the three lowest-frequency channels the vertical lines connect the first sample in each 1.068-minute sequence with a reading taken 7, 5, or 3 seconds later ( $f = 1.7, 3.9$ , and  $7.35$  kc/s, respectively).

periment was still thought to be of interest, since it was capable of detecting whistlers of higher amplitude. The expected result from an incident whistler would be signals of different amplitudes in each of the channels, which are approximately 1 second apart. Shortly before launch it became clear that the instrument could serve another function, as a detector of high-intensity, short-wavelength electrostatic oscillations.

##### 5. PRELIMINARY DESCRIPTION OF VLF OBSERVATIONS

The orbit of the spacecraft 1964-45A is such that it remains at essentially a constant local time near the 1-2 o'clock meridian, and so it has not been possible to explore the ambient fields in supposedly 'active' regions near dawn or dusk. Furthermore, the night- and day-side measurements correspond to essentially differ-

ent altitudes. Perigee remains on the night side, and the spacecraft travels through the inner zone of the radiation belts in sunlight. In this section we present the results obtained on a few early orbits and comment on some apparent persistent features of the fields. More detailed analysis of additional orbits and statistical evaluations will be presented in a future publication.

The indicated average electric fields in the four channels are shown in Figure 4 for orbit 47, August 19, 1964. The continuous line in the three lowest-frequency channels connects the first sample in each 1.068-minute sequence, and the dots represent readings taken 7, 5, or 3 seconds later ( $f = 1.7, 3.9$ , and  $7.35$  kc/s, respectively). The electric field strengths are derived using the free-space antenna capacitance,  $C_0$ , and an effective length of  $\frac{1}{2}l = 9$  inches; the true field strengths are related to the indicated

values by

$$E = \left(\frac{C_0}{C}\right) \left(\frac{l}{2 l_{eff}}\right) E_{ind} \quad (13)$$

It is argued in the appendix that above perigee the sheath correction factors should rarely cause  $E_{ind}/E$  to be greater than a factor of 3, but this analysis is subject to considerable uncertainty.

However, the very large values for the indicated background field strengths shown in Figure 4 are extremely significant, even if reduction factors as large as 3-5 are applied. The indicated background field is usually of the order of 1-2 mv/m in each channel, with infrequent dips to about 800  $\mu$ v/m. This behavior is typical for all orbits that have been examined to date, and field strengths near the receiver threshold level (300-600  $\mu$ v/m) are encountered on very rare and isolated occasions. Thus, even if the largest reasonable sheath reduction factor of 5 is appropriate, the VLF experiment reveals that the true background field is at least of the order of 200-400  $\mu$ v/m, in very good agreement with the prediction of equation 8.

We have already noted that, since the index of refraction at  $h \simeq 500-600$  km is near 50, the whistler background at this altitude for  $f = 1.7$  kc/s should be less than 5.5  $\mu$ v/m. The index of refraction has been calculated for the entire range of densities and geomagnetic field strengths along orbit 47, and we find  $24 \lesssim n(1.7 \text{ kc/s}) \lesssim 150$ . The corresponding range of values for  $|E| = c\Delta B/n$  are shown in Figure 5, and if the Injun 3 receiver noise level of  $10^{-3}$   $\gamma$  is used it can be seen that the whistler background should be no larger than 2-12  $\mu$ v/m for orbit 47. Thus, even when the maximum reasonable sheath reduction factor is applied, the observed electric field background at 1.7 kc is at least from 20 to 200 times too large to represent transverse waves. We therefore conclude that the observed background fields probably represent electrostatic ion waves.

It is also clear that VLF field strengths one or two orders of magnitude greater than background are frequently detected, especially in the 1.7-kc/s channel. Some of these are isolated spikes that might appear to be very large amplitude whistlers. For example, the two off-scale points in the 1.7-kc/s channel of Figure 4 represent bursts that are not detected when the

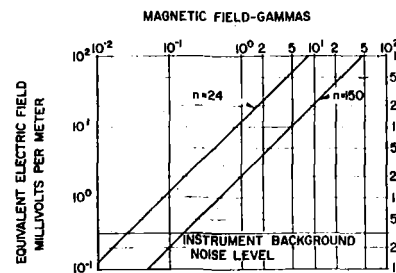


Fig. 5. Relation between electric and magnetic field strengths for whistlers. Over orbit 47 the index of refraction at  $f = 1.7$  kc/s varies between 24 and 150. The straight lines connect fields with  $E = cB/n$  for  $n = 24, 150$ , and the observed background field of about 1 mv/m then corresponds to a whistler magnetic background of 0.1-1  $\gamma$  at this frequency.

3.9-kc/s channel is sampled 1 second later. (The charge and discharge time constants are both of the order of 1 second, and the actual peak field strengths may be considerably higher than the indicated averages.) If the true electric field strengths are reduced to values of the order of  $4-8 \times 10^{-3}$  volt/m, Figure 5 indicates that the associated magnetic fluctuation amplitude is in the range of 0.2-5  $\gamma$ . These amplitude values are not inconsistent with the whistler observations on Vanguard 3; however, the isolated spikes do not appear to be normal whistlers in another sense. That is, most whistlers have a magnetic intensity spectrum that is quite flat between  $f_{min} \simeq 1$  kc/s and an upper frequency cutoff large in comparison with 1.7 kc/s, so that  $E_{wh} = c\Delta B/n$  should then vary as  $f^{1/2}$  in this range. On this basis, we should expect to observe whistler fields of even higher intensity in the higher-frequency channels; however, the very large spikes are definitely detected most frequently in the 1.7-kc/s channel. In fact, it is clear from Figure 4 that the small-amplitude signal variation over 7, 5, or 3 seconds (measured by the vertical lines) also decreases with increasing frequency. (Note that the Doppler shift is unimportant for whistlers, and in all channels  $l$  should be small compared with  $\lambda$ .)

It is even more difficult to explain the persistent ( $t \simeq 3-20$  minutes) rises in signal level that appear in Figure 4 on the basis of detection of transverse wave fields. Once again the signal levels become high ( $E_{ind} \simeq 8-15$  mv/m), and the main rise occurs in the 1.7 channel; but,

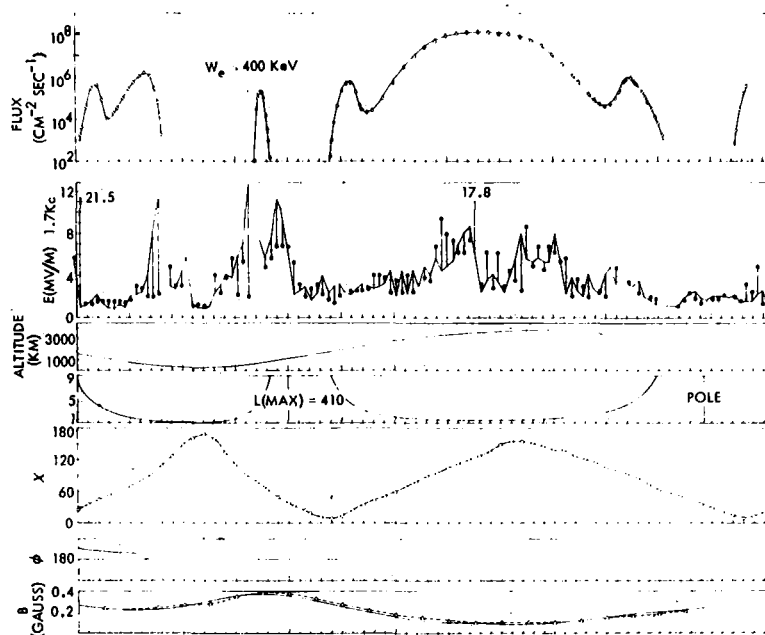


Fig. 6. The 1.7-kc/s response for orbit 47, various ephemeris parameters, and flux of electrons with  $E > 400$  kev. The quantity  $\chi$  is the angle between the antenna (spin axis) and the geomagnetic field;  $\chi$  and the observed  $B$  (dotted) are obtained from the STL triaxial fluxgate magnetometer (courtesy of G. Inouye, E. Greenstadt, and D. Judge). The solid  $B$  curve is the Jensen-Cain field. The angle  $\phi$  is solar longitude, and the spacecraft spends most of its time near the 1-2 o'clock meridian. The energetic electron fluxes are determined by the Aerospace solid-state detector (courtesy of G. A. Paulikas, J. B. Blake, and S. C. Freden).

in addition, these enhancements are too persistent to be normal whistler trains, they are seen on almost every orbit, and they are strongly correlated with passage through specific values of  $L$  and altitude (or local time). Furthermore, the well-defined enhancements on the night side (below the radiation belts) are strongly related to the presence of energetic precipitating electrons. These features are illustrated for orbits 47 and 85 in Figures 6 and 7, respectively, where the 1.7-kc/s channel signal and various ephemeris parameters ( $L$ ,  $h$ ,  $\chi = \cos^{-1}(l, B_{\text{geomag}})$ , etc.) are shown together, along with the response of the Aerospace solid-state detector. This instrument is sensitive to fluxes of electrons with energies greater than about 400 kev, and the data for Figures 6 and 7 were kindly furnished by G. A. Paulikas, J. B. Blake, and S. C. Freden.

There is some basis for the belief that the enhancements represent nonequilibrium amplitudes for ion waves rather than field strengths of transverse VLF oscillations: (1) If the waves

are electrostatic,  $\lambda \approx (\kappa T_e / M_i)^{1/2} / f$ , so that  $\lambda(1.7 \text{ kc/s}) \approx 1\text{--}2$  meters,  $\lambda(3.9 \text{ kc/s}) \approx 43\text{--}86$  cm, etc. Only the lowest-frequency channel has a range of wavelengths significantly greater than the effective antenna length ( $\approx 23$  cm), and so interference problems would be unimportant here. In fact, the signal does occasionally 'break through' in the upper channels, and an amplitude comparable to the 1.7-kc/s field is then seen at 3.9 and 7.35 kc/s. This behavior would be consistent with the conjecture that short-wavelength oscillations are being detected and that interference effects are operative. (2) The actual amplitudes again seem to be much too large to be compatible with magnetic field strengths of *sustained* VLF signals. For instance, the peak chorus and hiss fields were found to be of the order of  $10^{-2} \gamma$  on Injun 3. Even if we reduce the indicated electric field peaks from the range 8-15 to 1.5-3 mv/m, in order to include maximum hypothetical sheath corrections, Figure 5 shows that the equivalent magnetic amplitude would have to be of the order of

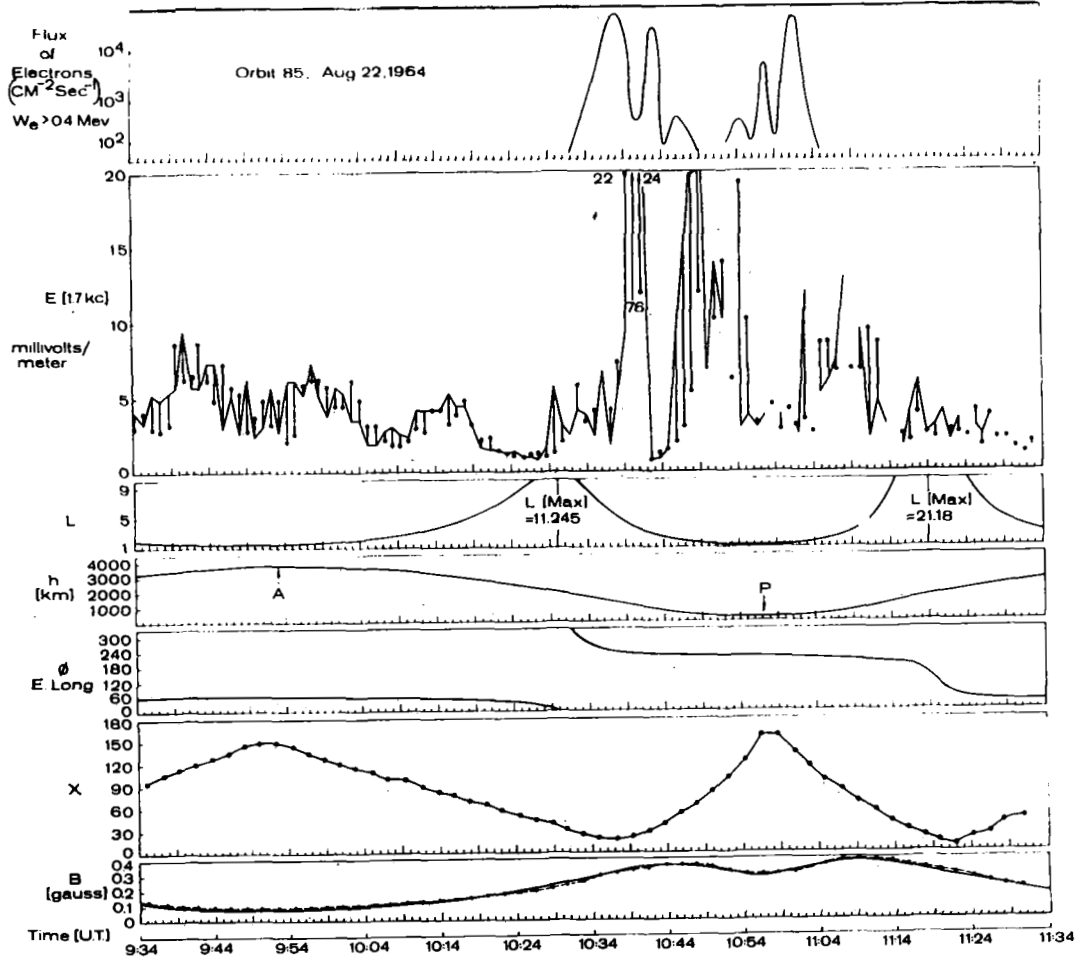


Fig. 7. Data similar to those of Figure 6 for orbit 85. Here  $\phi$  is conventional east longitude.

0.2–2  $\gamma$  for several minutes, if the waves were indeed transverse. (3) For transverse waves at these frequencies, we should expect the electric vector to tend to be polarized normal to the geomagnetic field. Furthermore, in a truly collisionless plasma, large currents can flow along the geomagnetic field, and there should be an antenna shunting effect when  $\sin \chi$  is small enough so that a geomagnetic field line passes through the top of the antenna and the spacecraft body. Thus, for transverse waves,  $E$  should become small when  $\sin \chi$  does, but Figures 6 and 7 indicate that the dependence on  $\chi$  is very weak, except perhaps when the fields are near the background value.

The apparent absence of a significant shorting effect definitely suggests that longitudinal ion

waves are present, for these fluctuations scatter electrons, limit the current flow, and produce a finite electrical conductivity in a collisionless plasma. In fact, if a dc or slowly varying ( $\omega \leq \nu$ , the collision frequency) electric field larger than the runaway field,

$$E_R = \frac{m}{e} \nu \left( \frac{\kappa T_e}{m} \right)^{1/2} \\ \simeq 10^{-6} \frac{N}{T} \ln \Lambda \left( \frac{\text{volts}}{m} \right) \\ \Lambda = 10^4 (T^{3/2} / N^{1/2}) \quad (14)$$

is suddenly imposed on a collisionless plasma, the distribution function rapidly becomes distorted so that ion waves grow and inhibit the

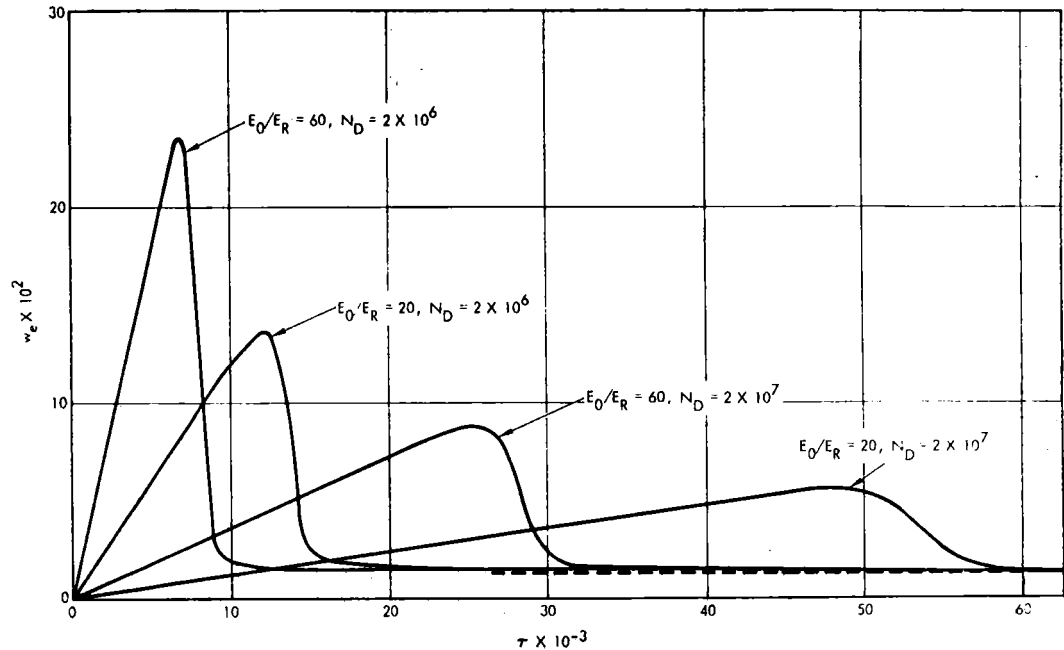


Fig. 8. Average electron drift velocity  $w_e = v_e/a$ , versus  $\tau = \omega_p t$  for various values for  $E_0/E_R$  ( $E_0$  is the applied field,  $E_R$  the runaway field) and  $N_D = \omega_p^2/\nu$  ( $\nu$  is the collision frequency). For a detailed discussion see *Field and Fried* [1964].

current, ultimately quenching the growth of the waves. The temporal variation has been studied by *Field and Fried* [1964], and Figure 8 shows some representative drift velocity versus time curves; after some  $10^4$  electron plasma periods, the 'self-regulation' has reduced the electron-proton drift speed to the value needed to quench the ion wave instability (see Figure 1).

At the spacecraft orbit, the critical or runaway field is very small. Near apogee,  $N_e \approx T_e \approx 3000$ , so that  $\nu \approx 0.8 \text{ sec}^{-1}$  and  $E_R \approx 17 \text{ } \mu\text{V/m}$  (above background); for  $N_e = 5 \times 10^4 \text{ cm}^{-3}$ ,  $T_e \approx 1500^\circ\text{K}$  ( $h \approx 500\text{--}600 \text{ km}$ ),  $\nu \approx 750 \text{ sec}^{-1}$ , and  $E_R \approx 350 \text{ } \mu\text{V/m}$ . However, in these regions the electron plasma period is of the order of  $0.1\text{--}0.3 \text{ } \mu\text{sec}$ , and so very large currents associated with any dc or slowly varying electric fields should be rapidly dissipated; the energy available distorts the electron population by producing anisotropies and energetic particles.

*Swift* [1965] has recently conjectured that large-amplitude, slowly varying electric fields may exist above the ionosphere, so that currents can flow along the magnetic field connecting the space charges to the conducting ionosphere.

The currents would then produce ion waves and also energetic electrons as indicated above. The theory was used by Swift to explain auroral bombardment and to interpret the weak VLF magnetic hiss detected on Injun 3 [*Gurnett and O'Brien*, 1964] in connection with enhancement of precipitated and trapped fluxes of 40-keV electrons. The observed hiss intensities (wide-band peak  $\approx 10^{-2} \gamma$ ) are somewhat higher than could reasonably be expected using  $\Delta B \approx VE/c^2$ , but Swift suggests gradient coupling between longitudinal and transverse waves to account for the discrepancy.

In many ways the observations shown in Figures 6 and 7 are compatible with this picture. Enhanced ion waves are found near  $L = 1.5$ ,  $L = 2\text{--}4$ , and  $L > 5\text{--}6$  (night side), and they could be associated with local currents produced by large-amplitude dc fields. The spikes appear to bound the regions where precipitating  $E > 400 \text{ keV}$  electrons are detected, suggesting that the fluxes at the spikes are already so low that they are undetectable. The data for orbit 47 are particularly interesting in this regard; the night-side enhancement at  $L \approx$

3, for instance, corresponds to a dip in the radiation belt flux on the day side at roughly the same  $L$  value. Similarly, the large auroral enhancement on the other side of the narrow precipitating electron spike appears to define a broad  $L$  shell ( $L > 6$ ) of reduced *trapped* flux. This precipitation would be consistent with the presence of a large dc field along the particular magnetic field line, but it seems unlikely that the  $E > 400$  kev electrons could be *produced* by such a field.

Of course, other mechanisms may be more important than the above. The enhanced ion waves could be generated by significant currents of particles energized in other regions of the magnetosphere, and gradients, anisotropies, etc., may also be significant. In the absence of a large-amplitude dc field parallel to  $B_{\text{geomag}}$ , we might try to account for the observed electron precipitation by conjecturing that the large-amplitude VLF fields are primarily oriented parallel to  $B_{\text{geomag}}$ , so that the VLF fields induce the precipitation directly. However, the P11 experiment yields no directional information, and equation 4 shows that ion wave electric fields can have any orientation with respect to  $B_{\text{geomag}}$ . If we consider the other extreme in which the ion wave fields are primarily normal to  $B_{\text{geomag}}$ , diffusion across  $L$  shells, rather than precipitation, becomes operative. This enhanced diffusion is discussed by Bohm [1949], Spitzer [1960], and Taylor [1961]; the maximum diffusion rate associated with microscopic electric fluctuations is

$$D_{\perp} \simeq \frac{10^8}{4} \frac{\kappa (T_e + T_i)}{B} \quad (15)$$

where  $\kappa T$  is in electron volts and  $D_{\perp}$  in centimeters<sup>2</sup> per second. For  $B \sim 0.3$  gauss and  $(T_e + T_i) \approx 3000^\circ\text{K}$ , the diffusion rate across field lines is of the order of  $2 \times 10^7$  cm<sup>2</sup>/sec. This value is not insignificant, and  $D_{\perp}$  rapidly increases with altitude.

#### 6. SIGNIFICANCE OF LARGE-AMPLITUDE ION WAVES

The results reported in section 5 strongly suggest that enhanced or nonequilibrium amplitudes for electrostatic ion waves are commonly present at the orbit of 1964-45A. Furthermore, it is clear that these field enhancements are related to precipitation of trapped particles from

the Van Allen belts (i. e., the fairly persistent rise near the 'slot' at  $L = 2-4$ ) and to auroral phenomena (large values are usually found near the night auroral and polar zones). There is, in fact, additional evidence that electric field amplitudes in the range of 100 mv/m may directly cause mid-latitude red arcs and type A red aurora [Megill and Carleton, 1964]. In this section we wish to speculate on the possible role of nonequilibrium electrostatic waves in the entire magnetosphere and transition region.

First, let us consider the magnetosphere. Ion acoustic waves with  $\mathbf{E} \times \mathbf{B}_{\text{geomag}} \simeq 0$  will precipitate particles, whereas those with  $\mathbf{E} \cdot \mathbf{B}_{\text{geomag}} \simeq 0$  will cause diffusion across  $L$  shells with  $D_{\perp}$  given approximately by equation 15. Near the equator at  $L = 3$ ,  $B_{\text{geomag}} \simeq 0.312/27$ ,  $T_e \simeq 7800^\circ\text{K}$  [Serbu, 1964], and equation 15 yields

$$D_{\perp}(L = 3) \simeq (0.025R_e)^2/\text{day} \quad (16)$$

This prediction is in good agreement with the equatorial observations of Frank *et al.* [1964] during the period December 7, 1962, to January 8, 1963. After December 20, the intensity of energetic electrons  $E > 1.6$  mev at  $L \sim 4.5$  declined gradually, but a pronounced dip initially at  $L = 3.8$  steadily moved inward to  $L = 3.2$  at a rate of  $\sim 0.02R_e/\text{day}$ .

It is unlikely that there could be recognizable diffusion and precipitation unless a significant source of energetic particles was also present. This observation is relevant because the most likely configurations for ion wave fields at the equator have finite  $E_{\parallel}$  (causing precipitation) and  $E_{\perp}$  (causing diffusion). In essence, the waves are strongly guided along  $B_{\text{geomag}}$ , but waves on adjacent field lines are randomly phased so that fluctuating transverse potential gradients develop [Spitzer, 1960]. Indeed, the observations of Frank, Van Allen, and Hills indicate that a local acceleration source did convert a small fraction of the 40-kev flux to  $E > 1.6$ -Mev electrons during this period. Once again, large-amplitude ion waves may be important in explaining this acceleration. In the presence of a magnetostatic field and an electrostatic wave, the equation of motion for an electron is

$$m\ddot{\mathbf{r}} = -e\dot{\mathbf{r}} \times \mathbf{B} + e\mathbf{k}\phi_0 \cos(\mathbf{k} \cdot \mathbf{r} - \omega t) \quad (17)$$

and it has been shown [Scarf *et al.*, 1965; Fredricks *et al.*, 1965] that resonance occurs if

$$\omega + k_{\parallel}v_{\parallel} = \beta\omega_c, \quad \beta = 1, 2 \quad (18)$$

with  $\omega/k \simeq (\kappa T_e/M_i)^{1/2}$ ,  $0 < \omega \ll \Omega_p$  for ion waves. At  $L = 3$ ,  $\omega/k \simeq 10^5$  cm/sec,  $f_p \simeq \Omega_p/2\pi \simeq 4.5$  kc/s, and  $f_c \simeq \omega_c/2\pi \simeq 30$  kc/s. Since a 40-keV electron has a speed near  $10^{10}$  cm/sec, which is far in excess of  $\omega/k$ , it is obvious that this resonance condition can easily be satisfied if the wave has a finite value for  $k_{\parallel}$ .

In the application to the transition region, equation 17 was solved for  $k_{\perp} = k_{\parallel}$  and large ion wave amplitudes ( $e\phi_0 \sim \kappa T_e$ ). It was found that velocity multiplication by a factor of 3-4 takes place very rapidly ( $t \simeq 43/\omega_c$ ), but that the acceleration is periodic if the field remains steady and the wave remains coherent. However, *Stix* [1964] has argued that, for these very large amplitudes, the ion wave is coherent only in a region of the order of  $k^{-1}$ . Thus, it was predicted [Fredricks *et al.*, 1965] that in the transition region electrons with initial energies of the order of 2-4 keV would be accelerated to 20-65 keV in times of the order of milliseconds. In the magnetosphere, very moderate ion wave amplitudes are anticipated, and the resonance condition, equation 18, involves a variety of ratios for  $k_{\perp}/k_{\parallel}$ . Thus, the transition-region calculations are not directly applicable. In particular, coherent waves can persist inducing many cycles of acceleration and deceleration, relativistic corrections are significant for electrons with initial 40-keV energies, and the trapped particles have complex orbits in the dipolar field. Nevertheless, the sample calculations, which yield velocity multiplication by a factor of 4, could be relevant in explaining a slow conversion of some of the  $E > 40$ -keV flux to MeV electrons. The slow growth of the  $E > 1.6$ -MeV flux could also imply that  $E_{\parallel}$  and  $k_{\parallel}$  remain extremely small, so that both precipitation and acceleration are inhibited while diffusion across  $L$  shells takes place.

As was mentioned above, we believe that ion wave instabilities are particularly important in the transition region. *Buneman* [1964] has recently stressed again that the only known mechanism that can distort the incident collisionless plasma so that a 'shocklike' transition region is formed involves scattering from electrostatic waves. This idea was developed by *Piddington* [1960], *Bernstein et al.* [1964], *Kellogg* [1964], *Scarf et al.* [1965], and *Fredricks et al.* [1965], and it was predicted that,

since the waves primarily heat the electrons,  $T_e/T_i$  rises so that the instability is maintained with moderate proton drift speeds (see Figure 1); recent data from Imp-B, Ogo-A [Wolfe and Silva, 1964], and Vela 2A, 2B [Strong *et al.*, 1964; Bame *et al.*, 1964] appear to confirm the expectations that, in the transition region,  $T_e/T_i$  is large, and that the protons are streaming.

#### APPENDIX. SHEATH CORRECTIONS

The P11 VLF antenna is an uninsulated rod ( $l = 45.7$  cm,  $r = 0.476$  cm) mounted parallel to the spin axis of the spacecraft. The free-space capacitance is computed assuming that the spacecraft body forms a ground plane, and this yields  $C_0 \simeq 2\pi\epsilon_0 l / \ln(l/r) \simeq 5.5 \times 10^{-12}$  farad.

In the collisionless magnetospheric plasma an insulating sheath forms around the antenna, and *Storey* [1963] has argued that this sheath keeps the antenna from being shorted by conduction along magnetic field lines when field lines cut both the antenna and the spacecraft body. However, the sheath modifies the antenna impedance so that  $C \neq C_0$ .

A simplified model to account for the change in  $C$  was also suggested by *Storey*. The highly conducting plasma beyond the sheath is regarded as a capacitor element, and the capacitance is recomputed accordingly. For  $R = R_{\text{sheath}} < l/2$ , we find

$$C/C_0 \simeq 2 \ln(l/r) / \ln(R/r) \simeq 9.1 / \ln(R/r) \quad (A1)$$

but for  $R > l/2$  these correction factors are insignificant, since the electric field pattern surrounding the antenna is dominated by the ground plane. However, even for  $R < l/2$ , it is quite difficult to define a 'radius' for the diffuse sheath that develops around the antenna. If  $R$  is defined as the radius that corresponds to half the potential drop across the sheath, the calculations of *Self* [1963] indicate that

$$R \approx 4 \sqrt{2} K_p^{-1} \quad (A2)$$

and, for  $h \simeq 500$ -600 km,  $K_p^{-1} \simeq 1$  cm, so that this gives  $C/C_0 \simeq 3.5$ . The sheath 'thickness' defined in equation A2 increases rapidly with altitude, and hence  $C$  should tend to  $C_0$  by, say,  $h \simeq 1000$  km.

Of course, these considerations concern a hypothetical stationary sheath in a quiet plasma.

If moderately enhanced ion waves are encountered ( $E_n < E \ll E_m$ ), the sheath becomes even more diffuse, since the plasma is then not a good conductor. In this case  $C$  should be closer to  $C_0$  than is indicated above, and there should be little dependence of  $C/C_0$  on  $\chi$ . Furthermore, if fields approaching the maximum ( $E_m \approx K_B k T_e / e$ ) are encountered, it seems unlikely that there would be any meaning to the concept of a plasma sheath, and then the antenna should sample the ambient fields directly.

Another aspect of the sheath has to do with the fact that the sheath electric fields are considerably larger than the runaway field,  $E_R$ . Under these circumstances, it might be asked whether nonuniformities or temporal variations in the sheath could actually *trigger* the ion waves observed on 1964-45A. This prospect seems highly unlikely, for a number of reasons. First, consider slowly varying or static sheath electric fields that have somehow 'protruded into' the ambient plasma with  $E < E_R$ . For the runaway effect to be significant we must have  $f < v/2\pi \approx (0.1-120)$  cps ( $h \approx 600$  km to apogee): but Figure 8 and the discussion in section 5 show that the instability associated with such a field would be quenched in milliseconds. Second, continuous moderate-amplitude sheath perturbations associated with ambient ion waves would not be magnified by a runaway process, because the observed ion wave frequencies appear to be too high. Finally, if the observed enhancements were somehow associated with sheath effects, there would be no conceivable way to explain their appearance near specific  $L$  shells or the correlation with energetic precipitating electrons.

**Acknowledgments.** The experimental program was sponsored by TRW/Space Technology Laboratories Independent Research Program and was carried out by the Space Physics Department of the Physical Research Division; one of the authors (Sarf) has been supported by the National Aeronautics and Space Administration under contract NASw-698.

We wish to thank Dr. A. Rosen, Dr. G. T. Inouye, and Mr. E. W. Greenstadt of TRW/Space Technology Laboratories for their encouragement and assistance in planning the experiment and having it built, and we are indebted to Drs. R. S. White and G. Paulikas of the Aerospace Corporation for their invitation to place the experiment on board the satellite and for their cooperation in making it successful. We are par-

ticularly grateful to Drs. Blake, Freden, and Paulikas of the Aerospace Corporation for making their particle data available, and to Dr. Inouye, Mr. Greenstadt, and Mr. Judge for supplying data from the STL triaxial magnetometer.

We have benefited from discussions with Drs. O. Buneman, B. D. Fried, and A. Kaufman, and from the opportunity to examine the reports of Dr. L. R. O. Storey before publication. J. P. Atkinson and M. Kovacevich are to be thanked for the construction and calibration of the instrument.

We also wish to acknowledge the cooperation of the Space Systems Division, Air Force Systems Command, and the efforts of the Lockheed Payloads Group at Vandenberg A. F. Base and Sunnyvale.

#### REFERENCES

- Bame, S. J., J. R. Asbridge, H. E. Felthausen, R. A. Olson, and I. B. Strong, Electron angular, spatial, and energy distributions measured near  $17R_E$  with an electrostatic analyzer (0.3 to 20 keV) and a GM tube (50 keV), *Trans. Am. Geophys. Union*, **45**, 624, 1964.
- Barrington, R. E., J. S. Behroze, and D. A. Keeley, Very low frequency noise bands observed by the Alouette 1 satellite, *J. Geophys. Res.*, **68**, 6539-6541, 1963.
- Bernstein, W., R. W. Fredricks, and F. L. Scarf, A model for a broad disordered transition between the solar wind and the magnetosphere, *J. Geophys. Res.*, **69**, 1201-1210, 1964.
- Bohm, D., in *The Characteristics of Electrical Discharges in Magnetic Fields*, edited by A. Guthrie and R. K. Wakerling, chapter 2, section 5, McGraw-Hill Book Company, New York, 1949.
- Buneman, O., Dissipation of currents in ionized media, *Phys. Rev.*, **115**, 503, 1959.
- Buneman, O., Excitation of field aligned sound waves by electron streams, *Phys. Rev. Letters*, **10**, 285-287, 1963.
- Buneman, O., Models of collisionless shock fronts, *Phys. Fluids*, **7**, S3-S8, 1964.
- Cain, J. C., I. R. Shapiro, J. Stolarik, and J. P. Heppner, Whistler signals observed with the Vanguard 3 satellite, *J. Phys. Soc. Japan*, **17**, Suppl. A-II, 84-88, 1962.
- Dawson, J. M., Nonlinear electron oscillations in a cold plasma, *Phys. Rev.*, **113**, 383, 1959.
- Dawson, J. M., One-dimensional plasma model, *Phys. Fluids*, **5**, 445, 1962.
- Evans, J. V., Ionospheric temperatures during the launch of NASA rocket 8.14 on July 2, 1963, *J. Geophys. Res.*, **69**, 1436-1444, 1964.
- Farley, D. T., Jr., Two-stream plasma instability as a source of irregularities in the ionosphere, *Phys. Rev. Letters*, **10**, 279-282, 1963.
- Field, E. C., and B. D. Fried, Solution of the kinetic equation for an unstable plasma in an electric field, *Phys. Fluids*, **7**, 1937-1951, 1964.
- Frank, L. A., J. A. Van Allen, and H. K. Hills, A study of charged particles in the earth's outer



- radiation zone with Explorer 14, *J. Geophys. Res.*, **69**, 2171-2191, 1964.
- Fredricks, R. W., F. L. Scarf, and W. Bernstein, Numerical estimates of superthermal electron production by ion acoustic waves in the transition region, *J. Geophys. Res.*, **70**, 21-28, 1965.
- Freeman, J. W., Detection of an intense flux of low-energy protons or ions trapped in the inner radiation zone, *J. Geophys. Res.*, **67**, 921-928, 1962.
- Fried, B. D., and R. W. Gould, Longitudinal ion oscillations in a hot plasma, *Phys. Fluids*, **4**, 139-147, 1961.
- Gdalevich, G. L., Measurements of the electrostatic field at the surface of a rocket during its flight in the ionosphere, *Artificial Earth Satellites*, **17**, 42-58, 1964.
- Gurnett, D. A., and B. J. O'Brien, High-latitude geophysical studies with satellite Injun 3, 5, Very low frequency electromagnetic radiation, *J. Geophys. Res.*, **69**, 65-89, 1964.
- Harris, E. G., Plasma instabilities associated with anisotropic velocity distributions, *J. Nucl. Energy*, Pt. C, **2**, 138-145, 1961.
- Helliwell, R., in Project Able-3 Final Mission Report, *Space Technol. Lab. Tech. Rept. STL/TR-59-V002-02903*, August 1960.
- Imyanitov, I. M., G. L. Gdalevich, and Ya. M. Shvarts, Measurements of the electrostatic field on the surface of geophysical rockets moving through the upper atmosphere, *Artificial Earth Satellites*, **17**, 66-81, 1964.
- Imyanitov, I. M., and Ya. M. Shvarts, Measurements of the electrostatic field strength on the third artificial earth satellite, *Artificial Earth Satellites*, **17**, 59-65, 1964.
- Jackson, E. A., Drift instabilities in a Maxwellian plasma, *Phys. Fluids*, **3**, 786-792, 1960.
- Kavadas, A., and D. W. Johnson, in *Space Research 4*, 365-370, edited by P. Muller (Interscience), John Wiley & Sons, New York, 1964.
- Kellogg, P. J., Shock waves in cool plasma, *Bull. Am. Phys. Soc.*, [2] **9**, 339, 1964.
- Klimontovich, Y., and V. P. Silin, in *Plasma Physics*, edited by J. E. Drummond, chapter 2, p. 82, McGraw-Hill Book Company, New York, 1961.
- Krall, N. A., and M. N. Rosenbluth, Low-frequency stability of nonuniform plasmas, *Phys. Fluids*, **6**, 254-265, 1963.
- Megill, L. R., and N. P. Carleton, Excitation by local electric fields in the aurora and airglow, *J. Geophys. Res.*, **69**, 101-122, 1964.
- Piddington, J. H., Geomagnetic storm theory, *J. Geophys. Res.*, **65**, 93-106, 1960.
- Rostoker, N., Fluctuations of plasmas, 1, *Nucl. Fusion*, **1**, 101-120, 1961.
- Scarf, F. L., W. Bernstein, and R. W. Fredricks, Electron acceleration and plasma instabilities in the transition region, *J. Geophys. Res.*, **70**, 9-20, 1965.
- Self, S. A., Exact solution of the collisionless plasma sheath equation, *Phys. Fluids*, **6**, 1762-1768, 1963.
- Serbu, G. P., Results from the Imp-1 retarding potential analyzer, *NASA Rept. X-615-64-109*, Goddard Space Flight Center, Greenbelt, Maryland, May 1964.
- Smith, C., and J. M. Dawson, Some computer experiments with a one-dimensional plasma model, *Rept. MATT-151, Plasma Phys. Lab., Princeton Univ.*, January 1963.
- Spitzer, L., Jr., Particle diffusion across a magnetic field, *Phys. Fluids*, **3**, 659-660, 1960.
- Stix, T. H., *The Theory of Plasma Waves*, McGraw-Hill Book Company, New York, 1962.
- Stix, T. H., Energetic electrons from a beam-plasma overstability, *Phys. Fluids*, **7**, 1960-1979, 1964.
- Storey, L. R. O., The design of an electric dipole antenna for VLF reception within the ionosphere, *Tech. Rept. 308 TC, Centre National d'Etudes des Télécommunications*, Département 'Télécommande,' July 1963.
- Storey, L. R. O., C. Renard, and G. Driancourt, The Aerobee experiment at Wallops Island in October 1963, *Tech. Rept. 327 TC, Centre National d'Etudes des Télécommunications*, Département 'Télécommande,' February 1964.
- Strong, I. B., J. R. Asbridge, S. J. Bame, H. E. Felthaus, and R. A. Olson, Positive ion angular spatial and energy distributions as measured near  $17R_E$  by an electrostatic analyzer (0.3 to 20 keV), *Trans. Am. Geophys. Union*, **45**, 624, 1964.
- Swift, D. W., A mechanism for energizing electrons in the magnetosphere, *J. Geophys. Res.*, **70**, 3061-3073, 1965.
- Taylor, J. B., Diffusion of plasma ions across a magnetic field, *Phys. Fluids*, **4**, 1142-1145, 1961.
- Wolfe, J. H., and R. W. Silva, Results of the NASA-Ames Research Center plasma probe on the interplanetary monitoring platform, *Trans. Am. Geophys. Union*, **45**, 604, 1964.

(Manuscript received February 15, 1965.)